Water holding of protein gels

Vaida Urbonaite

Thesis committee

Promotor
Prof. Dr E. van der Linden
Professor of Physics and Physical Chemistry of Foods
Wageningen University

Co-promotors
Dr L.A.M. Pouvreau
Senior scientist
NIZO Food research, Ede

Dr H.H.J. de Jongh
Senior scientist
Top Institute Food and Nutrition, Wageningen

Other members
Prof. Dr R.M. Boom, Wageningen University, NL
Prof. Dr C. Mills, University of Manchester, UK
Dr M. Charalambides, Imperial College London, UK
Dr T. Nicolai, Université du Maine, Le Mans, FR

Water holding of protein gels

Vaida Urbonaite

Skiriu Tėvams

Abstract

For foods, the ability of food products to entrap and exude water upon mechanical deformation is important for their texture, juiciness and, by means of concomitant release of tastants, the taste perception. For many food products the spatial volume is set by a protein network. Therefore, understanding how protein network characteristics determine entrapment and exudation of water is important. We have quantified the effects of the network coarseness at various scales and network stiffness on the gel water holding and the kinetics of water exudation. The knowledge enables a better control of texture, juiciness and taste in designing novel food products.

Table of Contents

Chapter 1

General introduction

1.1   Introduction

The current growth of the global population will require further exploitation of alternative protein sources. A better understanding of protein functionality and exchangeability from one source to another to ensure a sufficient and efficient food supply is essential to face future demands, where the use of plant proteins as structuring agents in food products has gained a lot of attention in the last decade. Ideally it would be desirable that any alternative protein has the functionality of the original protein. However, proteins from different sources usually show vastly different properties, like solubility, denaturation, assembly and according network-forming properties. This implies that exchanging a protein by another is difficult without affecting the textural and sensory properties of the final product. Since one of the important material properties that relate to texture and sensory is water holding, it is important to understand this material property in terms of the properties of the constituent proteins.

Water holding (WH) is defined as the ability of a matrix of molecules to entrap water in such a manner that exudation is prevented. Protein ability to gel (to form a spatial network) results in water entrapment within the gel, and therefore in a WH ability. For example, soy proteins are known for their functionality to retain water or to improve water holding of products, but the origin of this property is still largely unknown. Difficulty in understanding the origin of WH is caused by two reasons: (i) conditions at which exudation of water from gels is studied are not consistent in literature (**Tables 1.1-1.3**), and (ii) the large variation in the systems used to study WH differ in protein source and gelation conditions (**Tables 1.4-1.5**).

From the **Tables 1.1-1.3** it can be seen that water removal from the gel network by applying force is achieved by centrifugation, compression or using capillary suction. Within each methodology variables as sample size, mesh or membrane porosity, applied force, time under compression and temperature vary. As a result of an inconsistent methodology to measure WH and different systems studied, WH measurements cannot be compared between each other. Consequently, WH is often expressed as an additional parameter to characterize gels rather than being described as a gel property. Gels studied for their WH vary from protein gels to polysaccharide gels (**Table 1.4**). However, even for a single protein source, the gels differ in protein pre-treatment, protein concentration, pH, salts used and gelation conditions. An example for soy protein gels is shown in **Table 1.5**. A number of variables within methodologies and gels studied makes it difficult to conclude on the origin of WH property, as illustrated by the left column of **Table 1.5**, where numbers between 45 and 100% are reputed.

Table 1.1 WH of gels measured by centrifugation.

Ref.	Sample size (g)	Tube (ml)	Membrane pores	Speed (RCF)	Temp. (°C)	Time (min)	Adapted from
			Membrane fixed in the middle of the tube				
[1]	0.3-1.3	50	5.0 μm	120	15	5	
[2]	5	250	Cotton cloth	120	15	5	[1]
[3]	Gelled in the tube, 1	5	5 kDa	5000		20	[4]
[5]	Gelled in the tube, 0.5 ml	1.5	0.45 μm	8000 rpm		10	[3, 4]
[4]	Cylinder, 1 x 0.48 cm	1.5	0.45 μm & filter paper	153, 2451		2.5-25	
[6]	0.1	1.5	10 μm	120		5	
[7]	3		200 μm	790		30	
[8]	5			790		30	[7]
[9]	Cylinder, 1 x 0.48 cm	2		100, 300 & 500		45	[4]
[10]	Disk, 1.5 x 2.1 cm			224	RT*	1-60	[4, 11]
[11]	Cylinder, 1 x 0.38 cm		0.45 μm	268		5-120	
			Hanging membrane bag (2 cm from the bottom)				
[12]	Cylinder, 1 x 0.8 cm		0.45 μm	4000	15	10	[4]
[13]	Cylinder, 1 x 0.8 cm		0.45 μm	4000	15	10	[12]
			No membrane				
[14]	3		5	8000	RT*		[15]
[15]	5		50	8000	4		[16]
[17]	20			400-10000			
[18]	5		50	8000	4		[16]
			No membrane, samples wrapped in the filter paper				
[16]	Cubes, 0.3-0.5 cm			4000	15	10	[12]
[19]	1-1.5	50	Whatmann #1	124	10	5	

*Room temperature

Table 1.2 WH of gels measured by compression.

Ref.	Sample size (g)	Compression	Speed	Time under compression (min)	Temp. (°C)	Adapted from
[20]	Cylinder, 3 x 3.2 cm	to 50% initial height	0.17 mm/s	5	RT*	
[21]	~ 1	~3000 kPa		1	-	

*Room temperature

Table 1.3 WH measured by capillary suction.

Ref.	Sample size (g)	Filter paper	Ratio gel solids : filter paper	Equilibration time	Temp. (°C)	Adapted from
[9]	Slice, 1 x 1 x 0.2 cm	Whatmann #1	0.2 : 1	5 days	20	[22]
[22]		Whatmann #1	varied	72 h	6	

Table 1.4 Type of gels studied.

Gels	References
Soy protein	[1-3, 5, 13, 14, 16, 21, 23]
Whey protein isolate	[4, 19, 20]
Blood plasma protein	[7, 12, 24]
Mixed protein/protein	[8]
Mixed protein/polysaccharide	[17, 25]
Emulsion filled	[15, 18]
Polysaccharide gels	[10, 11]

Table 1.5 Example of soy protein gels (variables).

Ref.	Protein pretreatment	Protein conc. (%)	pH	Salt	Gelation	WH (%)
[23]		8-14	2.5-3.5		90°C for 30 min	80-100
[1]		10	2.75-8.0	NaCl, CaCl$_2$	90°C for 30 min	60-100
[3]	105°C for 5 min	6-9	7.0	CaCl$_2$		57-97
[5]	95°C for 10 min	4-8	6.9	GDL	95°C for 5 min	48-68
[13]		20	6.8		300-700 MPa	92-98
[14]	Sonication, heating 95°C for 20 min	10		GDL	95°C for 20 min	75-95
[16]	Oxidative modification	12			95°C for 20 min	45-82

Based on the literature overview, it can be seen that there is no uniform description of WH. Inconsistent methodology used and different systems studied do not allow to make comparisons and conclusions. Therefore, the objective of this thesis is to create clarity in WH by using a consistent approach and methodology, and make it generic.

1.1.1 Proteins studied in this thesis

Within this study globular proteins were used. Their densities approach that of crystalline hydrocarbons and amino acids [26]. Examples of globular proteins are whey proteins, egg white proteins (ovalbumin), and plant seed storage proteins, such as soy. We describe the proteins used in this thesis in more detail below.

Soy proteins

Soy protein isolate (SP) consists of two major components, β-conglycinin and glycinin. These are also referred to as 7S and 11S globulin, respectively. At neutral pH the denaturation temperature of β-conglycinin is about 70 °C and that of glycinin about 90 °C, [27]. Glycinin consists of one basic and one acidic polypeptide, linked by a disulphide bond, except for the acidic polypeptide A4 [28]. At least six acidic polypeptides and five basic polypeptides have been isolated [29]. At ambient temperatures and pH 7.6, glycinin forms hexameric complexes (11S), about 360 kDa. The isoelectric point (IEP) of glycinin is 4.90. β-Conglycinin has a molar mass of about 180 kDa and is a trimeric glycoprotein (7S). It consists of three types of subunits, in seven different combinations. The subunits are associated via hydrophobic and hydrogen bonding without any disulphide bonds. The isoelectric point of β-conglycinin is 4.64 [30].

Ovalbumin

Ovalbumin is a glycoprotein with molecular mass of ~ 45 kDa. It has 386 amino acids, an IEP of about 4.7, and a denaturation temperature of 80 °C [31]. Ovalbumin does not exhibit any protease-inhibitory activity [32]. Ovalbumin has 4 thiol groups with a single internal disulfide bond between Cys 74 and Cys 121 [33].

Whey proteins

Whey protein (here abbreviated as WPI) is present in a liquid byproduct of cheese production [34]. It is a mixture of proteins, of which the main ones are β-lactoglobulin and α-lactalbumin (61% and 22%, respectively). The protein β-lactoglobulin, is a small dimeric protein (molar weight of around 36 kDa (2 x 18 kDa)). It consists of 162 amino acid residues, two disulfide bonds (Cys66 – Cys160 and Cys106–Cys119), and a free thiol group (Cys121) [35]. It has an isoelectric point (IEP) of 5.2, and a defined secondary and tertiary structure. α-Lactalbumin is a Ca^{2+} binding protein, with an IEP 4.8 - 5.1 [36] and a molecular weight of around 14 kDa. Of WPI approximately 9.1% consists of immunoglobulin, having an IEP of 5.5 - 6.8 [37]. Of WPI, bovine serum albumin amounts to ~ 5.5%, with an IEP between 4.8 - 5.1 [37]. The heat denaturation of whey proteins starts to occur above 65 °C [38].

1.1.2 Protein aggregation and gelation

The microstructural aspects of the protein gel are set by e.g. the type of protein, protein concentration, pH, ionic strength and type of salts [3, 13, 27, 39, 40]. Globular proteins

form two types of gels classified as either fine or coarse-stranded, depending on the number of charges the native protein carries [41-43]. Structural elements composing the network define gel microstructure. When electrostatic repulsion dominates the system, the network will be composed of fine strands with a diameter in the order of nanometers in size [44]. Fine gels are characterized by thin protein strands, which cause low light scattering [20], and therefore the gels are visually transparent [44, 45]. Coarse-stranded networks exhibit strand dimensions in the range of 100 – 1000 nm [41, 46], dependent on the gelling conditions. The coarseness is maximal in the proximity of macroscopic phase separation [47]. Coarse gels are opaque in appearance and can show syneresis [48].

1.1.3 Gel microstructure and water holding

To be able to predict specific product properties as for example water holding, one has to know if protein structure or bigger length scales as microstructure determines the water holding property of the product. In literature, WH of a gel has been commonly related to microstructure (micrometer length scales) [1-3, 49], to gel strength [5, 21] or protein-protein and protein-water interactions [13, 16, 50]. When water holding in relation to gel coarseness is studied, network stiffness and time- or force-dependent changes in the gel morphology are often not taken into account. It is assumed that WH of a protein-based gel is predominantly defined by the gel morphology, but due to uncontrolled gel destruction during analysis, the relationship between WH and gel microstructure under applied deformation has been disputed. Consequently, WH and gel microstructure are not always linked [7], and length scales dictating WH remain difficult to identify.

With regard to a conceptual idea of length scales and gel WH, Hermansson proposed three different length scale-dependent water transport mechanisms in the gel: (i) hydrodynamic flow, (ii) capillary flow and (iii) molecular diffusion [40]. Hydrodynamic and capillary flows are apparent on macro- to micron scales. Hydrodynamic flow is active in large and open structures, and is driven by gravity or external forces. Capillary flow depends also on surface tension of the liquid, where an external pressure higher than the capillary pressure is needed to displace water [9, 40]. Molecular diffusion is apparent on nanometer scale and is more of importance for the mass transport of molecules or small particles in the gel matrix rather than for WH.

1.1.4 Approach to study gel WH

The aim of this thesis is to understand how structural aspects at different length scales affect protein gel water holding under applied pressure. Special attention is given to understanding which length scales contribute most to kinetics and quantity of water removed. The approach taken to study WH of gels under applied pressure was to evaluate different length scales contributions to gel water holding, and is schematically represented in **Figure 1.1**.
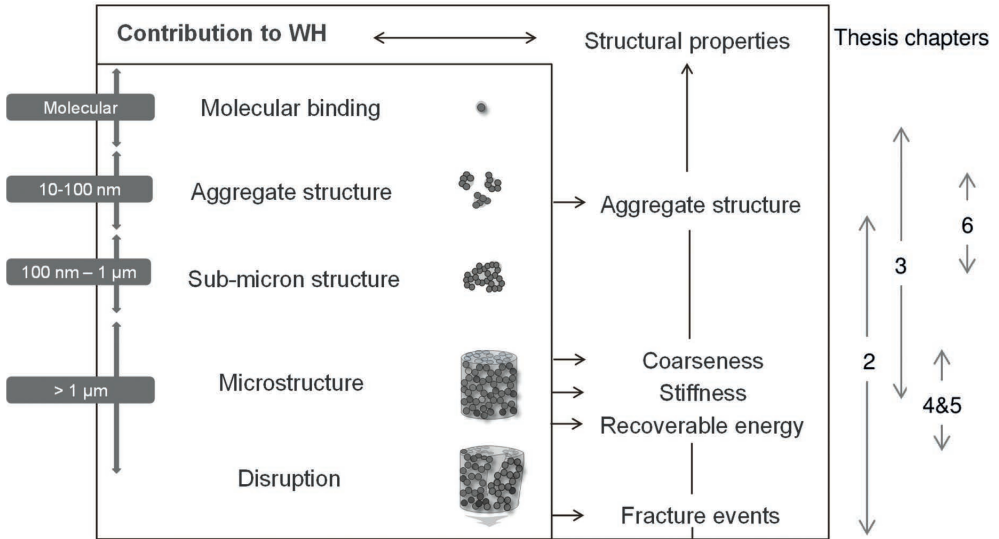
Figure 1.1 Approach to study protein gel WH at different length scales.

Within this study, protein gel WH is defined as sum of the five different contributions *(C)* representing water held within the gel microstructure at different length scales:

$$(\%)WH = C_{molecular \atop binding} + C_{aggregate \atop structure} + C_{sub-micron \atop structure} + C_{microstructure} + C_{disruption} \qquad (1.1)$$

where the $C_{molecular\ binding}$ refers to the retained water that is molecularly bound to the globular protein (0.06-0.07 g of water/g protein, where typically already 0.04 g water is required to hydrate peptide bonds) and is, in this research, assumed to be constant. The $C_{aggregate\ structure}$ represents water confined within aggregates. The $C_{sub-micron\ structure}$ includes water held by building blocks dictated by protein-protein and protein-water interactions. The $C_{microstructure}$ refers to porosity, connectivity and deformability of the spatial gel microstructure and covers micrometer length scales. The $C_{disruption}$ is determined by gel-water surface boundaries created by rupture events, which could be on sub(micron) or supra(micron) length scales.

1.1.5 Gel morphology

Within the gel structure different length scales are referred to nano, sub-micron, micron and macro structures. Depending on the length scales studied, different techniques to characterize these structures can be employed. Structures between 1-100 nm (nano scale) can be studied by small angle scattering techniques as small-angle neutron scattering (SANS) or small-angle x-ray scattering (SAXS). Sub-micron scale structures, which are in between 100 nm and 1 μm, can be visualized by electron microscopy, and structures above 1 μm (micron scale) by confocal laser scanning microscopy (CLSM). Macroscopic structures

could be seen by light microscopy or visually by the human eye. Gel coarseness in this work is defined as the microstructure inhomogeneity, and is derived from microscopic images. Since an image is made up of pixels, microstructure can be defined as an entity consisting of mutually related pixels and group of pixels [51]. A fine or homogeneous morphology is referred to an image in which two pixels next to each other have comparable intensity values. Microstructural details such as strand thickness and pore size, can be determined using public domain ImageJ software [52], after incorporating custom-made macro-instructions to obtain pair correlation functions [53].

1.1.6 Gel rheology

The study of protein network properties under deformation is essential to understand breakdown properties and thereby textural aspects. Gel network structure and interactions within network strands influence the rheological properties of gels [39, 54]. Large deformation rheology measurements are performed to obtain mechanical characteristics of the formed gels, where (fracture) stress reflects the hardness of the gel, (fracture) strain is an indication of cohesive properties, and small-strain moduli (shear stress/ shear strain) the stiffness of the network [39]. Fracture in protein gels possibly starts at a defect in the matrix or at a weak point created by a local inhomogeneity [55]. Additionally, the viscoelastic nature of gels adds complexity to their fracture mechanism(s) because viscosity is a time-dependent property. As a result, fracture stresses and strains are also dependent on the strain rate used in mechanical testing [39].

1.1.7 Gel water holding (centrifugation)

Within this thesis, we have chosen to measure water holding of protein-based gels by centrifugation, as described by Kocher and Foegeding [4]. A general schematic representation of the WH measurement set up is shown in **Figure 1.2**. To measure WH, a sample is placed in an Eppendorf tube and centrifuged over a range of time and forces. Removed water from the gel is collected at the bottom of the Eppendorf tube.

The WH is defined as the percentage of water in the gel remaining after centrifugation according to

$$WH = \frac{W_T - W_{RCF}}{W_T} \cdot 100 \quad (\%)$$
(1.2)

where W_T is the total initial amount of water in the sample and W_{RCF} denotes the amount of water removed from the sample at a given centrifugal force (RCF). Water removed from the sample is expected to be proportional to the applied RCF, which would hold to specific time of centrifugation. Data of WH versus RCF were fitted assuming a single exponential decay:

$$WH = A_{max} \cdot exp^{-k*RCF} + B$$
(1.3)

from which the fitting parameters A_{max} (the maximum percentage of water which can leave the system), B (percentage of water remaining in the gel, which represents WH) and k (the ease by which water leaves the system) are determined.
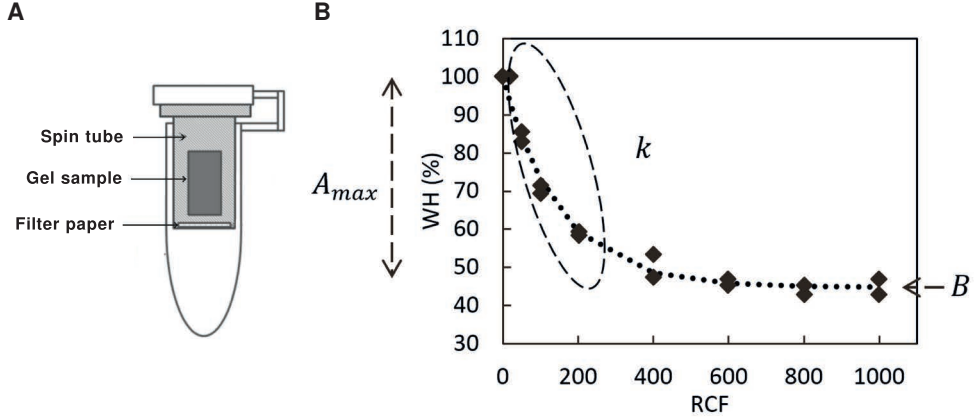
A   **B**

Figure 1.2 Schematic representation of WH method (panel A). Example of typical WH results (panel B).

1.1.7.1   Fracture events (centrifugation)

Once gel samples are exposed to centrifugation, e.g. to remove water, gels either fracture on microscopic or both on microscopic and macroscopic scales depending on the gel morphology and centrifugation speed used. A link between applied centrifugal forces and pressure, as applied for large deformation rheology measurements, is needed to better understand the effect of fracture events on gel WH. To evaluate the magnitude of pressures applied on the gel during centrifugation, relative centrifugal forces (RCF) can be converted to applied pressure (P) in Pascal (Pa) as follows:

$$P = \frac{(V_s \cdot \varnothing_{protein} \cdot \rho_{protein} + V_s \cdot \varnothing_{water} \cdot \rho_{water}) \cdot RCF \cdot g}{A} \qquad (1.4)$$

where V_S is volume of the sample (m³), Ø is the volume fraction of proteins or water in the sample, $\rho_{protein}$ = 1350 kg/m³ [56], g is gravitational acceleration (9.8 m/s²), and A is the area of the cylinder top surface (m²). As an example, 100 RCF is equivalent to 10 kPa applied on the gel for a 10% protein gel when centrifuged.

To evaluate the magnitude of applied pressure on the gel during centrifugation and to get an insight in the degree of gel deformation caused by centrifugation, large deformation data could be overlaid with RCF values recalculated to pressure kPa using equation 1.4 (**Figure 1.3**). In this manner it could be assumed that for a given gel sample shown in **Figure 1.3** up to 200 RCF no fracture events appear within gel network and above 1500 RCF the gel is fractured on a macroscopic scale.
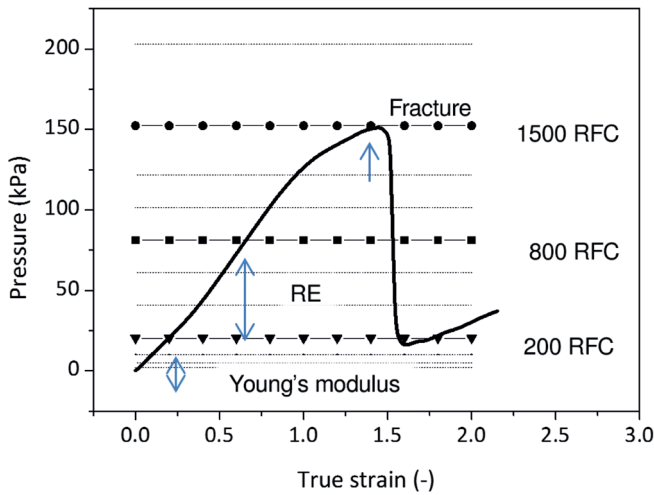
Figure 1.3 Gel large deformation data overlaid with RCF values recalculated to pressure kPa using equation 1.4.

1.1.8 Recoverable energy

The recoverable energy (RE), which is the measure of the energy that is stored within the network [57], serum release [58], and the critical stress intensity factor [59] are all relevant in foods and model systems, as they have an impact on the sensorial perception of food products. Energy distribution during crack initiation and spreading defines consumer perception of fracture of foods [60]. Once energy is applied on the food product, one part of the energy is stored and the other part dissipates. An energy balance model has been put forward by van Vliet et al. [61]. The authors dissect the dissipation into two contributions, i.e. friction and fracture. Choosing to refer to the total dissipation only we may write

$$W_{applied} = W_{stored} + W_{dissipated} \tag{1.5}$$

Where $W_{applied}$ denotes the applied work, W_{stored} the stored energy and $W_{dissipated}$ the dissipated energy. More recently de Jongh and colleagues dissected into six different contributions [62]:

$$W_{dissipated} = W_f + W_{db} + W_{mf} + W_{sf} + W_{pd} + W_{sr} \tag{1.6}$$

where they denote W_f as the energy used for the fracture events, W_{db} for de-bonding, W_{mf} as the friction between microstructural elements when a structure is deformed, W_{sf} as the viscous flow of the liquid entrapped in the network, W_{pd} as the plastic deformation of the material above the yielding-point, and W_{sr} as the energy lost via relaxation of elements within the network [63]. Munialo extensively studied both energy storage and dissipation in protein-based networks [64].

A measure for the stored energy (W_{stored}) is obtained from a uniaxial compression test using a texture analyzer. Typically samples are compressed to the 20-50% of their fracture strain at rates of 0.1-10 mm/s [62, 64, 65]. The ratio of energy to compress the sample and the energy released during decompression (times 100%) is referred to as recoverable energy (RE) [62]. Characteristics of this recoverable energy are extensively described in the thesis by Munialo [64].

1.1.9 Outline of the thesis

The aim of this thesis is to show how structural aspects at different length scales affect water holding under applied pressure in protein gels. A graphical representation of the thesis content is represented in **Figure 1.1**. **Chapter 1** gives an overview on the concept and the importance of gel WH property for textural properties and defines the challenges faced to understand which gel characteristics (at which length scale) are determinant for WH of protein gels.

In **Chapter 2**, water holding (WH) of soy protein gels was investigated to identify which length scales are most contributing to WH when a centrifugal force is applied. More specifically it was attempted to differentiate between the contributions of sub-micron and supra-micron length scale. $MgSO_4$ and $MgCl_2$ salt specificity on soy protein aggregation (sub-micron contribution) were used to create different gel morphologies (supra-micron contribution).

In **Chapter 3**, soy proteins were modified aiming to change protein clustering during network-assembly by means of modulation of calcium binding affinity to obtain gels with different morphologies at a constant ionic strength and constant protein concentration. Within this study it was aimed to differentiate between the gel microstructure and network stiffness contributions to WH of soy protein (SP) gels.

In **Chapter 4**, it was aimed to study the interplay of gel coarseness and gel stiffness on WH and water flow kinetics from the gel once force is applied onto the material. WH of ovalbumin heat-set gels obtained by varying ionic strength were measured both as a function of time and force applied. From experimental data (i) an effective gel permeability coefficient and (ii) an effective water flux coefficient were obtained and related to gel coarseness and stiffness.

In **Chapter 5**, it was aimed to show if relationship between gel stiffness and water holding for coarse and fine-stranded gels is different. A range of fine and coarse heat-set WPI gels were evaluated for their coarseness, stiffness and WH. It was shown that a cooperative effect between coarseness and stiffness proposes water removal mechanisms from the gel.

To address the effect of aggregate morphology on gel WH, in **Chapter 6** two types of water within aggregates were discriminated: (i) entrapped water and (ii) confined water. Entrapped water was defined as water associated to (pelleted) aggregates, which was not constrained in the exchangeability. Confined water in the aggregate was defined as hindered in its diffusion because of physical hindrance. It was shown that aggregates different in structure differ in entrapped water, but are comparable in confined water.

In the final chapter (**Chapter 7**), the findings of this thesis are integrated and discussed in a coherent view on the application of protein networks in food applications with a tailored mechanical response. A summary of the major findings discussed in thesis is also presented.

References

1. Puppo, M.C. and Añón, M.C., *Structural properties of heat-induced soy protein gels as affected by ionic strength and pH.* Journal of Agricultural and Food Chemistry, 1998. 46(9): p. 3583-3589.

2. Kao, F.J., Su, N.W., and Lee, M.H., *Effect of calcium sulfate concentration in soymilk on the microstructure of firm tofu and the protein constitutions in tofu whey.* Journal of Agricultural and Food Chemistry, 2003. 51(21): p. 6211-6216.

3. Maltais, A., et al., *Formation of soy protein isolate cold-set gels: protein and salt effects.* Journal of Food Science, 2005. 70(1): p. 67-73.

4. Kocher, P.N. and Foegeding, E.A., *Microcentrifuge-based method for measuring water-holding of protein gels.* Journal of Food Science, 1993. 58(5): p. 1040-1046.

5. Campbell, L.J., et al., *Effects of heat treatment and glucono-δ-lactone-induced acidification on characteristics of soy protein isolate.* Food Hydrocolloids, 2009. 23(2): p. 344-351.

6. He, J.S., et al., *Effects of sugars on the cross-linking formation and phase separation of high-pressure induced gel of whey protein from bovine milk.* Bioscience, Biotechnology and Biochemistry, 2006. 70(3): p. 615-625.

7. Hermansson, A-M. and Lucisano, M., *Gel characteristics—waterbinding properties of blood plasma gels and methodological aspects on the waterbinding of gel systems.* Journal of Food Science, 1982. 47(6): p. 1955-1959.

8. Chen, M.J. and Lin, C.W., *Factors affecting the water-holding capacity of fibrinogen/plasma protein gels optimized by response surface methodology.* Journal of Food Science, 2002. 67(7): p. 2579-2582.

9. Stevenson, C.D., Dykstra, M.J., and Lanier, T.C., *Capillary pressure as related to water holding in polyacrylamide and chicken protein gels.* Journal of Food Science, 2013. 78(2): p. 145-151.

10. Huang, Y., et al., *Effect of calcium concentration on textural properties of high and low acyl mixed gellan gels.* Carbohydrate Polymers, 2003. 54(4): p. 517-522.

11. Mao, R., Tang, J., and Swanson, B.G., *Water holding capacity and microstructure of gellan gels.* Carbohydrate Polymers, 2001. 46(4): p. 365-371.

12. Parés, D., et al., *Functional properties of heat induced gels from liquid and spray-dried porcine blood plasma as influenced by pH.* Journal of Food Science, 1998. 63(6): p. 958-961.

13. Molina, E., Defaye, A.B., and Ledward, D.A., *Soy protein pressure-induced gels.* Food Hydrocolloids, 2002. 16(6): p. 625-632.

14. Hu, H., et al., *Acid-induced gelation behavior of soybean protein isolate with high intensity ultrasonic pre-treatments.* Ultrasonics Sonochemistry, 2013. 20(1): p. 187-195.

15. Tang, C.-H., Chen, L., and Foegeding, E.A., *Mechanical and water-holding properties and microstructures of soy protein isolate emulsion gels induced by CaCl$_2$, glucono-δ-lactone (GDL), and transglutaminase: influence of thermal treatments before and/or after emulsification.* Journal of Agricultural and Food Chemistry, 2011. 59(8): p. 4071-4077.

16. Wu, W., et al., *Effects of oxidative modification on thermal aggregation and gel properties of soy protein by peroxyl radicals.* International Journal of Food Science & Technology, 2011. 46(9): p. 1891-1897.

17. Picone, C.S.F. and da Cunha, R.L., *Interactions between milk proteins and gellan gum in acidified gels.* Food Hydrocolloids, 2010. 24(5): p. 502-511.

18. Yang, M., Liu, F., and Tang, C.-H., *Properties and microstructure of transglutaminase-set soy protein-stabilized emulsion gels.* Food Research International, 2013. 52(1): p. 409-418.

19. Kuhn, K.R., Cavallieri, Â.L.F., and da Cunha, R.L., *Cold-set whey protein gels induced by calcium or sodium salt addition.* International Journal of Food Science & Technology, 2010. 45(2): p. 348-357.

20. Chantrapornchai, W. and McClements, D.J., *Influence of NaCl on optical properties, large-strain rheology and water holding capacity of heat-induced whey protein isolate gels.* Food Hydrocolloids, 2002. 16(5): p. 467-476.

21. Furukawa, T. and Ohta, S., *Mechanical and water-holding properties of heat-induced soy proteingels as related to their structural aspects.* Journal of Texture Studies, 1982. 13(1): p. 59-69.

22. Labuza, T.P. and Lewicki, P.P., *Measurement of gel water-binding capacity by capillary suction potential.* Journal of Food Science, 1978. 43(4): p. 1264-1269.

23. Puppo, M.C., Lupano, C.E., and Anon, M.C., *Gelation of soybean protein isolates in acidic conditions. Effect of pH and protein Concentration.* Journal of Agricultural and Food Chemistry, 1995. 43(9): p. 2356-2361.

24. Hermansson, A-M., *Gel characteristics—structure as related to texture and waterbinding of blood plasma gels.* Journal of Food Science, 1982. 47(6): p. 1965-1972.

25. He, J.-S., Azuma, N., and Yang, H., *Effects of pH and ionic strength on the rheology and microstructure of a pressure-induced whey protein gel.* International Dairy Journal, 2010. 20(2): p. 89-95.

26. Dill, K.A., *Theory for the folding and stability of globular proteins.* Biochemistry, 1985. 24(6): p. 1501-1509.

27. Renkema, J.M.S. and van Vliet, T., *Heat-induced gel formation by soy proteins at neutral pH.* Journal of Agricultural and Food Chemistry, 2002. 50(6): p. 1569-1573.

28. Staswick, P.E., Hermodson, M.A., and Nielsen, N.C., *Identification of the acidic and basic subunit complexes of glycinin.* Journal of Biological Chemistry, 1981. 256(16): p. 8752-8755.

29. Nielsen, N.C., *The Chemistry of Legume Storage Proteins.* Vol. 304. 1984. 287-296.

30. Renkema, J.M.S., Gruppen, H., and van Vliet, T., *Influence of pH and ionic itrength on heat-induced formation and rheological properties of soy protein gels in relation to denaturation and their protein compositions.* Journal of Agricultural and Food Chemistry, 2002. 50(21): p. 6064-6071.

31. Photchanachai, S., Mehta, A., and Kitabatake, N., *Heating of an ovalbumin solution at neutral pH and high temperature.* Bioscience, Biotechnology, and Biochemistry, 2002. 66(8): p. 1635-1640.

32. Stein, P.E., et al., *Crystal structure of uncleaved ovalbumin at 1·95 Å resolution.* Journal of Molecular Biology, 1991. 221(3): p. 941-959.

33. Kitabatake, N., Tahara, M., and Doi E., *Thermal denaturation of soybean protein at low water contents (Food & Nutrition).* Agricultural and biological chemistry, 1990. 54(9): p. 2205-2212.

34. Smithers, G.W., *Whey and whey proteins—from 'gutter-to-gold'.* International Dairy Journal, 2008. 18(7): p. 695-704.

35. Sakai, K., et al., *Conformation and stability of thiol-modified bovine blactoglobulin.* Protein Science, 2000. 9(9): p. 1719-1729.

36. Permyakov, E.A. and L.J. Berliner, *α-Lactalbumin: structure and function.* FEBS Letters, 2000. 473(3): p. 269-274.

37. Walstra, P., *Physical chemistry of foods.* Vol. 121. 2002: CRC Press.

38. Jovanović, S., Barać, M., and Maćej, O., *Whey proteins-properties and possibility of application.* Mljekarstvo, 2005. 55(3): p. 215-233.

39. Foegeding, E.A., Bowland, E.L., and Hardin, C.C., *Factors that determine the fracture properties and microstructure of globular protein gels.* Food Hydrocolloids, 1995. 9(4): p. 237-249.

40. Hermansson, A-M., *Structuring water by gelation food materials science*, Aguilera, J.M. and Lillford, P.J., Editors. 2008, Springer New York. p. 255-280.

41. Langton, M. and Hermansson, A-M., *Fine-stranded and particulate gels of β-lactoglobulin and whey protein at varying pH.* Food Hydrocolloids, 1992. 5(6): p. 523-539.

42. Clark, A. and Ross-Murphy, S., *Structural and mechanical properties of biopolymer gels*, in *Biopolymers*. 1987, Springer Berlin Heidelberg. p. 57-192.

43. Lefèvre, T. and Subirade, M., *Molecular differences in the formation and structure of fine-stranded and particulate β-lactoglobulin gels.* Biopolymers, 2000. 54(7): p. 578-586.

44. Ikeda, S. and Morris, V.J., *Fine-stranded and particulate aggregates of heat-denatured whey proteins visualized by atomic force microscopy.* Biomacromolecules, 2002. 3(2): p. 382-389.

45. Baussay, K., et al., *Influence of the ionic strength on the heat-induced aggregation of the globular protein β-lactoglobulin at pH 7.* International Journal of Biological Macromolecules, 2004. 34(1–2): p. 21-28.

46.   Stading, M. and Hermansson, A-M., *Large deformation properties of β-lactoglobulin gel structures.* Food Hydrocolloids, 1991. 5(4): p. 339-352.
47.   Ako, K., et al., *Micro-phase separation explains the abrupt structural change of denatured globular protein gels on varying the ionic strength or the pH.* Soft Matter, 2009. 5(20): p. 4033-4041.
48.   Baier, S.K. and McClements, D.J., *Influence of cosolvent systems on the gelation mechanism of globular protein: thermodynamic, kinetic, and structural aspects of globular protein gelation.* Comprehensive Reviews in Food Science and Food Safety, 2005. 4(3): p. 43-54.
49.   Hermansson, A-M., *Soy protein gelation.* 1986. 63(5): p. 658-666.
50.   Gu, X., Campbell, L.J., and Euston, S.R., *Influence of sugars on the characteristics of glucono-δ-lactone-induced soy protein isolate gels.* Food Hydrocolloids, 2009. 23(2): p. 314-326.
51.   Srinivasan, G. and Shobha, G., *Statistical texture analysis.* Proceedings of World Academy of Science, Engineering and Technology 2008. 36: p. 1264-1269.
52.   Rasband, W. *2009. ImageJ, U.S National Institutes of Health, Bethesda, Maryland, USA.* 1997; Available from: http://rsb.info.nih.gov/ij/.
53.   Ako, K., et al., *Quantitative analysis of confocal laser scanning microscopy images of heat-set globular protein gels.* Food Hydrocolloids, 2009. 23(4): p. 1111-1119.
54.   Li, H., Errington, A.D., and Foegeding, E.A., *Isostrength comparison of large-strain (fracture) rheological properties of egg white and whey protein gels.* Journal of Food Science, 1999. 64(5): p. 893-898.
55.   Stading, M., Langton, M., and Hermansson, A-M., *Microstructure and rheological behaviour of particulate β-lactoglobulin gels.* Food Hydrocolloids, 1993. 7(3): p. 195-212.
56.   Fischer, H., Polikarpov, I., and Craievich, A.F., *Average protein density is a molecular-weight-dependent function.* Protein science : a publication of the Protein Society, 2004. 13(10): p. 2825-2828.
57.   van den Berg, L., et al., *Breakdown properties and sensory perception of whey proteins/polysaccharide mixed gels as a function of microstructure.* Food Hydrocolloids, 2007. 21(5–6): p. 961-976.
58.   van den Berg, L., et al., *Serum release: The hidden quality in fracturing composites.* Food Hydrocolloids, 2007. 21(3): p. 420-432.
59.   Vincent, J., Saunders, D., and Beyts, P., *The use of critical stress intensity factor to quantify "hardness" and "crunchiness" objectively.* Journal of Texture Studies, 2002. 33(2): p. 149-159.
60.   van Vliet, T., *Rheology and Fracture Mechanics of Foods.* 2014: Boca Raton, FL [etc.], US: CRC [etc.]
61.   van Vliet, T., H. Luyten, and P. Walstra, *Fracture and yielding of gels.* Food polymers, gels and colloids, Dickinson, E., Editor. 1991.
62.   de Jong, S., van Vliet, T., and de Jongh, H.H.J., *The contribution of time-dependent stress relaxation in protein gels to the recoverable energy that is used as tool to describe food texture.* Submitted, 2015.
63.   de Jong, S., van Vliet, T., and de Jongh, H.J.H., *The contribution of time-dependent stress relaxation in protein gels to the recoverable energy that is used as tool to describe food texture.* Mechanics of Time-Dependent Materials, 2015. Submitted.
64.   Munialo, C.D., *Energy storage and dissipation in deformed protein-based networks on seconds time scale is controlled by submicron length scales*, 2015, Wageningen University: Wageningen.
65.   van den Berg, L., et al., *Energy storage controls crumbly perception in whey proteins/polysaccharide mixed gels.* Food Hydrocolloids, 2008. 22(7): p. 1404-1417.

1

Chapter 2

The origin of water loss from soy protein gels

Water holding (WH) of soy protein gels was investigated to identify which length scales are most contributing to WH when centrifugal forces are applied. More specifically it was attempted to differentiate between the contributions of sub-micron and supra-micron length scale. $MgSO_4$ and $MgCl_2$ salt specificity on soy protein aggregation (sub-micron contribution) were used to create different gel morphologies (supra-micron contribution). Obtained results showed that the micrometer length scale is the most important contribution to WH of gels under the applied deformation forces. WH of soy protein gels correlated negatively with Young's modulus and positively with recoverable energy. The occurrence of rupture events had only a limited impact on WH. The ease by which water may be removed from the gel, but not the total amount, seemed to be related to the initial building block size. These insights could be exploited in product development to predict and tune oral perception properties of (new) products.

Keywords: Young's modulus, gel stiffness, water holding, soy protein gels

2.1 Introduction

On a global scale, population growth will require further exploitation of alternative protein sources. A better understanding of protein functionality, and exchangeability of one source for another, in order to ensure a sufficient and efficient food supply on the global scale becomes more essential. Especially, a wider application of plant proteins is desired. This is exemplified by the fact that the use of soy proteins as structuring agent in food products has gained a lot of attention in the last decade. Soy proteins are known for their nutritional value and functionality to retain water and to improve water holding of products, but the detailed origin of this latter property is largely unknown.

The study of protein network (gel) formation and its macroscopic properties under deformation is essential to understand (oral) breakdown properties and thereby textural aspects. Externally applied energy on a protein gel is transformed into fracture, stored in the (continuous) network, or dissipates via other means, especially the friction developed during flow of serum during mechanical deformation [1]. Understanding the structural origins that determine these serum flow properties would provide industry guidelines to better control mechanical responses dictating oral perception of food products. However, such understanding is scarce.

Water holding (WH) is defined as the ability of a matrix of molecules (network) to entrap water in such a manner that exudation is prevented; however conditions defining exudation are not consistent. In literature, WH of a gel has been commonly related to microstructure (micrometer length scales) [2-4], to gel strength [5, 6] or protein-protein and protein-water interactions [7-9]. It is assumed that WH of a protein-based gel is affected by the gel morphology, but due to uncontrolled gel destruction during analysis, the relationship between WH and gel structure under applied deformation has been disputed. Consequently, WH and gel structure are not always linked [10], and in a number of studies WH measurement is just reported as an additional property to gel morphology to characterize a gel.

The WH of a gel has been measured by (i) centrifugation [10, 11] where a piece of gel is centrifuged at defined speed for a fixed time, (ii) by uniaxial sample compression to a fixed strain for a fixed time [12], or (iii) by capillary suction, when water removal is caused by water activity differences between a gel and filter paper in contact with that gel [13, 14]. Centrifugation is the most commonly used method but the methodology varies between different studies in sample size (0.1 - 5 g), pore size of the membrane (5 kDa - 5 μm), centrifugation speed (120 – 10.000 g), time (5 – 60 min) and temperature (4 - 25°C), as well as the definition of WH itself. In few studies low centrifugal forces (120 - 224 g) were used to limit structure destruction [2, 4, 11], though the majority of papers on WH show results of released or retained water when the gel is macroscopically destroyed [3, 5, 8].

In this paper water holding (WH) is assumed to be the effect of different contributions originating at different length scales. Four different contributions (C) retaining water in the gel are considered, over their according different length scales:

$$(\%) \; WH = C_{molecular \atop binding} + C_{sub-micron \atop structure} + C_{microstructure} + C_{disruption}$$

where the $C_{molecular \; binding}$ refers to the retained water that is molecularly bound to the globular protein (0.06-0.07 g of water/ g protein, where typically already 0.04 g water is required to hydrate peptide bonds) and is, in this research, assumed to be constant. The $C_{sub-micron \; structure}$ includes water held by building blocks dictated by protein-protein and protein-water interactions. The $C_{microstructure}$ refers to porosity, connectivity and deformability of the spatial gel microstructure and covers micrometer length scales. The $C_{disruption}$ is determined by gel-water surface boundaries creating the rupture events, which could be on sub(micron) or supra(micron) length scales.

The aim of this chapter is to show which length scales are most contributing to WH of soy protein-based gels when centrifugal compression is applied. In the presence of divalent salts and by varying their concentration during the gelation process, a variety of different gel structures can be obtained, for which morphology was analyzed by confocal scanning laser microscopy (CSLM) and large deformation rheological responses were determined in relation to the WH for different centrifugal forces.

2.2   Materials and Methods

2.2.1   Materials

Defatted soy flour was provided by Cargill BV (Amsterdam, The Netherlands). Anhydrous magnesium sulfate ($MgSO_4$) and magnesium chloride ($MgSO_4$) were obtained from Sigma-Aldrich (Steinheim, Germany). Reagents were of analytical grade and used without further purification.

2.2.2   Preparation of enriched soy protein solution

Defatted soy flour was suspended in reverse osmosis (RO) water at a ratio 1:10 (w/w) at 45°C and stirred for 30 min. Then the pH was adjusted to 8.0 with 5 M NaOH and stirred for an additional 30 min. The supernatant was collected by centrifugation (30 min, 6000 g, 13°C). Isolation of the globulins (glycinin and β-conglycinin) was achieved by isoelectric precipitation (pH 4.5, 6 M HCl). After mild stirring of the precipitate overnight at 4°C, suspension was centrifuged (30 min, 6000 g, 7°C). The pellet was resuspended 3 times at pH 4.5 in RO water at a ratio 1:3 (w/w) to remove impurities followed by centrifugation (30 min, 6000 g), and was finally suspended in RO water at a ratio 1:4 (w/w) at pH 7.0 using 5 M NaOH. This material was denoted as enriched soy protein solution (SP). Protein content

of SP was determined by Kjeldahl (calculated using N x 6.25) and was between 11 and 12% (w/w). The ratio of glycinin:β-conglycinin was estimated to be 50:50 by gel electrophoresis and reversed phase high-performance liquid chromatography (results are not shown). SP was stored at 4°C in solution in the presence of 0.02% (w/w) sodium azide and used within a month after preparation. The enthalpy change, indicative for the protein nativity, was 15.2 J/g protein measured by differential scanning calorimetry (DSC) (Q1000, TA Instrument, New Castle, DE).

2.2.3 Preparation of soy protein aggregates

Soy protein aggregates were prepared in 20 mM MOPS buffer pH 7.0 by mixing 0.1% (v/v) SP with 0.1-1.5 mM $MgSO_4$ or $MgCl_2$ salt at: (i) 25°C for 15 min, (ii) 25°C, 50°C and 70°C for 25 min, or (iii) 95°C for 30 min and cooled to 25°C. Prior to the experiments, all solutions were filtered with disposable syringe filters before mixing (Machery-Nagel Chromafil RC-20/25, pore size 0.2 µm).

2.2.4 Turbidity

Turbidity was measured with a Hewlett Packard 8435 diode array spectrophotometer with integrated heating element and magnetic stirrer at 600 nm. Cuvettes with a light path of 10 mm were used. Samples were stirred at 200 rpm during measurements. Two different measurements were performed: 1) change in turbidity as function of increased salt concentration after 15 min mixing protein with salt, and 2) twenty-five min measurements at a fixed protein and salt concentration, immediately after the addition of salt. Samples were measured at least in duplicate.

2.2.5 Aggregate size

The size of protein aggregates was determined using a Zetasizer Nano ZS (Malvern Instruments Ltd, Worcestershire, United Kingdom) by 173° angle backward scattering. Measurements were performed at 25 °C and repeated ten times per sample and data were analyzed using general purpose model.

2.2.6 Preparation of gels

SP was diluted to 10% (w/w) protein at pH 7.0 using Tris buffer to a final Tris concentration of 20 mM. The protein solution was mixed with different concentrations of $MgSO_4$ or $MgCl_2$. Gelation was performed in 20 ml syringes (20 mm in diameter), lubricated with paraffin oil, and closed airtight to reduce air bubble formation during heating at 95°C for 30 min in the water bath and subsequently cooled overnight at room temperature. Every sample was prepared in triplicate.

2.2.7 WH measurements

The centrifugation procedure was adapted from Kocher and Foegeding [11]. A micro-centrifuge filtration unit was composed of an inner spin tube and a 2 ml Eppendof tube (Axygen Biosciences, Inc., Union City, USA). Gels were cut in 10 mm height and 4.8 mm diameter cylinders using a cork borer and carefully placed on the bottom of the spin tube. The bottom of the spin tube was covered with a 5.5 mm diameter filter paper to reduce grid size. Centrifugation was performed at different maximal g-force ranging from 20 g to 1000 g for 10 min at 20°C. No changes in WH were seen above 1000 g. Exuded serum from the gel was collected at the bottom of the Eppendorf tube. Some samples exposed to high g-forces fractured in a number of pieces of which part co-eluted in the exuded serum. In that case a strip of filter paper was used to carefully remove serum from the bottom of the Eppendorf tube to eliminate the contribution of gel residue, and the removed weight was determined. The WH was calculated as the remaining water (%) in the gel after centrifugation (equation 2.1), where W_T is the total amount of water in the sample (g), and W_{RCF} is removed water from the sample at a given centrifugal force (RCF). Measurements were performed in duplicates.

$$WH = \frac{W_T - W_{RCF}}{W_T} \cdot 100 \quad (\%) \qquad (2.1)$$

Obtained WH (%) at various centrifugal forces were fitted using an exponential decay (equation 2.2) analogous to the exponential decay as a function of time at constant force as reported by Kocher and Foegeding [11]. A_{max} represents the maximum amount of water that can leave the system between applied 0 and 1000 g force, (equals 100-A_{max}) refers to the amount of water remaining in the gel, and k represents the coefficient reflecting how easy water leaves the system under applied force (in units of the gravitational acceleration, g).

$$WH = A_{max} \cdot e^{-k_{RCF}} + B \qquad (2.2)$$

Parameters A_{max} and k were obtained by least square minimization fitting of the experimental data on WH as a function of applied g force with Excel optimization tool Solver. Fitting the curves using two exponential decay did not give an improvement.

2.2.8 Confocal laser scanning microscopy (CLSM)

Samples for microstructural analysis were stained with 0.1% (w/w) fluorescent dye Rhodamine B to visualize proteins. Imaging of the samples was performed using a Leica TCS-SP5 confocal laser scanning microscope (Leica Microsystems (CMS) GmbH., Mannheim, Germany). Leica objective lenses HC PL APO 20x/0.70 IMM/CORR CS and HCX PL APO 63x/1.20 W CORR CS were used. The excitation wavelength and emission spectral regime of Rhodamine B was 561 nm and 570-725 nm, respectively.

2.2.9 Large deformation rheology

Gels were sliced with a gel slicer into cylinders of 20 mm in height and 20 mm in diameter. Fracture stress and fracture strain were measured by uniaxial compression with an AP-501 rheometer (Anton Paar, Graz, Austria) mounted with the 5 kg load cell. Paraffin oil was applied on top and bottom of the gel to prevent friction during compression. Gel samples were compressed to 90% of their initial height between two parallel plates at a constant deformation rate of 1 mm/s. Measurements were performed at 20°C in triplicate, and mean values of fracture stress and strain were calculated. The compressive stress and strain was recalculated to true Hencky's stress and strain. True Hencky's strain, ε_h, is defined as:

$$\varepsilon_h = \ln \frac{h(t)}{h_0} \quad (-)$$

(2.3)

where h_0 is the initial height of the gel sample and $h(t)$ the height after certain deformation time t. The true strain is negative for compression but is expressed as an absolute value. It was assumed that the volume of gel samples did not change during deformation and that the cylindrical shape was retained. Therefore, the contact surface area A of the gel sample at compression time t can be defined as:

$$A(t) = \frac{h_0}{h(t)} \cdot A_0 \quad (m^2)$$

(2.4)

where A_0 is the initial contact surface area of the gel sample. The true stress σ in the gel sample at time t is defined as:

$$\sigma(t) = \frac{F(t)}{A(t)} \quad (Pa)$$

(2.5)

in which $F(t)$ is the force per unit of area $A(t)$. Fracture of the gel is described as a peak or discontinuity of the stress over strain curve. Young's modulus, E, was calculated from the linear part of the stress over strain curve within region of 0.05-0.15 of fracture strain, and is defined as:

$$E = \left(\frac{d\sigma}{d\varepsilon_h} \right) \quad (Pa)$$

(2.6)

Recoverable energy was measured by compressing each gel to 50% of its fracture strain with a deformation speed of 1 mm/s. The measure that was used for the recoverable elastic energy (RE) was defined as the ratio of the released energy during decompression over the applied energy during compression. The areas below the stress over time curve (before and after the transition point between compression and decompression) were used to calculate the recoverable energy:

$$RE = \frac{\int_{t_{end}}^{t_{trans}} \sigma dt}{\int_{0}^{t_{trans}} \sigma dt} \times 100 \quad (\%)$$

(2.7)

We note that the measure we have defined for recoverable energy is a ratio and does not have a unit. We nonetheless refer to it as recoverable energy.

2.2.10 Fracture events (centrifugation)

Over a range of centrifugal forces used (10-1000 RCF), the gel either fractures on microscopic and/or macroscopic scales, depending on gel morphology and centrifugal speed used. To estimate which centrifugal force, F, leads to macro-fracture of a gel, applied centrifugal forces (RFC) were transformed to uniaxial compression pressure (Pa) as follows:

$$F = m * RCF * g \qquad (2.8)$$

where m is the mass of protein network (kg) (equation 2.9) and $g = 9.807$ m/s². Writing

$$m = \rho_{prot} * V \qquad (2.9)$$

with ρ_{prot} = 1350 kg/m³ [15], and V – volume of the cylinder shaped gel (m³). Calculated force (N) was converted to Pa (force/ area) using the definition:

$$P = F / A \qquad (2.10)$$

where A – area of the cylinder top surface (m²).

Obtained values were plotted on true stress over true strain curve to estimate in which region (linear, non-linear, fracture or above fracture) recalculated centrifugal force appears on the fracture curve. To make it more explicit, 200 RCF used in centrifugation would be similar to 7 kPa in under uniaxial deformation while compression of 10% (w/w) soy protein gels. Compression speed in both texture analyzer (TA) and centrifuge tube were comparable, but time under compression differed.

2.3 Results

The ability of a protein gel to retain or hold water has often been correlated to rheological properties, like gel strength and is suggested to be related to gel morphology. However, a concise study where it is attempted to link the macroscopic ability to retain water to properties at different length scales has not been reported. In this chapter, it was aimed to create a variety of soy protein gels, based on either different microstructural building blocks or different gel morphologies. These gels were then subjected to WH measurements, microscopic imaging and rheological characterization.

2.3.1 Variation in aggregate size

To investigate the contribution to WH of a gel determined by the aggregate level, $C_{sub\text{-}micron\ structure}$, we studied the effect of $MgSO_4$ or $MgCl_2$ salts on soy protein aggregation. By varying salt concentration different types of aggregates can be created, as measured by turbidity. Results of 0.1% SP (v/v) mixed with 0.1-1.5 mM $MgSO_4$ or $MgCl_2$ salts at

ambient temperature are shown in **Figure 2.1**. At a concentration higher than about 0.1 mM a proportional dependence of turbidity with increasing salt addition was observed, suggesting larger or higher number of aggregates. Both salts showed the same salt concentration-turbidity dependence, however $MgCl_2$ showed slightly higher turbidity above 0.7 mM concentration compared to $MgSO_4$.
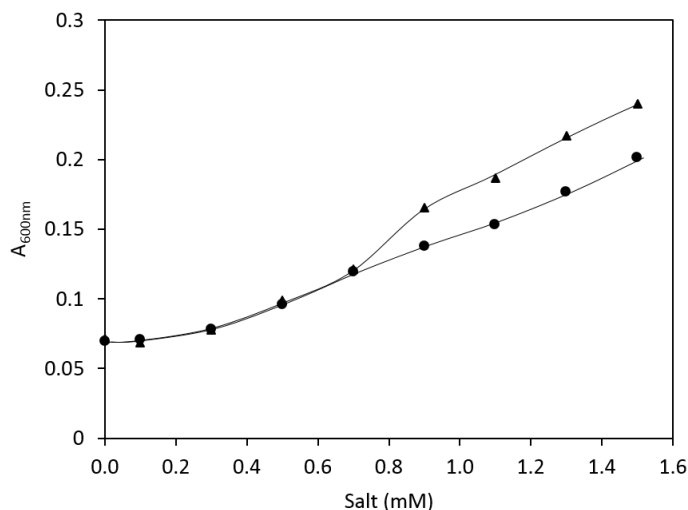

Figure 2.1 Turbidity measurement of 0.1% (v/v) SP mixed with 0.1-1.5 mM $MgSO_4$ or $MgCl_2$ (25°C, reaction time 15 min); (●) $MgSO_4$, (▲) $MgCl_2$. The solid lines are fits to guide the eye.

Heat-induced soy protein aggregation kinetics in presence of magnesium salts was monitored by changes in turbidity over time: firstly, to investigate the effect of the anion (SO_4^{2-} or Cl^-) on aggregate formation and secondly, to mimic the initial aggregation during heating and the gel formation. The protein to salt ratio was kept the same in both aggregation and gelation experiments. Results of 0.1% SP (v/v) mixed with 1.0 mM $MgSO_4$ or $MgCl_2$ at 25°C, 50°C and 70°C in time are shown in **Figure 2.2**. The major change in turbidity was completed within the first 5 min. At 50°C and 70°C, higher turbidity was measured indicating the formation of aggregates either larger or higher in number. Samples containing $MgCl_2$ salt showed a significant turbidity increase compared to those containing $MgSO_4$. With increasing temperatures the impact on turbidity of chloride over sulfate became more pronounced. The above-described effect of different salts on aggregate size was confirmed by Zetasizer measurements (**Figure 2.3**).
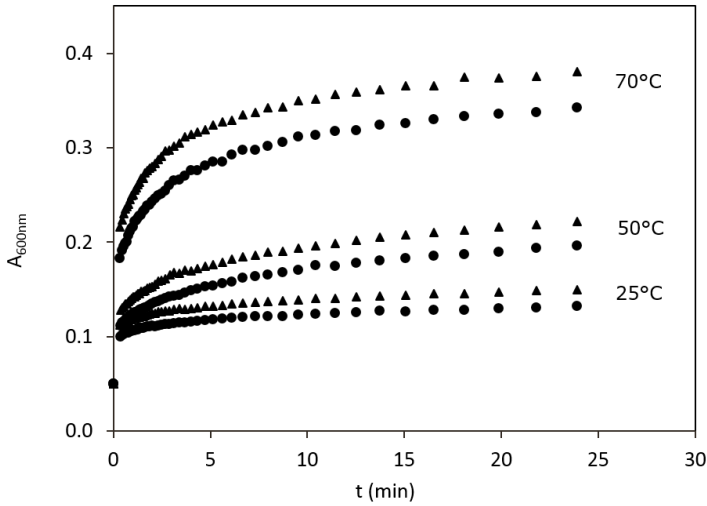
Figure 2.2 Turbidity measurements of 0.1% (v/v) SP with 1.0 mM salt in time at 25°C, 50°C and 70°C: (●) $MgSO_4$, (▲) $MgCl_2$.
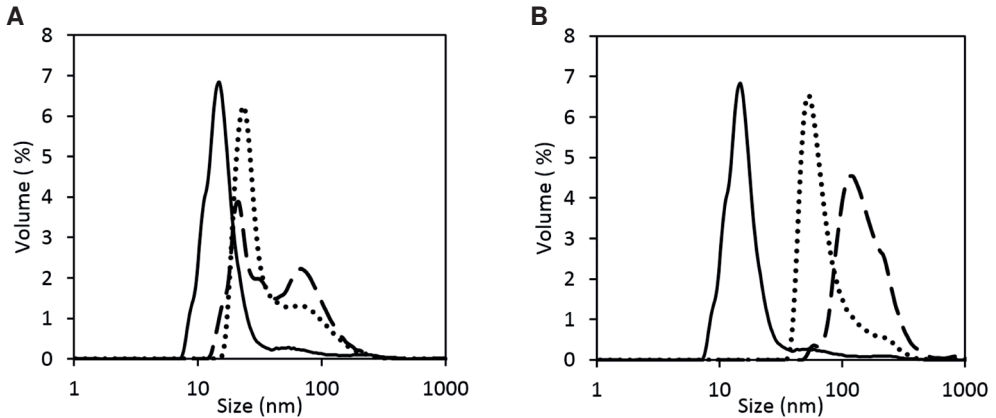

Figure 2.3 (A) Aggregate size of 0.1% (v/v) SP (solid line), 0.1% (v/v) SP with 0.5 mM $MgSO_4$ (dotted line) and 0.1% (v/v) SP with 0.5 mM $MgCl_2$ mixed for 30 min at 25°C (dashed line). (B) Aggregate size of 0.1% (v/v) SP (solid line), 0.1% (v/v) SP heated at 95°C for 30 min (dotted line) and 0.1% (v/v) SP with 0.5 mM $MgCl_2$ heated at 95°C for 30 min (dashed line). All measurements were performed at 25°C.

In **Figure 2.3A**, protein aggregate sizes in 0.1% SP (v/v) mixed with or without 0.5 mM $MgSO_4$ or $MgCl_2$ at 25°C (no heating) are shown. The addition of $MgSO_4$ increased the aggregate size from approximately 14 nm to 22 nm, while $MgCl_2$ resulted in a mixture of 20 - 65 nm aggregates. Effect of heating on soy protein aggregate size is shown in **Figure 2.3B.** Heating of 0.1% SP (v/v) in the absence of salt increased aggregate size from approximately 14 nm to 50 nm, while the addition of 0.5 mM $MgCl_2$ salt resulted in aggregate size of approximately 110 nm. From these results it can be concluded that heating of SP in

the presence of $MgSO_4$ and $MgCl_2$ results in typical different aggregates that will serve (at higher concentrations) as building blocks for network formation.

2.3.2 Soy protein gels: variation in morphology

To study the effect of the $C_{microstructure}$ contribution to WH of a 10% (w/w) SP gels, we aimed to create a range of different morphologies of self-supporting gels without observable syneresis. As discussed above, by varying the type of salt ($MgCl_2$ and $MgSO_4$) different building blocks were created, and by varying the salt concentration (5-100 mM) different gel morphologies were obtained. With increasing salt concentration the visual appearance of the gels changed. These varied from being translucent to white. Typically, $MgSO_4$ gels appeared smoother and more homogeneous compared to chloride gels. The 40-60 mM $MgCl_2$ gels showed syneresis and therefore these gels were discarded in this study.

Gel morphology was visualized with CLSM and imaged at 250 µm and 25 µm length scales (**Figure 2.4A**, **B**) (scale bars are indicated in the top left parts only). Heating in the presence of salts resulted in mixed or particulate soy protein networks with different microstructures in terms of pore size, strand thickness and homogeneity. As intended, a wide range of microstructures varying from fine stranded to very coarse were obtained by using either $MgSO_4$ or $MgCl_2$ salts.

2.3.3 Rheological gel characteristics

Large deformation rheology measurements were performed to obtain mechanical characteristics of the formed gels. Young's modulus, which reflects the stiffness of the material, was determined from the initial slope of the resulting stress by applying a strain deformation. **Figure 2.5A** shows that both $MgSO_4$ and $MgCl_2$ SP gels increased in Young's moduli with increasing salt concentration indicating the formation of firmer structures, reaching a maximum around 30-40 mM of salt and decreased again with further salt increment. The fracture stress (**Figure 2.5B**) followed the same pattern as the Young's moduli showing more brittle structures with increasing salt concentration and more elastic structures formed at high salt concentrations. All gels were comparable in fracture strain with the exception of 40-50 mM $MgSO_4$ gels with the higher fracture strain, and 30 and 80 mM $MgCl_2$ SP gels with the lower fracture strain (**Figure 2.5C**). Typically, SP gels in the presence of $MgCl_2$ had lower fracture stress and strain compared to those with a similar concentration $MgSO_4$.
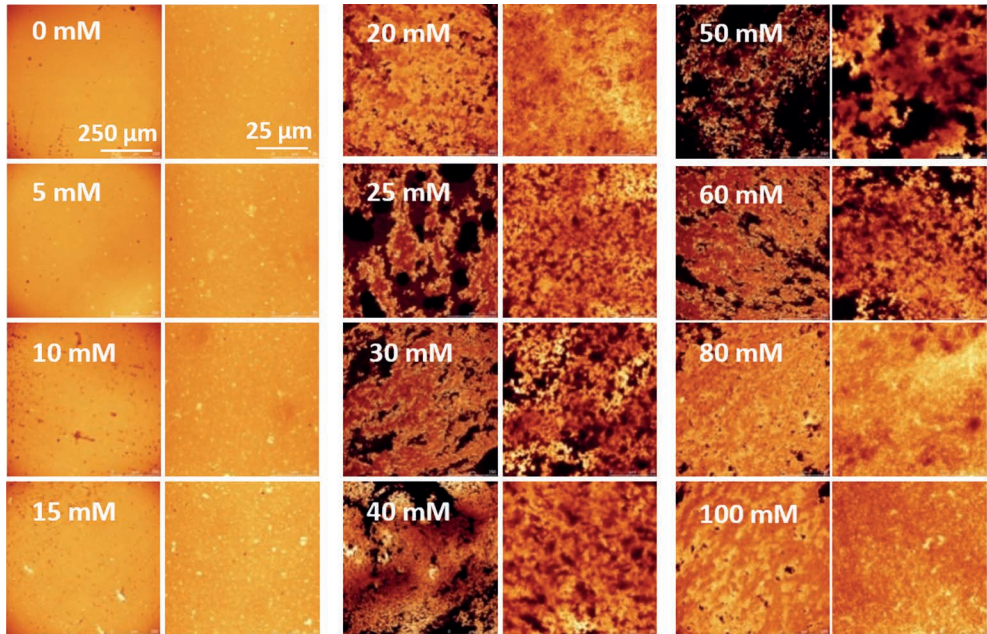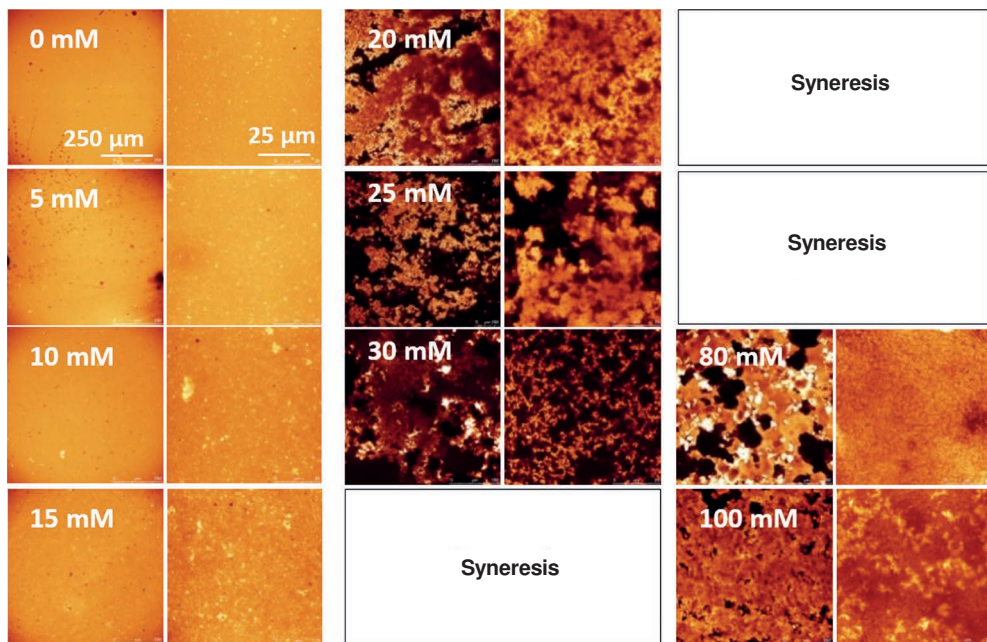
Figure 2.4 CLSM images of 10% (w/w) SP gels in the presence of 10-100 mM (A) MgSO$_4$ and (B) MgCl$_2$. Left image side stands for 250 µm scale, right side for 25 µm.
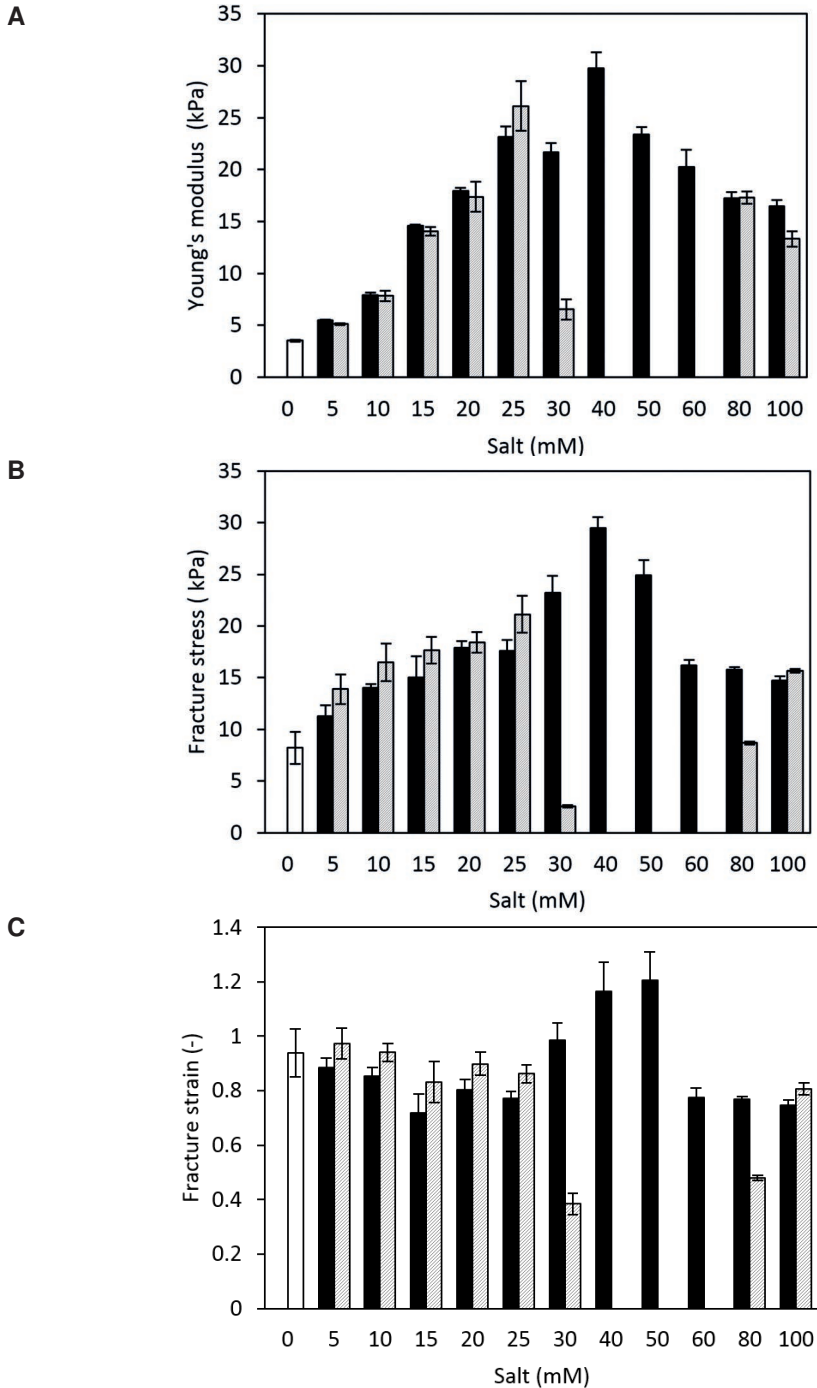
A

B

C

Figure 2.5 Large deformation rheology measurements of 10% (w/w) SP gels without salt (open bars), and mixed with 5-100 mM $MgSO_4$ (filled bars) or with 5-100 mM $MgCl_2$ (striped bars).

2.3.4 Recoverable energy

Recoverable energy represents the energy that is elastically stored during deformation. Recoverable energy was measured by compressing a gel to half of its fracture strain followed by decompression (equation 2.7). Recoverable energy results of $MgSO_4$ and $MgCl_2$ SP gels are shown in **Figure 2.6**. Recoverable energy decreased from approximately 70 to 40% with increasing salt concentration and increased with higher salt concentration (80-100 mM) up to 60%. Between 15 mM and 60 mM, $MgSO_4$ gels gave significantly higher RE values compared to $MgCl_2$ gels.
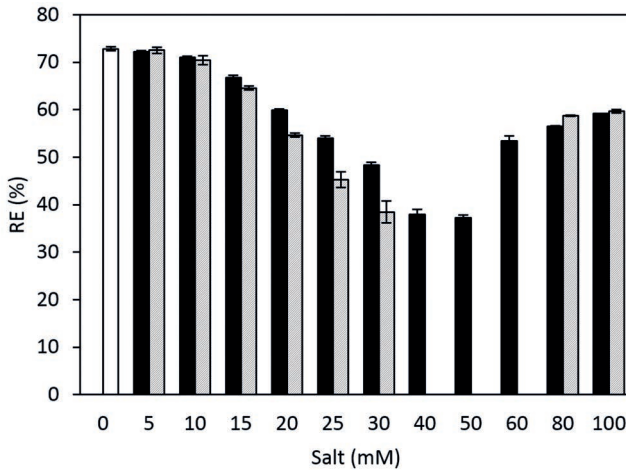

Figure 2.6 Recoverable energy of 10% (w/w) SP gels measured at half of fracture strain: without salt (open bar), and mixed with 5-100 mM $MgSO_4$ (filled bars) or with 5-100 mM $MgCl_2$ (striped bars).

2.3.5 WH measurements

To measure WH, SP gels were centrifuged from 20 to 1000 g for fixed time (10 min). The WH results of 10% (w/w) SP gels with 0-100 mM $MgSO_4$ and $MgCl_2$ salts are shown in **Figure 2.7**. Large differences in WH were observed by varying type of salt and its concentration. These data were further analyzed using equation 2.2 (dashed lines, **Figure 2.7**). The results of the obtained fitting parameters A_{max} and k are plotted in **Figure 2.8**. Up to 30 mM salt concentration both k and A_{max} increased, indicating easier water removal (k) from the gel under applied force, as well as increased amount or removable water (A_{max}) from the gel. The 30-60 mM $MgSO_4$ gels were comparable in k and A_{max}. At higher salt concentrations, k slightly decreased as well as the amount of removable water (A_{max}).
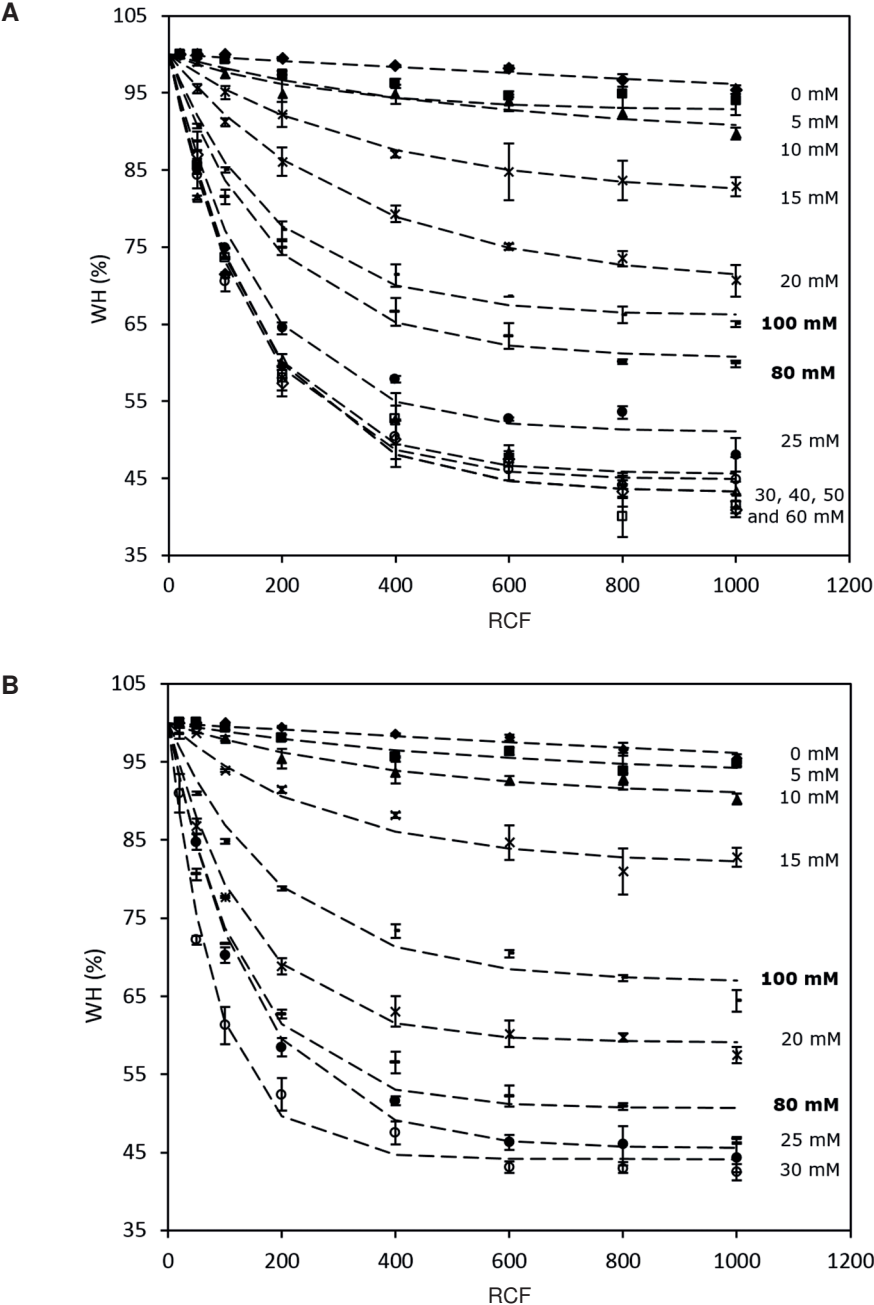
A

B

Figure 2.7 WH of 10% (w/w) SP gels with 5-100 mM (A) $MgSO_4$ gels and (B) $MgCl_2$ gels. The dashed lines represent the fits following the analysis as described in the text.
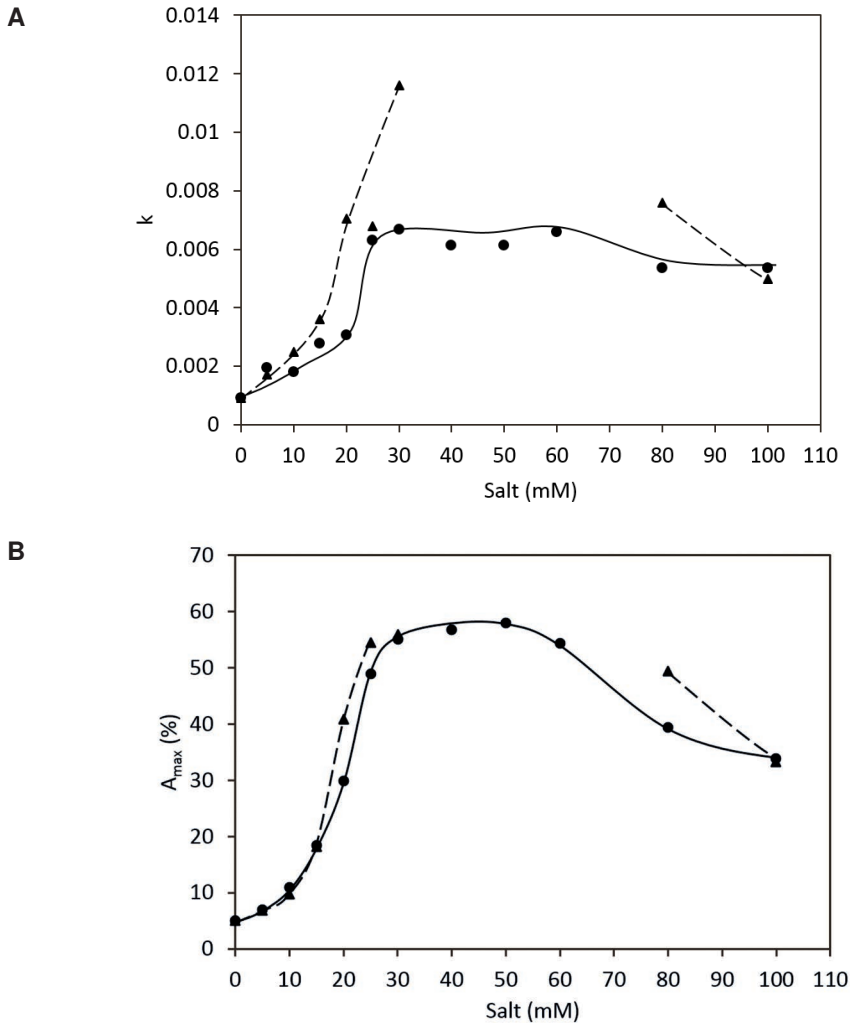
A

B

Figure 2.8 Fitting parameters as a function of salt concentration: (A) k parameter and (B) A_{max} parameter, where (●) $MgSO_4$, (▲) $MgCl_2$. The lines are fits to guide the eye.

2.4 Discussion

In this chapter it was aimed to show which length scales are most contributing to WH of soy protein gels when centrifugal compression is applied. More specifically, it was attempted to differentiate between the contributions of sub-micron (aggregate level) and supra-micron length scales (morphology) to WH by varying salt concentration, and by employing the salt specificity ($MgSO_4$ and $MgCl_2$) on protein aggregation. Moreover, by applying different g-forces the influence of macroscopic gel disruption on WH could be assessed.

2.4.1 Gel microstructure and WH

CSLM and scanning electron microscopy (SEM) imaging has been used to visualize gel microstructure on a (sub-)micron scale and observed differences in coarseness have been linked to WH results [4, 16-18] or used to estimated capillary pressure [12, 14]. Fine stranded gels are homogeneous through different length scales, whereas coarse gels can be homogeneous on a (sub-)micron scale but may be heterogeneous on sub-mm level. It was shown that addition up to 15 mM magnesium salt yielded gels with comparable microstructures on sub-micron to sub-mm length scales (**Figure 2.4**), but displayed different WH properties (**Figure 2.7**). Alternatively, e.g. 30-60 mM $MgSO_4$ gels were different in microstructure, but had a comparable WH. This illustrates that WH cannot be simply explained by a single length scale evaluation of gel microstructure. To ensure that the differences in coarseness provide a differentiation in porosity and pore dimensions, leading to differences in capillary pressures especially when salts are present as well, a more detailed study on WH was performed using capillary suction. This has been reported in the supplemental material of this chapter. The outcome of that study is that capillary pressures in the different gels do not relate to the observed water holding capacities described for the various SP gels under the type of centrifugal deformation we applied.

2.4.2 Gel stiffness or fracture properties and WH

A correlation plot of WH (**Figure 2.7**) against the Young's moduli (**Figures 2.5A)** of the various SP gels is shown in **Figure 2.9**. A clear negative relation can be observed. The stiffer the gel, the more energy is needed to deform the network for a given deformation. The correlation shown in **Figure 2.9** illustrate that such higher stiffness coincides with the inability of a gel network to hold water well. Correlation plots between WH and the fracture stress (**Figure 2.5B**) or fracture strain (**Figure 2.5C**) did not show any correlation (not shown), illustrating that the ability of a protein network to retain water in its structure under applied force does not show a relation to the inability of the network to withstand stress build-up leading to fracture events. Also Hermansson and Lucisano suggested that WH and rheological properties of blood plasma gels are not related [10]. Yet few other studies on blood plasma gels indicated that stronger gels can lose more water than weaker ones [10, 19] in contrast to another study by Hu et al. on SP gels [20]. Alternatively, Pares and colleagues reported on gels with different strengths but comparable in WH [17]. Yang et al. found a positive correlation of elastic modulus G' and WH of SP emulsion filled gels [21].
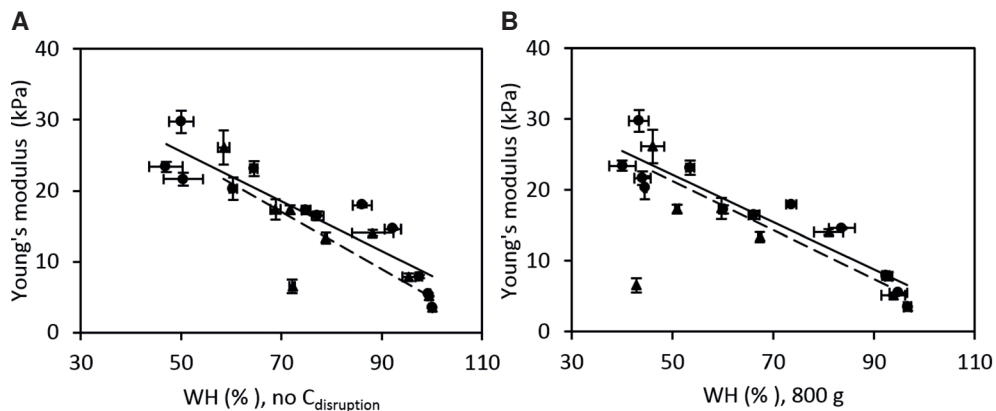
Figure 2.9 Correlation plots of WH as a function of Young's moduli, where (●) MgSO$_4$ and (▲) MgCl$_2$. (A) WH when $C_{disruption}$ is eliminated, (B) WH when fracture events are present. Horizontal error bars stand for WH, vertical for Young's moduli. Linear fitting was done to guide the eye, where solid line stands for MgSO$_4$ and dashed line for MgCl$_2$.

2.4.3 RE and WH

Once energy is applied to the system, the energy can be stored in the system or dissipated by fracture, friction or serum flow. RE can be regarded as the difference between applied and dissipated energy. When limited deformation is applied while determining the RE, macroscopic fracture events can be neglected and a loss of RE might reflect predominantly the energy required to displace serum within the gel. **Figure 2.10** shows RE (**Figure 2.6**) as a function of the WH (**Figure 2.7**) for the various SP gels. A clear positive correlation can be observed, showing an extrapolated intercept close to zero. This latter would imply that when a protein gel would not be able to retain any water during mechanical deformation, it would also not be capable to store energy in the gel that can be regained after decompression. A comparable finding was obtained by Chantrapornchai and McClements for WPI gels [12]. The slope of the correlation shown in **Figure 2.10** could be a measure for the efficiency by which a deformed protein network transduces its energy to viscous flow of the serum phase and thereby dissipates the applied energy.

2.4.4 Influence of gel disruption on WH

A positive correlation of fracture strain to WH was reported in gellan gels [22, 23], but thus far no information is available of fracture properties in relation to WH for protein-based gels. As already stipulated above, no correlations were found between gel fracture stress or fracture strain and WH of that gel (results are not shown). Comparing the correlation plots shown in **Figure 2.9** and **2.10** at relative low applied g force (panels A) where the exerted stress in the systems is much lower than the recorded fracture stress (see method section for the pressure-to-stress conversion), with those at high g-force (panels B), may provide insight in the contribution of gel disruption on the WH of these gels. When looking

at the RE, the correlation with WH at higher applied g-force (**Figure 2.10B**) illustrates a general shift to lower WH and an offset in RE at zero WH. It can thus be suggested that the generation of microcracks introduces a small reduction in WH of a few percentage. Rupture of the protein network has thus a limited effect on WH and the fragmented pieces (either at macro- of micro-length scale) of the network still behave predominantly as an ensemble of intact smaller gel pieces.

Alternatively, when the stiffness of the gel under non rupturing conditions is correlated to WH as determined at high g-force (**Figure 2.9B**) a similar dependence is found as compared to low applied g-force (**Figure 2.9A**). This supports the idea that upon rupturing of the gel the individual fragmented pieces behave as smaller intact gel pieces where the stiffness sets the WH ability of the gel pieces.
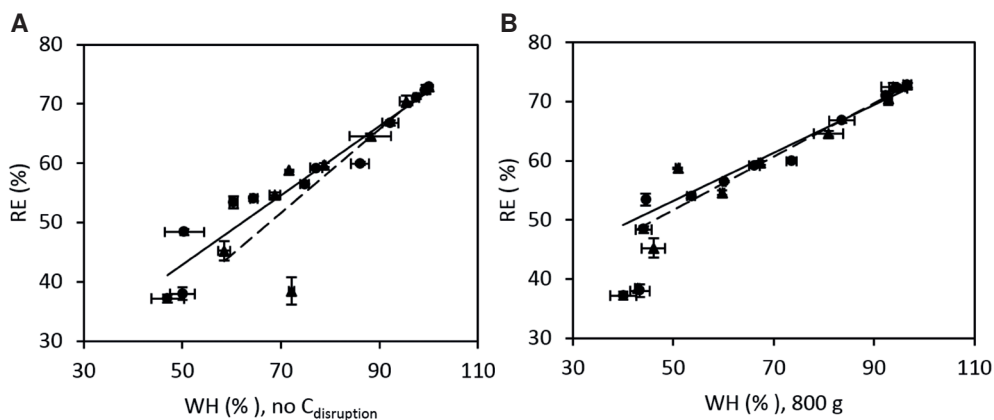

Figure 2.10 Correlation plots of WH as a function RE, where (●) MgSO$_4$ and (▲) MgCl$_2$. (A) WH results when $C_{disruption}$ is eliminated, (B) WH results when fracture events are present. Horizontal error bars stand for WH, vertical for RE. Linear fitting was done to guide the eye, where solid line stands for MgSO$_4$ and dashed line for MgCl$_2$.

2.4.5 Discrimination of sub- and supra-micron contributions to WH

In this chapter it was aimed to show which length scale was most important for WH of SP gels under compression and defined WH consisting of four different contributions covering from molecular to macro length scales. To this end different gel morphologies (supra-micron) were created based on different protein aggregates (sub-micron). The correlation graphs shown in **Figure 2.9** and **2.10** show the datasets of both MgSO$_4$ (dashed lines) and MgCl$_2$ (solid lines) containing gels, where the first ones were based on smaller aggregates (**Figure 2.1-2.3**). It can be concluded that, when considering the Young's modulus (**Figure 2.9**) the aggregate level has no significant impact. But also for the RE (**Figure 2.10**) it cannot be concluded that there is an obvious effect when the outlier around a WH of around 72% (panel A) for MgCl$_2$ is discarded.

It is then interesting to evaluate whether there might be a sub-micron differentiation when the kinetics is considered, as described in **Figure 2.8** from fitting of the g-force curves. This is shown in **Figure 2.11** for both the Young's modulus (panel A) and the RE (panel B) as a function of the k and A_{max} parameters. It can be observed that the $MgCl_2$ gels show a significant less steep dependence compared to the $MgSO_4$ gels when the ease by which water is removed from the gel (k) is considered. The physical implication of this finding is still unclear. On the other hand the maximum quantity of water that can be removed (A_{max}) does not show a clear discrimination between the two different types of aggregates.
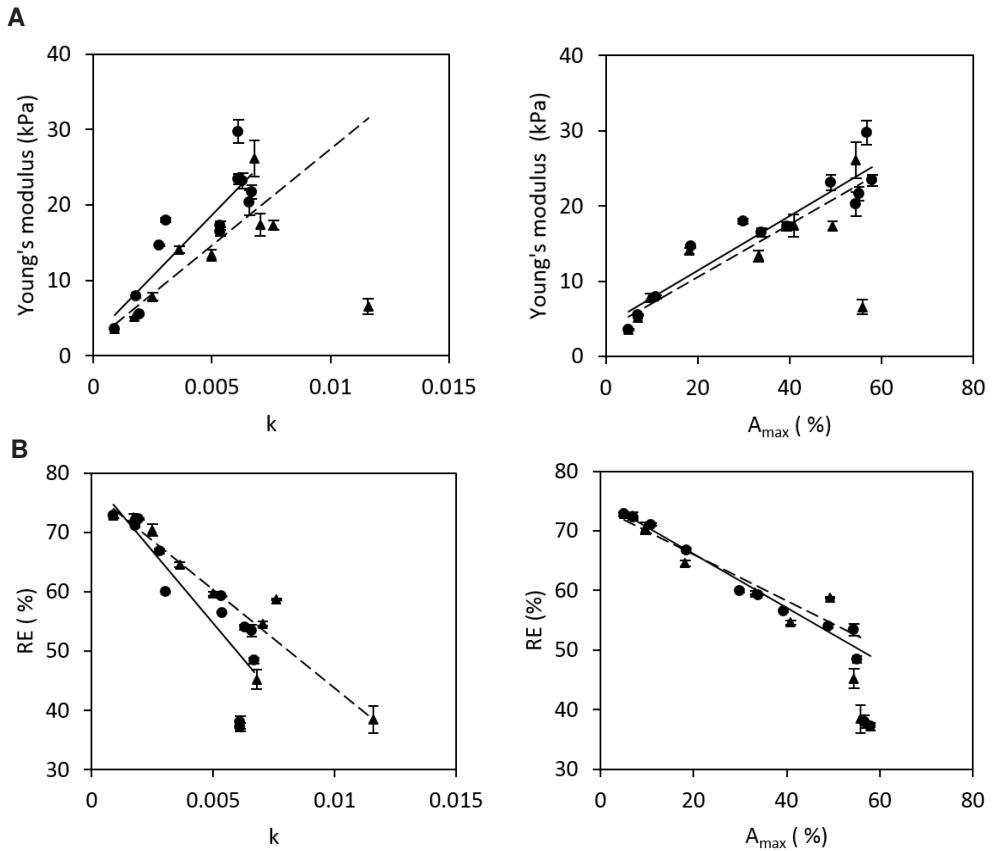
A

B

Figure 2.11 Correlation plots of fitting parameters k and A_{max} against (A) Young's moduli and (B) RE, where (●) $MgSO_4$, (▲) $MgCl_2$. Vertical error bars stand for moduli and RE. Linear fitting was done to guide the eye, where solid line stands for $MgSO_4$ and dashed line for $MgCl_2$.

Summarizing, this work shows that straight forward microstructural analysis (CSLM or SEM) does not predict the WH of SP gels. The stiffness of the gels does show a negative correlation with WH, which in turn might set the propensity of the gel to reversibly store energy in the system during mechanical deformation. Fracturing characteristics, like

fracture stress and strain, have no correlation with the ability of the gel to hold water, while the occurrence of rupture events, either as micro or macroscopic cracks, has only a limited impact on WH, as the WH of the retained gel fragments is still dominated by the inherent stiffness of these pieces. Comparison of gels derived from differently sized soy protein aggregates did not provide an indication that length scales at the sub-micron level are a determinant factor for WH of soy protein gels, and that this latter property is predominantly set by larger length scales. The ease by which water may be removed from the gel (not the total amount) seems to be related to the initial building block size, which could be speculated to be related to the fine-structure on the microstructure elements that set-up the network. Different aggregate characteristics might of course directly influence the gel morphology (coarseness of the network) that can be derived and thereby set the WH capacity of the gels.

2.5   Acknowledgement

References

1. Van Vliet, T. and P. Walstra, *Large deformation and fracture behaviour of gels.* Faraday Discussions, 1995. 101: p. 359-370.

2. Kao, F.-J., N.-W. Su, and M.-H. Lee, *Effect of calcium sulfate concentration in soymilk on the microstructure of firm tofu and the protein constitutions in tofu whey.* Journal of Agricultural and Food Chemistry, 2003. 51(21): p. 6211-6216.

3. Maltais, A., et al., *Formation of soy protein isolate cold-set gels: protein and salt effects.* Journal of Food Science, 2005. 70(1): p. 67-73.

4. Puppo, M.C. and Añón, M.C, *Structural properties of heat-induced soy protein gels as affected by ionic strength and pH.* Journal of Agricultural and Food Chemistry, 1998. 46(9): p. 3583-3589.

5. Campbell, L.J., et al., *Effects of heat treatment and glucono-δ-lactone-induced acidification on characteristics of soy protein isolate.* Food Hydrocolloids, 2009. 23(2): p. 344-351.

6. Furukawa, T. and Ohta, S., *Mechanical and water-holding properties of heat-induced soy protein gels as related to their structural aspects.* Journal of Texture Studies, 1982. 13(1): p. 59-69.

7. Gu, X., L.J. Campbell, and Euston, S.R., *Influence of sugars on the characteristics of glucono-δ-lactone-induced soy protein isolate gels.* Food Hydrocolloids, 2009. 23(2): p. 314-326.

8. Molina, E., A.B. Defaye, and D.A. Ledward, *Soy protein pressure-induced gels.* Food Hydrocolloids, 2002. 16(6): p. 625-632.

9. Wu, W., et al., *Effects of oxidative modification on thermal aggregation and gel properties of soy protein by peroxyl radicals.* International Journal of Food Science & Technology, 2011. 46(9): p. 1891-1897.

10. Hermansson, A-M. and Lucisano, M., *Gel characteristics—water binding properties of blood plasma gels and methodological aspects on the waterbinding of gel systems.* Journal of Food Science, 1982. 47(6): p. 1955-1959.

11. Kocher, P.N. and Foegeding, E.A., *Microcentrifuge-based method for measuring water-holding of protein gels.* Journal of Food Science, 1993. 58(5): p. 1040-1046.

12. Chantrapornchai, W. and McClements, D.J., *Influence of NaCl on optical properties, large-strain rheology and water holding capacity of heat-induced whey protein isolate gels.* Food Hydrocolloids, 2002. 16(5): p. 467-476.

13. Labuza, T.P. and Lewicki, P.P., *Measurement of gel water-binding capacity by capillary suction potential.* Journal of Food Science, 1978. 43(4): p. 1264-1269.

14. Stevenson, C.D., M.J. Dykstra, and Lanier, T.C., *Capillary pressure as related to water holding in polyacrylamide and chicken protein gels.* Journal of Food Science, 2013. 78(2): p. 145-151.

15. Fischer, H., I. Polikarpov, and Craievich, A.F., *Average protein density is a molecular-weight-dependent function.* Protein science : a publication of the Protein Society, 2004. 13(10): p. 2825-2828.

16. Picone, C.S.F. and da Cunha, R.L., *Interactions between milk proteins and gellan gum in acidified gels.* Food Hydrocolloids, 2010. 24(5): p. 502-511.

17. Parés, D., et al., *Functional properties of heat induced gels from liquid and spray-dried porcine blood plasma as influenced by pH.* Journal of Food Science, 1998. 63(6): p. 958-961.

18. He, J.-S., N. Azuma, and Yang, H., *Effects of pH and ionic strength on the rheology and microstructure of a pressure-induced whey protein gel.* International Dairy Journal, 2010. 20(2): p. 89-95.

19. Hermansson, A-M., *Gel characteristics—structure as related to texture and waterbinding of blood plasma gels.* Journal of Food Science, 1982. 47(6): p. 1965-1972.

20. Hu, H., et al., *Acid-induced gelation behavior of soybean protein isolate with high intensity ultrasonic pre-treatments.* Ultrasonics Sonochemistry, 2013. 20(1): p. 187-195.

21. Yang, M., F. Liu, and Tang, C-H., *Properties and microstructure of transglutaminase-set soy protein-stabilized emulsion gels.* Food Research International, 2013. 52(1): p. 409-418.

2

22.   Mao, R., J. Tang, and Swanson, B.G., *Water holding capacity and microstructure of gellan gels.* Carbohydrate Polymers, 2001. 46(4): p. 365-371.

23.   Huang, Y., et al., *Effect of calcium concentration on textural properties of high and low acyl mixed gellan gels.* Carbohydrate Polymers, 2003. 54(4): p. 517-522.

2

Supplementary material

Introduction

To investigate whether capillary suction measurements would give deeper insight in water holding (WH) of protein based gels, as alternative to the centrifugal measurements described in the main chapter, studies were performed using equilibration of the gel in contact to filter paper. The capillary pressure difference of a spherical cavity in comparison to its surrounding is given by the Young-Laplace equation: $\Delta P = 2\gamma/R$, where γ is the interfacial tension between the cavity and its surrounding, and R is the radius of the cavity. Accordingly, water should be more tightly held in gels with smaller pore size, more hydrophilic network surface (small contact angle), and higher solvent surface tension [1]. This chapter describes a number of gel morphologies based on soy protein, formed in the presence of 0-100 mM magnesium salts. From the results it was concluded that gel microstructure (gel coarseness) was not the unique determinant to WH. This supplementary material treats the capillary effect on WH in these results.

Materials and Methods

The capillary suction method was adapted from Labuza and Lewicki [2]. A custom designed plate containing twelve 22.5 mm in diameter and 4.5 mm in height cylinder wells was made. Gels were cut in 2 mm height and 14 mm diameter cylinders using a cork borer and carefully placed in the middle of each well and covered with 7 layers of filter paper 20 mm in diameter (Whatman grade nr.1). Dimensionality of the porosity was determined by image analysis of the filter paper and varied from 70 μm to 20 nm (**Figure 2.12**). The ratio of total water present in the sample and maximum amount of water that could be absorbed by the filter paper (1 : 2.5) was determined by dipping filter papers in demi water and weighing the maximum amount of water adsorbed. Using a lower or higher ratio permits faster or slower equilibration, but does not affect the equilibration amount. A filled plate was covered with silicone rubber, an aluminum plate and a 2 kg weight load was placed on top to reduce pressure build-up in the well while assembling the stack and to prevent evaporation of water during equilibration. After storage for 24 h at 4°C, the filter papers were carefully removed and weighted. Absorbed water by capillary suction was recalculated to remaining water in the gel named WH_{CS} (%) (eq. 2.11), where W_T is total amount of water in the sample (g), and W_r is removed water from the sample. Measurements were performed in triplicates.

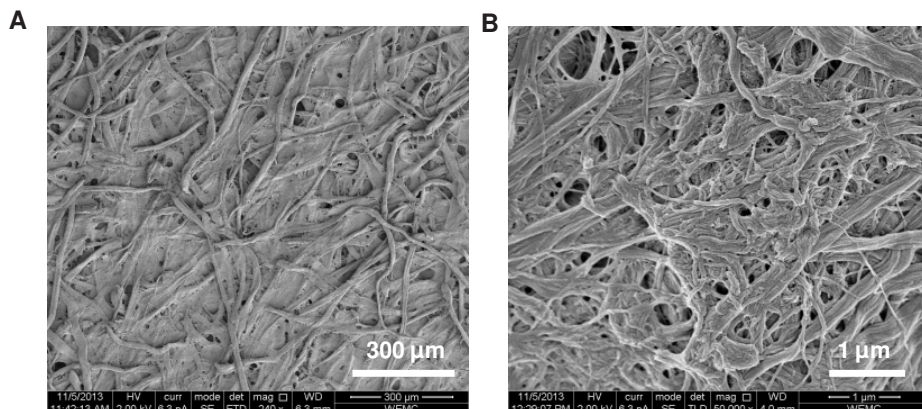$$WH_{CS} = \frac{W_T - W_r}{W_T} \cdot 100 \quad (\%) \tag{2.11}$$

Figure 2.12 SEM images of filter paper (A) 300 μm and (B) 1 μm length scale.

Results

In **Figure 2.13** a positive linear correlation of WH and RE, shown in the main chapter (**Figure 2.10A**), is presented in a 3D graph to illustrate if the salt concentration affects WH and RE. Careful analysis of the ion concentration on the gel structure formation and WH (**Figure 2.13**) does not provide an indication that WH is proportional to ionic strength. Though, it could be argued that the osmotic pressure in the gels is different by employing different salts and concentrations. To evaluate whether the determination of WH by capillary forces would show such an ionic strength dependence, studies were performed using equilibration of the gel in contact to a filter paper as described in the method section.
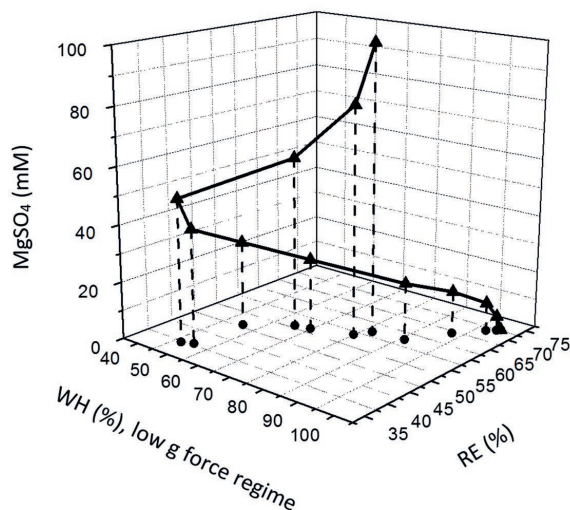

Figure 2.13 Salt concentration dependency on WH-RE relation of 10% (w/w) SP gels prepared in the presence of 0-100 mM $MgSO_4$.

A steady state capillary suction method was used to investigate WH of a gel. Results of WH_{CS} are shown in **Figure 2.14**. It can be observed that neither salt concentration (ionic strength), nor the anion type influence the WH as measured by static capillary suction. No obvious pattern of increasing osmotic pressure with increasing ionic strength on WH was observed. WH varied between gels (45 - 60%), but did not depend on salt concentration.
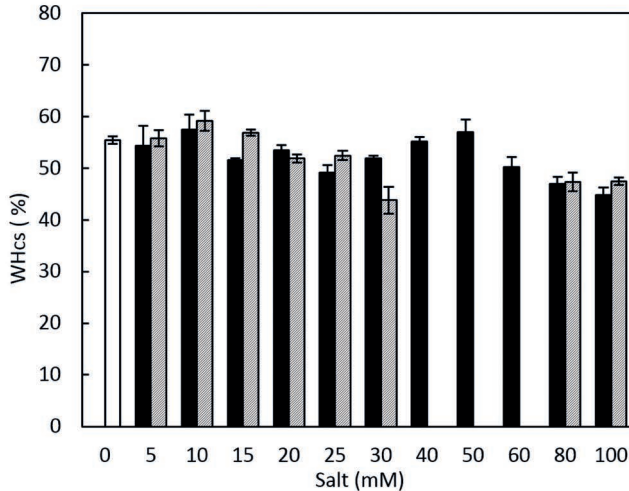

Figure 2.14 WH measurements by static capillary suction method of 10% (w/w) SP gels without salt (open bars), and mixed with 5-100 mM MgSO$_4$ (filled bars) or with 5-100 mM MgCl$_2$ (striped bars).

As discussed in the main chapter, WH measured by centrifugal forces shows a clear correlation with Young's modulus and RE. Exudation of water from a gel changes its spatial structure (density) and thereby its osmotic potential [2]. Consequently both morphology (stiffness and elasticity) and ionic strength of the gel were expected to have an effect on WH. In **Figure 2.15A** and **B** correlation plots of WH_{CS} and Young's modulus, and WH_{CS} - RE are shown for all soy protein gels studied in the main paper. No obvious correlations were found between these properties. The obtained results suggest that neither gel morphology nor ionic strength have an effect on WH measured by capillary suction. From this study can be concluded that not the ionic strength or osmotic pressure, but apparent gel morphology sets the WH measured by centrifugal forces.

The capillary suction pressure has an order of magnitude of $0.1/R$ ~10^5 Pa (when using a surface tension ~0.1 N/m and R ~10^{-6} m). The centrifugal pressure equals $h \cdot \Delta\rho \cdot g_c$, where h is the height of the sample, $\Delta\rho$ the density difference between aqueous phase and protein, and g_c the centrifugal force. With the sample height of 0.2 cm that was used, and approximating $\Delta\rho$=100 kg/m^3, the centrifugal pressure has an order of magnitude of $200 \cdot g_c$.
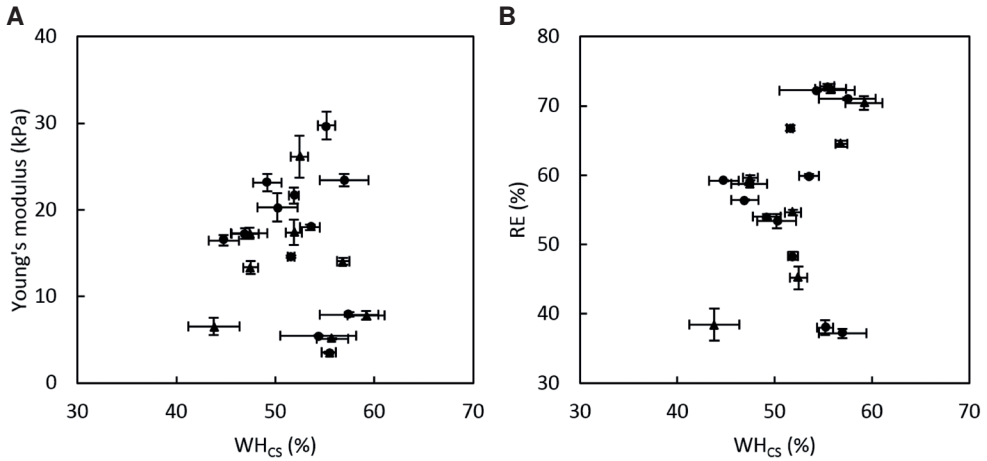
Figure 2.15 WH_{CS} as a function of (A) Young's moduli and (B) RE, with (●) $MgSO_4$ and (▲) $MgCl_2$. Horizontal error bars stand for WH, vertical for Young's moduli and RE.

The capillary pressure becomes negligible when $0.1/R < 200 \cdot g_c$ or when $R > 5 \cdot 10^{-4}/g_c$. Taking g_c in units of g (gravitational acceleration), and R in microns, we find that the capillary pressure is negligible when $R/\text{micron} > 50/(g_c/g)$. For a typical $10\ g < g_c < 100\ g$, we find $0.5\ \text{micron} < R < 5\ \text{micron}$.

Summarizing, the ionic strength contribution to capillary forces that might be present in determination of WH using gravitational pressure is not apparent. Moreover, evaluation of the pore sizes suggests that a contribution of capillary pressures on WH may be negligible in these systems.

References

1. Stevenson, C.D., M.J. Dykstra, and T.C. Lanier, *Capillary pressure as related to water holding in polyacrylamide and chicken protein gels.* Journal of Food Science, 2013. 78(2): p. 145-151.
2. Labuza, T.P. and P.P. Lewicki, *Measurement of gel water-binding capacity by capillary suction potential.* Journal of Food Science, 1978. 43(4): p. 1264-1269.

Chapter 3

Water holding of soy protein gels is set by coarseness, modulated by calcium binding, rather than gel stiffness

This chapter aims to differentiate between the contributions to water holding (WH) by gel microstructure and network stiffness of soy protein (SP) gels. SP were succinylated to increase calcium binding affinity, and the presence of different calcium salts were used to generate gels with different morphologies while keeping ionic strength and protein concentration constant. It was found that not gel stiffness, but coarseness (gel microstructure inhomogeneity) is more dominant in setting the WH ability. A higher energy dissipation of applied stress onto the protein network was related to inability of a gel network to retain water.

Keywords: calcium binding affinity, gel coarseness, soy protein gels, water holding, microstructure

3.1 Introduction

Population growth requires a more intense exploration and implementation of alternative protein sources in production, especially a wider application of plant proteins is desired for the structuring of food products. Particularly the use of soy proteins as structuring - gelation agents in food products has gained a lot of attention as this protein source is known to form gels with a high water holding (WH) capacity.

Two gel characteristics, microstructure and stiffness, are reported to determine this water holding propensity. The microstructural (morphological) aspects of the gel network appear relevant. These are set by e.g. the type of protein, protein concentration, pH, ionic strength and type of salts [1-5]. The impact of morphology on the water holding capacity has been reported for different protein systems and attempts to link it to typical length scales in the network have been made [6-10]. It has been reported that pore size diameters in the range of 0.1 - 2 μm are relevant for WH [11] and more recently, a dissection to identify the most relevant length scale that sets WH in soy gels was presented, showing that the structure contributions at the supra-micron level were most important, as discussed in **Chapter 2**. However, as modulation of coarseness of gels typically coincides with variation in, for example, osmotic pressures within the network, a conclusive picture has not emerged yet.

Alternatively, when WH is evaluated under an applied external force, like during oral processing, WH becomes also a function of the deformability of the network. Van den Berg and colleagues were able to demonstrate the deformation of the porosity of the continuous serum phase and how this affects the exudation of liquid [12]. The impact of gel stiffness represented by the Young's modulus on the ease of water removal from the gel was reported for soy gels more recently [13], and is discussed in **Chapter 2**.

The measurement of water holding capacity comprises two distinct outcomes: (i) the maximum amount of water that is removed from the protein gel, given an applied force, and (ii) the kinetics of this removal [14]. The variation in how the water holding capacity is assessed experimentally, together with variation in microstructure and deformability when comparing different gels, has prohibited thus far a complete understanding of how WH can be set by controlling gel network formation.

This work aims to differentiate between the contributions to WH by microstructure and network stiffness for soy protein gels. To this end, the approach has been taken to keep protein concentration, ionic strength and pH constant to derive a series of different types of gel morphologies. The obtained gels are then analyzed for their coarseness, their mechanical deformability and their WH capacity.

3.2 Material and Methods

3.2.1 Material

Defatted soy flour was provided by Cargill BV (Amsterdam, The Netherlands). Calcium sulphate dihydrate ($CaSO_4 \cdot 2H_2O$), calcium chloride dihydrate ($CaCl_2 \cdot 2H_2O$) and succinic anhydride (dihydro-2,5-furandione) were obtained from Sigma-Aldrich (Steinheim, Germany). Reagents were of analytical grade and used without further purification.

3.2.2 Preparation of enriched soy protein solution

Defatted soy flour was suspended in reverse osmosis (RO) water at a ratio 1:10 (w/w) at 45°C and stirred for 30 min. Then the pH was adjusted to 8.0 with 5 M NaOH and stirred for an additional 30 min. The supernatant was collected by centrifugation (30 min, 6000 g, 13°C). Isolation of the globulins (predominantly glycinin and β-conglycinin) was achieved by isoelectric precipitation (pH 4.5, 6 M HCl). After mild stirring of precipitate overnight at 4°C, the suspension was centrifuged (30 min, 6000 g, 7°C). The pellet was resuspended 3 times at pH 4.5 in RO water at a ratio 1:3 (w/w) to remove any remaining insoluble material followed by centrifugation (30 min, 6000 g), and was finally suspended in RO water at ratio 1:4 (w/w) at pH 7.0 using 5 M NaOH. This material was denoted as enriched soy protein solution (SP). Protein content of SP was determined by Kjeldahl (calculated using N x 6.25), where typical isolation procedure yielded 11-12% (w/w). The ratio of predominant proteins glycinin:β-conglycinin was estimated to be 50:50 by gel electrophoresis and reversed phase high-performance liquid chromatography (results are not shown). SP was stored at 4°C in solution in the presence of 0.02% (w/w) sodium azide and used within a month after preparation. The enthalpy change, indicative for the protein nativity, was 15.2 J/g protein measured by differential scanning calorimetry (DSC) (Q1000, TA Instrument, New Castle, USA).

3.2.3 Succinylation

Succinylation of SP was performed by diluting the protein solution to 5% w/w with phosphate buffer at pH 8.0 to a final buffer concentration of 75 mM. Samples were prepared in 50 ml aliquots. Succinic anhydride (10, 40 and 100 mg/g protein) was added in portions of 5-10 mg while constant stirring and maintaining the pH at 8.0 ± 0.2 by manual addition of 2 M NaOH. Between each succinic anhydride addition, the solution was allowed to equilibrate for at least 5 min. After the final addition samples were stirred for another 15 minutes. Succinylated samples were dialyzed in a dialysis tube (MW cut off: 12- 14 kDa) against demi water in 100 times excess 4 times for at least 3 hours. After dialysis, pH was adjusted to 7.0, samples were freeze-dried followed by resolubilization in demi water to 11% w/w protein. Protein content of succinylated SP was checked by Kjeldahl (calculated using N x 6.25). Succinylated SP was stored at 4°C in solution with 0.02% azide and used within a month.

3.2.4 Degree of succinylation

The degree of succinylation was determined by OPA (o-Phthaldialdehyde) assay adapted from Church et al. [15]. OPA reacts with primary amine groups (N-terminus and lysine ε-amino groups) in the presence of DMA (2-(dimethyl amino) ethanethiol hydrochloride) and results in the formation of alkyl-iso-indole fluorescent moieties. The OPA reagent was freshly prepared in a 50 ml volumetric flask by dissolving 40 mg OPA dissolved in 1 ml methanol, 25 ml 0.1 M borax solution, 200 mg DMA, 5 ml 10% (w/w) SDS solution and demi water. Presence of alkyl-iso-indole derivatives were measured at 340 nm in a UV-1800 spectrophotometer (Shimadzu, Kyoto, Japan) of 1 ml OPA reagent mixed with 100 μl 0.05% (w/w) succinylated SP, equilibrated for 1 h at room temperature in the dark. A linear calibration curve was obtained by measuring absorbance at 340 nm of 0.08-0.6 mM L-leucine as described above. Using this calibration curve the amount of NH_2 (mM) of protein prior and after modification was obtained. Degree of modification was expressed as % of modified lysine residues.

3.2.5 Apparent isoelectric point (IEP)

The zeta-potential was determined at 25 °C by a Zetasizer Nano ZS (Malvern Instruments, Worcestershire, UK). Reagents and protein solutions were filtered using 0.2 μm pore size syringe filter (Chromafil RC-20/25, Macherey-nagel, Düren, Germany). To determine the zeta-potential, 2.5 mg/ml (modified) SP was mixed with 5 mM $NaNO_3$ buffer previously adjusted to a series of pH from 3.0 up to 5.0. Measurements were performed in triplicates. The apparent IEP was determined by plotting a linear regression line across measured zeta potential values (mV) over defined pH range and taking the x-axis intercept as apparent IEP.

3.2.6 Differential scanning calorimetry (DSC)

Differential scanning calorimetry (DSC) measurements of (modified) SP were performed using DSC Q1000 (TA Instruments, New Castle, USA). Samples containing 10% w/w (modified) SP were heated from 20 to 120°C with a heating rate of 0.5°C/min. The enthalpy change and denaturation temperature was determined using standard software (TA Universal analysis) provided by the supplier. Measurements were performed in duplicates.

3.2.7 Intrinsic tryptophan fluorescence

Fluorescence spectra of 0.2 mg/mL SP (modified and non-modified) at pH 7.0 were recorded on a Varian Eclipse fluorescence spectrophotometer (Agilent Technologies, Amstelveen, The Netherlands). Excitation was performed at 295 nm and the resulting emission spectrum was recorded from 305 to 405 nm, using a scan speed of 10 nm/min. Both the excitation and the emission slit were set at 5 nm. Spectra were recorded 3-fold and averaged. Spectra were corrected by subtracting the spectrum of a protein free sample, obtained under identical conditions.

3.2.8 Far UV-CD

Far UV-CD spectra was obtained using a Jasco J-815 spectropolarimeter (Tasco Corp., Tokyo, Japan) to evaluate the protein secondary structure at room temperature. Measurements of (modified) SP samples (protein concentration: 0.1 mg/mL) were performed in quartz cuvettes with an optical path length of 0.1 cm. The scan range was 180 – 265 nm, the scan speed 100 nm/min, the band width 5.0 nm, spectral resolution 0.2 nm, and the response time was 1.0 s. Spectra were recorded in 32-fold and averaged. Far-UV CD spectra were analyzed for the estimated secondary structure content of the proteins using a nonlinear least-squares fitting procedure using reference spectra as described previously [16].

3.2.9 Determining calcium binding affinity

The average number of calcium ions bound per protein was determined with a calcium Ionplus Sure-flow ion selective electrode (Thermo Fisher Scientific, Beverly, USA) connected to a Orion Star A214 meter (Thermo Fisher Scientific, Beverly, USA). Calibration was performed with 1-100 mM $CaCl_2$ solutions (pH 7.0) in 20 mM TRIS buffer and 100 mM KCl to provide a constant ionic strength background. Samples were prepared in 10 ml aliquots containing 1% w/w protein in 20 mM TRIS buffer pH 7.0 containing 100 mM KCl. The 1 M $CaCl_2$ solution was titrated in 10, 15, 25 and 30 µl increments to the protein solution. After each increment, the solution was mixed for 3 min and measured. Millivolt values were converted to concentrations of free calcium using the calibration curve. The amount of added calcium was known, the bound calcium was derived from the difference between free and total calcium ions. The absolute amount of bound calcium (B) was calculated as follows (equation 3.1):

$$B = \frac{Ca_{total} - Ca_{free}}{P} \quad (\text{mol} / \text{mol})$$
(3.1)

where Ca_{total} is Ca²⁺ titrated in protein solution (mol), Ca_{free} is free Ca²⁺ measured in the solution (mol) in the presence of proteins, and P is protein concentration in moles (mol). As SP is a mixture of proteins with different molar weights and quaternary structures, a molecular weight average of complex 7S and 11S mixture of 270 kDa was used for calculations and materials prepared. Scatchard plots were obtained by plotting the ratio of bound calcium per protein (mol/mol) (B) over the free calcium concentration (B/Ca_{free}, mM⁻¹) against B. The calcium binding constant (K_d) was obtained from the slope of the curve, and the number of calcium-binding sites (n) from the x-axis intercept.

3.2.10 Preparation of gels

(Modified) SP was diluted to 10% (w/w) protein at pH 7.0 using TRIS buffer to a final TRIS concentration of 20 mM. The protein solution was mixed with 100 mM $CaCl_2$ or $CaSO_4$. Gelation was performed in 20 ml syringes (20 mm in diameter), lubricated with paraffin oil, and closed airtight to reduce air bubble formation during heating the samples at 95 °C for 30 min in the water bath and subsequently cooled overnight at room temperature. Every sample was prepared in duplicate.

3.2.11 WH measurements

The centrifugation procedure of gels was adapted from Kocher and Foegeding [14]. A microcentrifuge filtration unit was composed of an inner spin tube and a 2 ml Eppendof tube (Axygen Biosciences, Inc., Union City, USA). Gels were cut in 10 mm height and 4.8 mm diameter cylinders using a cork borer and carefully placed on the bottom of the spin tube. The bottom of the spin tube was covered with a 5.5 mm diameter filter paper to reduce grid size. Centrifugation was performed at 20 – 800 relative centrifugal forces (RCF) for 10 min at 20°C. Expulsed serum from the gel was collected at the bottom of the Eppendorf tube. Some samples exposed to high RCF fractured in a number of pieces, of which several co-eluted in the expulsed serum. In those cases, in order to determine the amount of expulsed serum, a strip of filter paper was used to carefully absorb the serum and determine its weight, thereby excluding the effect of the small co-exuded particles. The WH was defined as the percentage of water in the gel remaining after centrifugation according to

$$WH = \frac{W_T - W_{RCF}}{W_T} \cdot 100 \quad (\%) \tag{3.2}$$

where W_T is the total amount of water in the sample and W_{RCF} denotes the amount of water removed from the sample at a given RCF. Measurements were performed in duplicate. Water removed from the sample is expected to be proportional to applied RCF, which would hold to specific time of centrifugation. Plots of WH versus RCF were fitted assuming a single exponential decay

$$WH = A_{max} \cdot exp^{-k*RCF} + B \tag{3.3}$$

from where the fitting parameters A_{max} (the maximum percentage of water which can leave the system), B (percentage of water remaining in the gel) and k (the ease by which water leaves the system) were determined. Fitting the curves (using Origin 6.0) assuming two exponential decay functions did not give a significant improvement of fittings.

3.2.12 Confocal laser scanning microscopy (CLSM)

A 10% (w/w) soy protein solution was mixed with fluorescent dye Rhodamine B to a final dye concentration of 0.001% (v/w). Samples for microstructural analysis were gelled in glass cuvettes using 125 µl Gene Frame adhesive system (Fisher Scientific, Loughborough, UK). Imaging of the samples was performed using a Leica TCS-SP5 confocal laser scanning microscope (Leica Microsystems (CMS) GmbH., Mannheim, Germany). Leica objective lenses HC PL APO 20x/0.70 IMM/CORR CS and HCX PL APO 63x/1.20 W CORR CS were used. The excitation wavelength and emission spectral regime of Rhodamine B was 561 nm and 570-725 nm, respectively.

3.2.13 CLSM image analysis

CLSM images were analyzed to obtain a pair correlation function, $g(r)$, of the protein concentration as a function of the distance r using the procedure described by Ako et al. [17]. Pair correlation functions $g(r)$ were fitted assuming a stretched exponential decay [17] according to

$$g(r) = B_1 \cdot exp^{-\left(\frac{r}{\xi}\right)^{\beta}} + 1 \tag{3.4}$$

where B_1, ξ and β are fitting parameters. Theoretically the minimum value of distance (r) that can be explored by CLSM is 0.3 μm (63x water immersion objective). The σ^2, which is $g((r = 0.3$ μm$) - 1)$ is used as an indication of heterogeneity of gels and is valid for the case where one compares pictures imaged in the presence of constant protein and fluorescent dye concentrations. The σ^2 value at $r = 0$ follows from the fitting parameter B_1.

3.2.14 Scanning electron microscopy (SEM)

Gels were prepared in 1 ml pipette tips (narrowest part removed, sides cut to aid the diffusion of used reagents) and placed for 8 h into an aqueous 1% (v/v) glutaraldehyde solution for crosslinking. After crosslinking, excess of glutaraldehyde was removed by placing tips overnight into demi water. Demi water consequently was replaced with 50% DMSO in 3 steps (two steps for 4 h, third step - equilibration overnight). Samples were slowly frozen in liquid nitrogen, the pipette tips were peeled away from the gel. Remaining cylinder shaped gel was cut into slices using a razor blade. Obtained slices were thawed in the 50% DMSO solution which later was replaced by demi water and subsequently water was replaced for acetone in a few steps. Slices in acetone were dried by critical point drying (CPD) and attached on sample holders with CCC Carbon Adhesive (Electron Microscopy Sciences, Washington, USA). After evaporation of the solvent from the adhesive the samples were sputter coated with a 15 nm thick layer of iridium (MED 020, Leica, Vienna, Austria) and analyzed in a field emission scanning electron microscope (Magellan 400, FEI, Eindhoven, the Netherlands) at a working distance of about 4 mm, with SE detection at 2 kV and 6.3 pA. The digital images were contrast optimized with Photoshop CS5.

3.2.15 Large deformation rheology

10% (w/w) (modified) SP gels were sliced with a gel slicer into 20 mm in height and 20 mm diameter cylinders. Fracture stress and fracture strain were measured by uniaxial compression with an AP-501 rheometer (Anton Paar, Graz, Austria) mounted with a 5 kg load cell. Paraffin oil was applied on top and bottom of the gel to prevent friction during compression. Gel samples were compressed to 90% of their initial height between two parallel plates at a constant deformation rate of 1 mm/s. Measurements were performed at 20°C in triplicate. Young's modulus, E, was calculated from the linear part of the stress over strain curve within region of 0.05-0.15 and was calculated as described by Renkema et al. [18].

Recoverable energy was measured by compressing each gel to 50% of its fracture strain at a deformation speed of 1 mm/s. The recoverable elastic energy (RE) was determined as the ratio of the released energy during decompression and the applied energy during compression. The energies were determined from the areas below the stress-strain curve, as already discussed in the previous chapter.

3.3 Results and discussion

3.3.1 Changes in calcium binding affinity by succinylation

Soy proteins were modified aiming to change protein agglomeration during network-assembly by means of modulation of calcium binding affinity to obtain gels with different morphologies at a constant ionic strength and constant protein concentration.

Different degrees of succinylation of soy proteins was achieved by increasing the number of negative charges on the surface of the protein by chemical reaction of the primary amines (lysine residues) with succinyl group of succinic anhydride. Using the OPA assay 106 (±1) primary amines were detected in non-modified SP (mM primary amines/ mM protein, based on an average molecular weight in the complex 7S and 11S mixture of 270 kDa). Succinylated samples resulted in 87 (±3), 44 (±1) and 28 (±12) primary amines, indicating average degrees of succinylation (DS) of 17, 58 and 73% respectively (**Table 3.1**). These materials will be referred to SP17, SP58 and SP73. SP0 refers to the non-succinylated SP. Clearly, increasing DS increases the net (negative) charge of the protein, and is in line with the measured apparent IEP (**Table 3.1**).

Table 3.1 Chemical characterization of SP modified by succinylation.

Sample	DS (%)*	Apparent IEP	K_d (mM)	n
SP0	0	4.7±0.0	0.8	4.3±0.3
SP17	17.2±2.2	4.5±0.0	1.3	5.6±0.4
SP58	58.3±0.5	4.1±0.0	2.3	9.4±1.0
SP73	73.0±7.7	3.8±0.0	3.2	14.1±2.6

*DS - degree of succinylation

Calcium binding constants (K_d) as well as the number of calcium-binding sites (n) (summarized in **Table 3.1**) were obtained from calcium-binding curves (**Figure 3.1**) once converted into the so-called Scatchard plots [19]. Increasing DS yielded additional calcium binding sites on the protein as well as higher calcium binding affinity. Analysis of Scatchard plots showed that SP0 and SP17 had a linear relationship between bound calcium per protein (mol/mol) (B) and free calcium concentration (B/Ca_{free}, mM^{-1}), indicating a more specific binding affinity. Samples SP58 and SP73 deviated from such a linear relation, suggesting a less-specific calcium binding. This change in specificity can be deduced

from the standard deviation in Scatchard plot of binding sites (*n*) data (**Table 3.1**) (the standard deviation increases with increasing DS). The appearance of multiple or less-specific binding sites could be related to partial unfolding of proteins due to the increased net charge of the proteins. To verify this structural integrity of the soy proteins was studied.
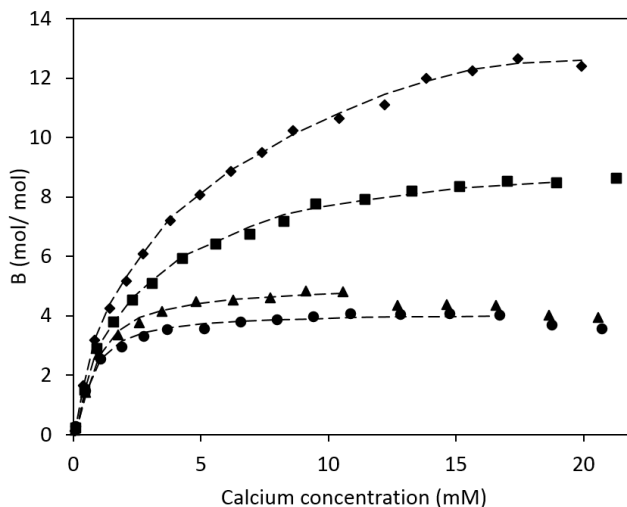

Figure 3.1 Ca binding: 1% (w/w) protein solution with 0 to 20 mM CaCl$_2$: SP0 (●), SP17 (▲), SP57 (■) and SP73 (◆). The dashed lines are fits to guide the eye.

3.3.2 Conformational changes of soy proteins by succinylation

Changes in tertiary structure of (modified) SP were probed using intrinsic tryptophan fluorescence (results are not shown). A fluorescence emission maximum below 340 nm is characteristic for a tertiary folded protein in which tryptophans are buried in the interior of the molecule [20]. No shift of the emission maximum, typically around 330 nm, was observed with increasing degree of succinylation, illustrating that the local environment of the tryptophan residues remained unaffected by the succinylation, even up to a substantially high degree of modification and concomitant increase in net charge. This preserved apparent global packing of the proteins is contradictive to the evaluated thermal stability of the proteins, as recorded by DSC. The enthalpy change of denaturation decreased strongly with increasing DS (**Figure 3.2A**), indicating either a lower cooperativity in unfolding, or that the different folding domains within a protein exhibit different thermal stabilities as often encountered in multi-domain proteins like the plant storage protein family.

Possible changes on the secondary structure level of (modified) SP were investigated using far UV-CD spectra (not shown). The spectrum of SP0 showed a positive extreme around 190 nm and negative extremes around 208 nm and 222 nm, and a zero-crossing at 198 nm. These features are indicative for an ordered secondary structure with high contributions of α-helices [21, 22]. Upon succinylation, the zero crossing shifted to lower wavelengths, the intensity of the negative and positive extreme diminished, reflecting the loss of ordered

secondary structure. From far-UV CD spectral analysis (**Figure 3.2B**) the contributions of α-helix, β-structures (β-strand and β-turn), and random coil were estimated. These results confirmed that increasing DS lowered progressively the α-helix content and increased random coil structures in (modified) SP, indicating unfolding of the protein at the secondary structure level.
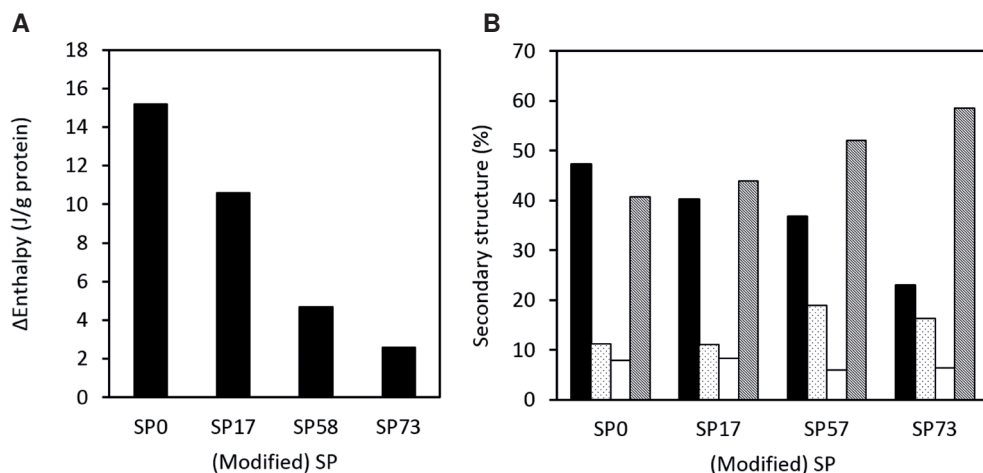

Figure 3.2 (A) Change in enthalpy of (modified) SP. (B) Estimated contributions to secondary structure of (modified) SP: α-helix (filled column), β-strand (dotted column), β-turn (open column) and random coil (stripped).

To conclude, despite the loss of local secondary structure in the protein upon progressive succinylation and a diminished enthalpic transition involved during heat denaturation, succinylated soy proteins still remain tertiary folded and responsive to heat treatment even at high degree of succinylation. These properties demonstrate the protein ability to develop a gel-network upon heat-treatment.

3.3.3 Gel microstructure

The presence of 100 mM $CaSO_4$ or $CaCl_2$ in 10% w/w (modified) SP solutions resulted in heat-set gels varying from translucent to white, while keeping ionic strength and protein concentration constant. Obtained gel microstructures were visualized at different length scales ranging from 250 to 0.5 µm using CLSM and SEM (**Figure 3.3**). In the presence of calcium salts gel coarseness typically decreased with increasing DS. Also the (modified) SP gels in the presence of $CaCl_2$ were coarser than those with $CaSO_4$. All gels obtained were ranked from least coarse (G1) to most coarse (G8) by visual evaluation of gel microstructure on different length scales (CLSM, SEM) (**Figure 3.3**). Ranking criteria was based on gel coarseness, which was defined in this study as the inhomogeneity within the gel microstructure over different length scales.
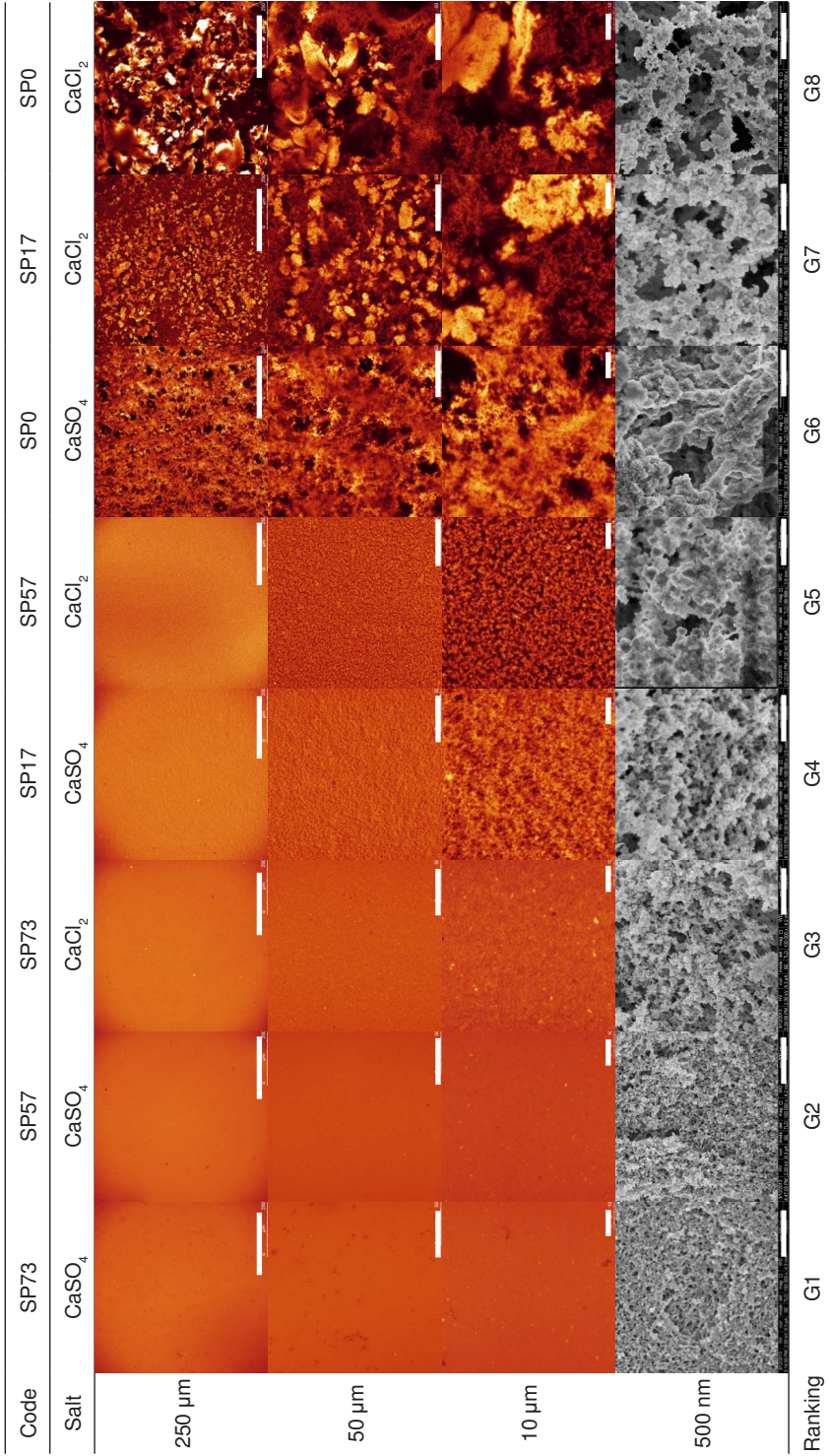
Figure 3.3 Apparent coarseness of 10% w/w 100 mM $CaSO_4$ and $CaCl_2$ SP gels ranked from least coarse (G1) to most coarse (G8) by visual evaluation on different length scales (CLSM, SEM).

Assessment of gel microstructure obtained by both CLSM and SEM provides a good representation of structure inhomogeneity over different length scales. For example, gels G1-G2 differ only in a nanometer scale range (SEM). Gels G3-G4 have a pronounced difference in coarseness on a 10 µm scale (CLSM), yet are still comparable on nanometer scale. Most coarse gels G6-G8 appeared to be more inhomogeneous over all length scales.

To obtain a more quantitative measure for apparent coarseness, image analysis of the CLSM pictures was performed. The advantage of this method is that correlation functions of single gel images at different magnifications yield one master correlation function [17]. This allows one to obtain a representative coarseness parameter of a gel microstructure over a range of length scales. Obtained pair correlation functions for gels G1-G8 are shown in **Figure 3.4A**. Quantification of coarseness by means of σ^2 (**Figure 3.4B)** yields a correlation with the visually observed coarseness. The B_1 values obtained by fitting (results are not shown) had comparable values to σ^2, but for the gels G1 and G2 showed high standard deviations, confirming present limitation of the method below 0.3 µm length scale.
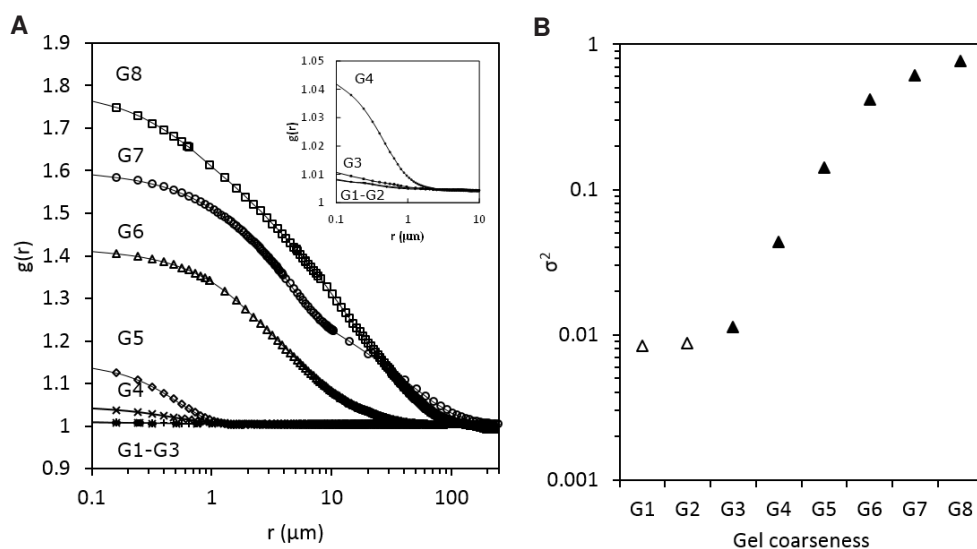

Figure 3.4 Image analysis. (A) Semi-logarithmic representation of pair-correlation functions of gels G1-G8. The insert shows enlarged pair-correlation functions of G1-G4 gels. (B) σ^2 of gels G1 to G8, ranked according to an increasing coarseness as observed visually. Open symbols stands for data points below the CSLM resolution limit.

Correlation lengths (ξ) and slopes (β) of gels G1-G8 obtained by fitting (equation 3.4) are listed in **Table 3.2**. Typically, decrease of the correlation function has been related to intensity fluctuations, reflecting structural properties of the gel network [17]. Results shown in **Figure 3.4** and **Table 3.2** indicate that gels G1 and G2 are homogeneous through all length scales analyzed, and no structure elements above 0.3 µm are observed. Gels G3-

G5 have a stepwise change in correlation length from 0.3 μm to 0.5 μm and increased correlation slopes. Gels G6-G8 have correlation lengths up to approximately 11 μm, and lower slopes when compared to G3-G5 gels indicating coarse structures.

Table 3.2 Correlation length (ξ) and slope (β) for the samples G1-G8.

Gel	ξ (μm)	β
G1	0.20±0.02*	0.34±0.01*
G2	0.19±0.01*	0.41±0.02*
G3	0.30±0.01	0.99±0.03
G4	0.46±0.01	1.35±0.10
G5	0.53±0.03	1.53±0.07
G6	4.66±0.08	0.67±0.01
G7	8.67±0.29	0.51±0.01
G8	10.96±0.15	0.61±0.01

*Below CLSM resolution limit

Summarizing, SP calcium binding affinity modulation yielded gels with different coarseness over different length scales. Coarseness over length scales was evaluated qualitatively as well as quantitatively by means of coarseness parameter (correlation length)**.**

3.3.4 Water holding and gel microstructure

The results for WH versus the applied RCF of (modified) SP gels G1-G8 are presented in **Figure 3.5**. It can be observed that from the least coarse gels G1-G2 no water could be removed for all RCF applied. From gels G3-G5 pronounced water loss as well as increased water removal kinetics was seen with increasing coarseness. Gels G6-G8 resulted in comparable amount of water removed, where 200 RCF was enough to expulse the majority of total removable water (under conditions used) followed by a plateau. Latter gels have large network building blocks which are seen back in gel microstructure. Calcium addition to non-succinylated or low degree succinylated SP solutions results in a sudden color change from transparent to white indicating protein aggregation to occur at lengths scales larger than 100-200 nm. Coarseness could be accounted for maximum water removal already at low RCF applied.

These WH results were quantified for the different gels by deriving fitting parameters A_{max} and k using equation 3.3 (dashed lines**, Figure 3.5**) and are presented in **Figure 3.6**. The results illustrate clearly that the maximum amount of removable water (A_{max}) and easiness of water removal (k) under applied deformation increase with increasing gel coarseness, and that above a certain coarseness (> G6) the maximum amount of water to be removed is the same, while the ease by which this water is expulsed still increases.
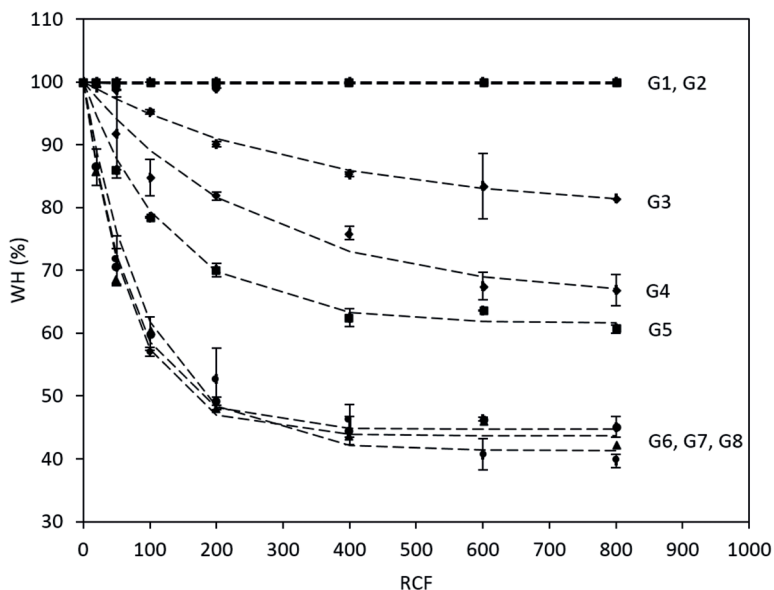
Figure 3.5 WH values of 10% w/w (modified) SP gels G1 to G8, where 1 to 8 refer to a visual ranking in increasing coarseness. The dashed lines represent fits obtained using equation 3.3.
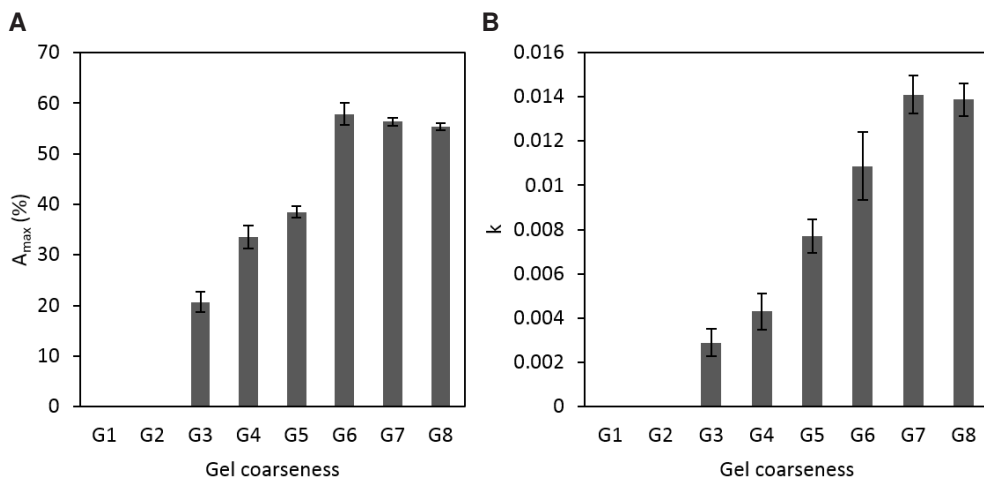
A

B

Figure 3.6 Fitting parameter values of 10% (w/w) (modified) SP gels G1 to G8, where 1 to 8 refer to a visual ranking in increasing coarseness. (A) A_{max} parameter and (B) k parameter.

Figure 3.7 shows the correlation of gel coarseness and WH of a gel obtained by plotting correlation lengths (**Table 3.2**) as a function of A_{max} (**Figure 3.6A**) and k (**Figure 3.6B**). When the correlation length is below 0.3 μm, no water could be removed from the gel network. With increasing gel coarseness from approximately 0.3 to 0.5 μm amount of water removal increases from approximately 20 to 40%. The ease of water removal

from the gel increases with increasing gel coarseness. Above 4 µm length scales, the total amount of water that can be removed is maximized at approximately 60%, while correlation lengths between approximately 4 and 8 µm still differ in ease of water removal from the gel (k). Length scales above 8 µm does not matter for final amount (A_{max}) or ease of water removal (k) from the gel network. Overall, image analysis suggests that critical correlation length defining WH lies between 0.3 and approximately 4-5 µm for SP gels. Similarly, Hermansson reported that blood plasma and whey protein gels with pore sizes (established by SEM) below approximately 0.1 µm barely release water when a centrifugal force is applied (without breaking the gel), while pore size in the range of 0.2-2 µm already shows pronounced loss of water [5].
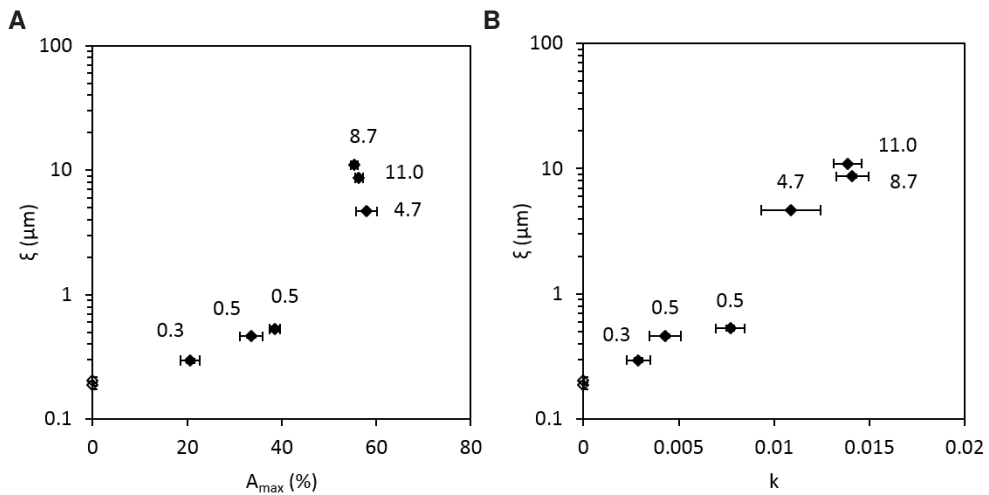

Figure 3.7 Correlation length (ξ) of gels G1-G8 obtained by image analysis as a function of (A) max removed water from the gel (A_{max}), and (B) the ease by which water can be removed (k). Open symbols stand for data points below the CSLM resolution limit.

3.3.5 Water holding and gel stiffness

The above shows that WH of a gel is clearly proportional to its coarseness. To study to what extent contribution of the gel stiffness, as reflected by the Young's modulus, comes into relation to WH, large deformation rheology of gels G1-G8 was performed to analyze Young's modulus as shown in **Figure 3.8A**. There is an optimum in Young's modulus for the array of gels G1-G8, and is found for gel G4. This can be explained by that fact that increasing coarseness yields thicker strands, and lower number of connectivity points within the sample (**Figure 3.3**, 500 nm scale). The first effect could yield an increase and the latter a decrease in Young's modulus.

In **Figure 3.8B**, the gel stiffness is plotted against WH results (A_{max} parameter), but no relationship could be found. Gels G6 and G8 have the same WH, but different Young's modulus, e.g. gels G3 and G6 have comparable Young's modulus, but differ in WH. This

result is in contrast to results of heat-induced SP gels prepared in the presence of $MgSO_4$ and $MgCl_2$, which did show a relation between WH and Young's modulus as discussed in **Chapter 2**, and suggests that gel microstructure contribution (coarseness) in studied modified (SP) gels is more dominant in defining WH. A possible explanation may be that in the latter study the aggregation was modulated by type of salt and salt concentration to obtain different gel morphologies, while in the current study different SP gel morphologies were obtained at similar ionic strength.
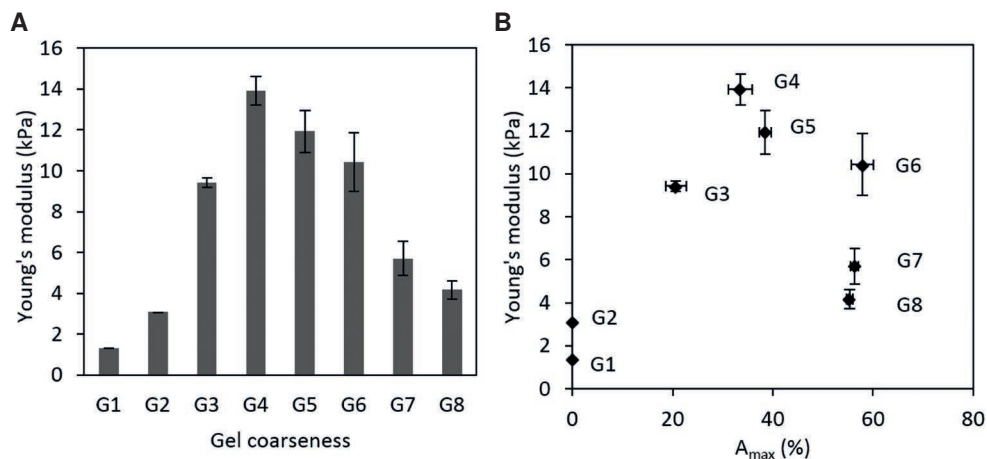

Figure 3.8 (A) Young's modulus of 10% w/w (modified) SP G1-G8 gels ranked according to an increasing coarseness as observed visually. (B) A plot of Young's modulus versus maximum amount of water removed (A_{max}) from gels G1-G8.

3.3.6 Water holding and energy dissipation

During mechanical deformation, part of the energy to deform a gel is stored elastically, and another part is dissipated due to e.g. viscous flow or fracture [23]. The recoverable energy is therefore not only determined by microstructure characteristics as, for example, strand thickness, stiffness or coarseness, but also sensitive to the flow properties of the entrapped liquid phase. RE analysis of gels G1-G8 are presented in **Figure 3.9A**. Obtained results show that RE decreased from approximately 75% (G1) to 43% (G8) with increasing gel coarseness. Least coarse gels have a high RE, whereas coarser gels have a low RE, indicating a higher proportion of dissipating energy during deformation. These results are in line with results previously reported in **Chapter 2** [13]. It could be suggested that the lower RE found for G6 is caused by (micro-)fracture events initiated by compression to more than half of the gel actual fracture strain. Nonetheless, careful analysis of the loading and unloading curves did not give an indication of fracture events being apparent.

Correlation plot between WH and RE is shown in **Figure 3.9B**, where a relation between WH (A_{max}) and energy dissipation can be observed. As macroscopic fracture events can

be neglected while the measurement is performed, the loss of RE may reflect largely serum displacement from the gel. The higher the water holding capacity of the protein gel, the smaller the dissipated energy. Coarser gels have more dissipation via serum flow as they are less able to hold water, causing more energy to dissipate during deformation, leading to a lower RE. This relation is valid up to the point where a WH limit is reached, as seen in case of gels G6-G8. The slope of the correlation shown in **Figure 3.9B** could be a measure for the efficiency by which a deformed protein network transduces its energy to viscous flow of the serum phase and thereby dissipates the applied energy and may reflect how the entrapped serum phase moves together with the network during deformation. Displacement of water from the network has been shown as a relevant mechanism for energy dissipation [24].
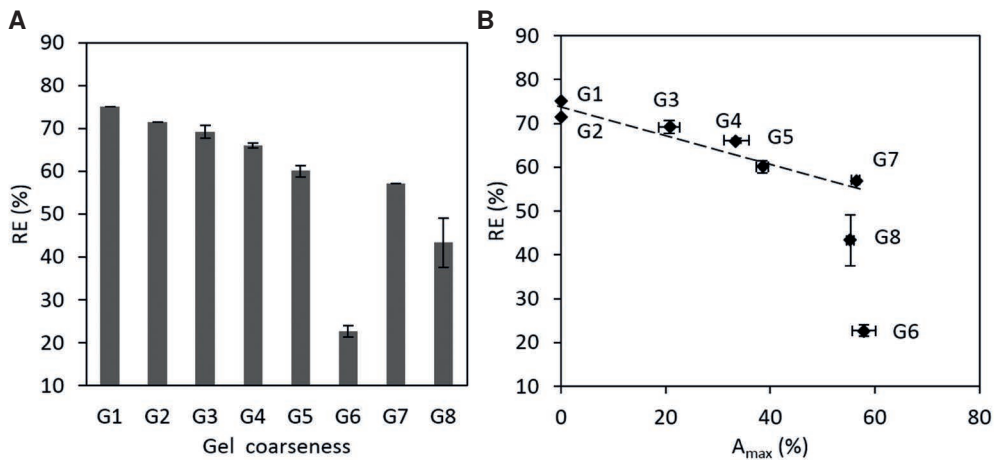

Figure 3.9 (A) RE measurments of 10% (w/w) (modified) SP G1-G8 gels ranked according to an increasing coarseness as observed visually. (B) A plot of RE versus maximum amount of water removed (A_{max}) for gels G1-G8.

3.4   Conclusions

This chapter aimed to differentiate between the microstructure and network deformability contributions to WH for (modified) SP gels. Gels G1-G8 based on single protein concentration and a constant ionic strength, where osmotic pressure differences can be neglected, showed that not gel stiffness but coarseness (gel microstructure inhomogeneity) sets WH propensity. Coarser gels result in lower RE and therefore higher energy dissipation related to WH property, but no correlation was found between stiffness and WH of (modified) SP gels, indicating that WH in the studied system is strongly dominated by gel microstructure. Image analysis suggested that a pronounced water loss is in the range of 0.3 - 4.7 µm, and critical length scale where no more water could be removed from the gel for SP gels is above 4.7 µm. Overall, coarser gels are less able to hold water

under applied force and have higher energy dissipation by serum displacement from the gel. This work brings understanding on length scales determining pronounced water loss and shows that coarseness is dominant in setting WH of a gel. These insights could be exploited in product development to predict and tune WH of (new) products.

3.5 Acknowledgements

3

References

1. Molina, E., A.B. Defaye, and Ledward, D.A., *Soy protein pressure-induced gels.* Food Hydrocolloids, 2002. 16(6): p. 625-632.

2. Maltais, A., et al., *Formation of soy protein isolate cold-set gels: protein and salt effects.* Journal of Food Science, 2005. 70(1): p. 67-73.

3. Renkema, J.M.S. and van Vliet, T., *Heat-induced gel formation by soy proteins at neutral pH.* Journal of Agricultural and Food Chemistry, 2002. 50(6): p. 1569-1573.

4. Foegeding, E.A., Bowland, E.L., and Hardin, C.C., *Factors that determine the fracture properties and microstructure of globular protein gels.* Food Hydrocolloids, 1995. 9(4): p. 237-249.

5. Hermansson, A-M., *Structuring water by gelation food materials science*, J.M. Aguilera and P.J. Lillford, Editors. 2008, Springer New York. p. 255-280.

6. Chantrapornchai, W. and McClements, D.J., *Influence of NaCl on optical properties, large-strain rheology and water holding capacity of heat-induced whey protein isolate gels.* Food Hydrocolloids, 2002. 16(5): p. 467-476.

7. Hermansson, A-M., *Gel characteristics—structure as related to texture and water binding of blood plasma gels.* Journal of Food Science, 1982. 47(6): p. 1965-1972.

8. Puppo, M.C. and Añón, M.C., *Structural properties of heat-Induced soy protein gels as affected by ionic strength and pH.* Journal of Agricultural and Food Chemistry, 1998. 46(9): p. 3583-3589.

9. Stevenson, C.D., Dykstra, M.J., and Lanier, T.C., *Capillary pressure as related to water holding in polyacrylamide and chicken protein gels.* Journal of Food Science, 2013. 78(2): p. 145-151.

10. Puppo, M.C., Lupano, C.E., and Anon, M.C., *Gelation of soybean protein isolates in acidic conditions. Effect of pH and protein Concentration.* Journal of Agricultural and Food Chemistry, 1995. 43(9): p. 2356-2361.

11. Hermansson, A-M., *Fat and water holding in functional properties of food macromolecules.* Functional Properties of Food Macromolecules, ed. J.R. Mitchell and D.A. Ledwards. 1986, London and New York: Elsevier Applied Science Publishers.

12. van den Berg, L., et al., *Serum release: The hidden quality in fracturing composites.* Food Hydrocolloids, 2007. 21(3): p. 420-432.

13. Urbonaite, V., et al., *Origin of water loss from soy protein gels.* Journal of Agricultural and Food Chemistry, 2014. 62(30): p. 7550-7558.

14. Kocher, P.N. and Foegeding, E.A., *Microcentrifuge-based method for measuring water-holding of protein gels.* Journal of Food Science, 1993. 58(5): p. 1040-1046.

15. Church, F.C., et al., *Spectrophotometric assay using o-phthaldialdehyde for determination of proteolysis in milk and isolated milk proteins1.* Journal of Dairy Science, 1983. 66(6): p. 1219-1227.

16. de Jongh, H.H.J., Goormaghtigh, E., and Killian, J.A., *Analysis of circular dichroism spectra of oriented protein-lipid complexes: toward a general application.* Biochemistry, 1994. 33(48): p. 14521-14528.

17. Ako, K., et al., *Quantitative analysis of confocal laser scanning microscopy images of heat-set globular protein gels.* Food Hydrocolloids, 2009. 23(4): p. 1111-1119.

18. Renkema, J.M.S., J.H.M. Knabben, and T. van Vliet, *Gel formation by β-conglycinin and glycinin and their mixtures.* Food Hydrocolloids, 2001. 15(4–6): p. 407-414.

19. Fu, H. and Wilkinson, K., *Quantitative analysis of protein-protein interactions*, in *Protein-Protein Interactions*. 2004, Humana Press. p. 15-31.

20. Pain, R.H., *Determining the fluorescence spectrum of a protein*, in *Current Protocols in Protein Science*. 2001, John Wiley & Sons, Inc.

21. Johnson, W.C., *Secondary structure of proteins through circular dichroism spectroscopy.* Annual Review of Biophysics and Biophysical Chemistry, 1988. 17(1): p. 145-166.

22. Achouri, A. and Zhang, W., *Effect of succinylation on the physicochemical properties of soy protein hydrolysate.* Food Research International, 2001. 34(6): p. 507-514.

3

23.   Van Vliet, T. and Walstra, P., *Large deformation and fracture behaviour of gels.* Faraday Discussions, 1995. 101: p. 359-370.

24.   de Jong, S., T. van Vliet, and H.H.J. de Jongh, *The contribution of time-dependent stress relaxation in protein gels to the recoverable energy that is used as tool to describe food texture.* Submitted, 2015.

3

Chapter 4

Permeability of gels is set by the impulse applied on the gel

To better understand sensory perception of foods, water exudation studies on protein-based gels are of a high importance. It was aimed to study the interplay of gel coarseness and gel stiffness on water holding (WH) and water flow kinetics from the gel once force is applied onto the material. Ovalbumin heat-set gels were used as a model system, where protein volume fraction was kept constant and ionic strength was varied to obtain a range of different gel morphologies and stiffness. WH of gels was measured both as a function of time and force applied. From experimental data (i) an effective gel permeability coefficient and (ii) an effective water flux coefficient were obtained and related to gel coarseness and stiffness. Gel coarseness determined maximum amount of water removed from the gel at defined conditions, where lower (≤0.1 μm) and upper (≥0.4 μm) limiting scales for water removal were identified. Gel stiffness is the major determinant for water removal kinetics from the gel. The combination of gel coarseness and gel stiffness showed a cooperative effect on gel WH. The insights can be exploited in product development to predict and tune oral perception properties of (new) products.

Keywords: Young's modulus, gel stiffness, gel coarseness, water holding, ovalbumin gels effective gel permeability coefficient, effective water flux coefficient

4.1 Introduction

To better understand sensory perception of foods, water exudation studies on protein-based gels are of a high importance. The water holding (WH) property of a gel is determined by gel characteristics [1-3]. First, the microstructural (morphological) aspects of the gel network appear to be relevant. Secondly, deformability of the network by an applied force affects water exudation from the gel.

As previously discussed, the morphological aspects of the gel network are set by e.g. the type of protein, its concentration, the pH, ionic strength and type of salts present [4-8]. The impact of morphology on WH capacity has been reported for different protein systems and attempts to link it to typical length scales in the network have been made [2, 3, 9-13]. It has been reported that pore size diameters in the range of 0.1 - 2 µm are relevant for WH [14]. More recently, the water loss of soy protein gels was reported to be most sensitive in the pore size range of 0.3 - 4.7 µm [3].

The extent the gel structure deforms upon applied force is crucial for exudation of water [8]. Van den Berg and colleagues showed that serum flow rate from the gel was a direct function of the network porosity and was higher at higher compression rates [15]. In **Chapter 2** we have shown that gel stiffness was related to WH property in soy protein gels, where stiff gels had low WH and less stiff gels had high WH [2].

Once a single protein gel system obtained by e.g. varying pH or salt concentration is studied, typically gel coarseness is dominant in determining WH [3]. However, when two different protein systems differing in protein source or processing condition are compared, gels comparable in apparent coarseness may result in different WH. This suggests that gel microstructure is not a single determinant in WH property. Gel coarseness and stiffness parameters are interrelated, but thus far to our knowledge no attempt to dissection the effect of gel coarseness and gel stiffness on gel WH under applied pressure was reported.

When water transport mechanisms in relation to gel coarseness are studied, in most studies network stiffness and time- or force-dependent changes in the gel morphology are not taken into account. Water transport simulations in porous media based on Darcy's law are applicable only for laminar flow in solid non-deformable porous medium [16]. Such analysis leads to permeability coefficients reflecting gel coarseness [17, 18]. In relation to coarseness, Hermansson (2008) proposed three different length scale-dependent water transport mechanisms in the gel: (i) hydrodynamic flow, (ii) capillary flow and (iii) molecular diffusion [8]. Hydrodynamic and capillary flows are apparent on macro- to micron scales. Hydrodynamic flow is active in large and open structures, and is driven by gravity or external forces. Capillary flow depends also on surface tension of the liquid, where an external pressure higher than capillary pressure is needed to displace water [8, 12]. Molecular diffusion is apparent on nanometer scale and is more of importance for the mass transport of molecules or small particles in the gel matrix rather than for WH.

To measure hydrodynamic and capillary flow, an external force has to be applied. The measurement of WH comprises two distinct aspects: (i) the maximum amount of water that is exuded from the protein gel, at a given force, and (ii) the kinetics of this exudation, or as often referred to, the 'ease of flow' [19]. In this chapter we aim to show how gel coarseness, defined as microstructure inhomogeneity, and gel stiffness affect water flow from the gel under applied force. As a model system for this study ovalbumin heat-set gels were used. Ovalbumin, as the main protein in egg white, is highly relevant for the food industry for a range of applications, and is well-studied for its aggregation and gelation mechanisms [20]. The approach was taken to have a constant protein volume fraction and to vary ionic strength to obtain a range of different gel morphologies. Obtained gels are then analyzed for their coarseness using image analysis of CLSM and SEM images, their stiffness using large deformation rheology, and WH capacity measured by centrifugation in time over a range of forces applied or at constant forces applied as a function of time.

4.2 Material and Methods

4.2.1 Material

Ovalbumin was purchased from Neova (lot no: BB13191, Abbotsford BC, Canada) with a purity of 90%. Sodium chloride (NaCl) was obtained from Sigma-Aldrich (Steinheim, Germany). Reagents were of analytical grade and used without further purification.

4.2.2 Preparation of gels

Ovalbumin was dissolved in milliQ water to 12% (w/w) protein at pH 7.5. The protein solution was mixed with different concentrations of NaCl. The protein solution prior to gelling was de-aerated under vacuum for 5 min (vacuum pump MZ 2C NT, Vacuubrand, Wertheim, Germany). Gelation was performed in 20 ml syringes (20 mm in diameter), lubricated with paraffin oil, and closed airtight to reduce air bubble formation during heating the samples at 95°C for 20 min in a water bath and subsequently cooling overnight at room temperature. Every sample was prepared at least in duplicate.

4.2.3 WH measurements at given time and pressure

The centrifugation procedure of gels was adapted from Kocher and Foegeding [19]. A microcentrifuge filtration unit was composed of an inner spin tube and a 2 ml Eppendof tube (Axygen Biosciences, Inc., Union City, USA). Gels were cut in 10 mm high and 4.8 mm diameter cylinders using a cork borer and carefully placed on the bottom of the spin tube. The bottom of the spin tube was covered with a 5.5 mm diameter filter paper to reduce grid size. Centrifugation was performed at 20 – 1000 relative centrifugal forces (RCF) for 10 to 40 min at 20°C. Expulsed serum from the gel was collected at the bottom of the Eppendorf tube. The WH was defined as the percentage of water in the gel remaining after centrifugation according to

$$WH = \frac{W_T - W_{RCF}}{W_T} \cdot 100 \quad (\%) \tag{4.1}$$

where W_T is the total amount of water in the sample and W_{RCF} denotes the amount of water removed from the sample at a given RCF. Measurements were performed in duplicate.

To evaluate the magnitude of pressure applied on the gel RCF was converted to applied pressure (P) in Pascal (Pa) as follows:

$$P = \frac{(V_s \cdot \varnothing_{protein} \cdot \rho_{protein} + V_s \cdot \varnothing_{water} \cdot \rho_{water}) \cdot RCF \cdot g}{A} \tag{4.2}$$

where V_S is volume of the sample (m³), $\varnothing$ is volume fraction of proteins or water in the sample, $\rho_{protein}$ = 1350 kg/m³ [21], g is gravitational acceleration (9.8 m/s²), and A is area of the cylinder top surface (m²). As an example, 100 RCF is equivalent to 10 kPa applied on the gel. Water removed from the sample is expected to be proportional to applied force, which would hold for a specific time of centrifugation. Using above described experimental set-up, WH of gels was measured (i) as a function of applied pressure (P), when the time was fixed (e.g. gels centrifuged at 20-1000 RCF for 1 min, 2 min, 3 min etc. up to 40 min), and (ii) as a function of time (t), when the pressure was fixed (e.g. gels centrifuged at 1-40 min at 20 RCF, 50 RCF, 100 RCF etc. up to 1000 RCF). Obtained WH data versus applied pressure (P) at fixed times, and time (t) at fixed applied pressures were fitted using equation 4.3 assuming a single exponential decay

$$WH = A_{max} \cdot exp^{-k_i f(P,t)} + B \tag{4.3}$$

from where the fitting parameters A_{max}, the maximum percentage of water which can leave the system, B, percentage of water remaining in the gel, and k_i, kinetics parameter either as a function of applied pressure or time were determined. Fitting parameter k as a function of pressure at fixed different times was denoted as *k1* and reflects effective gel permeability coefficient change over time. Parameter k as a function of time at fixed different applied pressures was denoted as *k2* and reflects water flux coefficient from the gel change over applied pressure. Fitting the curves (using Origin60) assuming two exponential decay functions did not yield a significant improvement of the fit. Change in *k2* slope was calculated using Excel slope function between second and third points of each curve. Calculated values of the initial slope depended on the pressure-interval chosen. However, independent of the pressure where the differences were analyzed, the outcome and conclusive lines were similar.

4.2.4 Confocal laser scanning microscopy (CLSM)

12% (w/w) protein solution was mixed with fluorescent dye Rhodamine B to a final dye concentration of 0.001% (v/w). Samples for microstructural analysis were gelled in glass cuvettes using 125 µl Gene Frame adhesive system (Fisher Scientific, Loughborough, UK). Imaging of the samples was performed using a Leica TCS-SP5 confocal laser scanning

microscope (Leica Microsystems (CMS) GmbH., Mannheim, Germany). Leica objective lenses HC PL APO 20x/0.70 IMM/CORR CS and HCX PL APO 63x/1.20 W CORR CS were used. The excitation wavelength and emission spectral regime of Rhodamine B was 561 nm and 570-725 nm, respectively.

4.2.5 CLSM image analysis

CLSM images were analyzed to obtain a pair correlation function, $g(r)$, of the protein concentration as a function of the distance r using the procedure described by Ako et al. [22]. Pair correlation functions $g(r)$ were fitted assuming a stretched exponential decay [22] according to

$$g(r) = B \cdot exp^{-\left(\frac{r}{\xi}\right)^{\beta}} + 1 \qquad (4.4)$$

where B, ξ and β are fitting parameters. The parameter ξ represents correlation length. Theoretically the minimum value of distance (r) that can be detected by CLSM is 0.3 μm (63x water immersion objective). The σ^2, which is $g(r = 0.3$ μm) - 1) is used as an indication of heterogeneity of gels and is valid for the case where one compares pictures imaged in the presence of constant protein and fluorescent dye concentrations. The σ^2 value at $r = 0$ follows from the fitting parameter B.

4.2.6 Scanning electron microscopy (SEM)

Gels were cut in 1.3 cm height and 1 cm diameter cylinders using a gel slicer and a cork borer and placed for 8 h into an aqueous 2.5% (v/v) glutaraldehyde solution for crosslinking. After crosslinking, excess of glutaraldehyde was removed by placing gel pieces in demi water overnight. Samples were gently rotated during the process. Demineralized water was subsequently replaced for acetone in a few steps. Gel pieces in acetone were dried by critical point drying (CPD), fractured and attached on sample holders with CCC Carbon Adhesive (Electron Microscopy Sciences, Washington, USA). After evaporation of the solvent from the adhesive the samples were sputter coated with a 15 nm thick layer of iridium (MED 020, Leica, Vienna, Austria) and analyzed in a field emission scanning electron microscope (Magellan 400, FEI, Eindhoven, the Netherlands) at a working distance of about 4 mm, with SE detection at 2 kV and 6.3 pA. The digital images were contrast optimized with Photoshop CS5.

4.2.7 SEM image analysis

ImageJ 1.49d was used as a tool to measure building block sizes visualized in SEM images at magnifications of 20,000, 100,000 and 200,000. On average 15 images were analyzed per gel. Building block sizes were obtained by direct visual inspection of the gel and are representative numbers over the different magnifications and multiple spot analysis in each of the images. The derived building block sizes were averaged.

4.2.8 Large deformation rheology

12% (w/w) ovalbumin gels were sliced with a gel slicer into 20 mm in height and 20 mm diameter cylinders. Fracture stress and fracture strain were measured by uniaxial compression with an AP-501 rheometer (Anton Paar, Graz, Austria) mounted with a 50 kg load cell. Paraffin oil was applied on top and bottom of the gel to prevent friction during compression. Gel samples were compressed to 90% of their initial height between two parallel plates at a constant deformation rate of 1 mm/s. Measurements were performed at 20°C in triplicate. Young's modulus, E, was calculated from the linear part of the stress over strain curve within the region of 0.05-0.15 of true fracture strain, and mean values of fracture stress and strain were calculated as described by Renkema et al. [23]. The 1 mm/s deformation rate was chosen for this study to relate our results to oral processing conditions where entrainments speeds are up to 20-50 mm/s [24], however such speeds were technically not feasible with the current instrumentation.

4.3 Results and discussion

4.3.1 Gel microstructure

Gel coarseness in this work is defined as microstructure inhomogeneity derived from microscopy images. Since an image is made up of pixels, microstructure can be defined as an entity consisting of mutually related pixels and group of pixels [25]. A fine or homogeneous morphology is referred to an image when two pixels next to each other do not differ.

To study the effect of gel coarseness and gel stiffness on water holding and water flow kinetics from the gel once force is applied, the protein volume fraction was kept constant and ionic strength was varied to obtain a range of different gel morphologies. Heat treatment of a 12% w/w ovalbumin solution (pH 7.5) in the presence of 0-300 mM NaCl resulted in heat-set gels varying from transparent to white in their appearance. Obtained gel microstructures were visualized at different length scales ranging from macroscopic to nanometer scales and are shown in **Figure 4.1**. In all cases fine gels were obtained with no observable differences in morphology on 50 micrometer length scale. Differences in gel microstructure do become observable on 10 and 5 micrometer length scales. Most pronounced differences between gels in building block sizes and their connectivity were visible on 1 to 0.5 micron length scales. Generally, addition of 50-300 mM NaCl increased gel coarseness on nanometer length scale. Gels with no salt added and with 20 mM NaCl had fine microstructures through all length scales visualized.

To obtain a quantitative measure for gel coarseness, defined here as gel microstructure inhomogeneity, image analysis of CLSM images by means of pair correlation function, and SEM image analysis by measuring typical building block sizes was performed. A pair

correlation function describes how density varies as a function of distance from a reference point. A decrease of the correlation function is related to intensity fluctuations, reflecting the morphology of the gel [22]. Obtained correlation functions for gels are shown in **Figure 4.2A**. Quantification of coarseness by means of σ^2 (**Figure 4.2B)** and *B* values (results are not shown) obtained by fitting confirmed that 0-50 mM gels have structural units smaller than 0.3 µm (i.e. below CLSM resolution limit), and marginal difference in coarseness was detected between 100-300 mM NaCl gels. The correlation length (ξ) (**Figure 4.2C**) of latter gels changed from 0.3 to 0.4 µm. SEM images analysis results (**Figure 4.2C**) were in agreement with CLSM image analysis. Building blocks in gels with 0-20 mM NaCl varied from 0.09 to 0.13 µm, and the gel containing 50 mM NaCl was composed of on average 0.22 µm building blocks. More coarse gels with 100-300 mM NaCl increased in building block size from approximately 0.26 to 0.45 microns. Quantitative analysis showed a change of intensities in CLSM images and a change in building block size in SEM images from approximately 0.09 to 0.45µm, representing increased gel coarseness with increasing ionic strength.

4.3.2 Mechanical responses

Large deformation rheology of different gels was performed to determine Young's modulus. Young's modulus reflects the stiffness of the material determined from the linear stress over strain curve region at small strain. The obtained results are presented in **Figure 4.3**. There is an optimum found for the gel containing 50 mM NaCl. Increase in Young's modulus with increasing NaCl concentration, followed by a decrease at higher NaCl concentrations is in accordance with the literature [26]. Addition of salt reduces electrostatic repulsion between proteins and therefor affects protein aggregation and gel microstructure. This can be explained by two opposing contributions. First, increasing coarseness yields thicker strands and therefore higher Young's modulus. Second, strands increasing in thickness result in a lower number of connectivity points in the network (**Figure 4.1**, 500 nm scale) and therefore decrease Young's modulus. Accordingly, gels with no salt added and 300 mM NaCl are good examples of the latter contributions, as they are comparable in Young's modulus (**Figure 4.3**) but largely differ in coarseness (**Figure 4.1**).
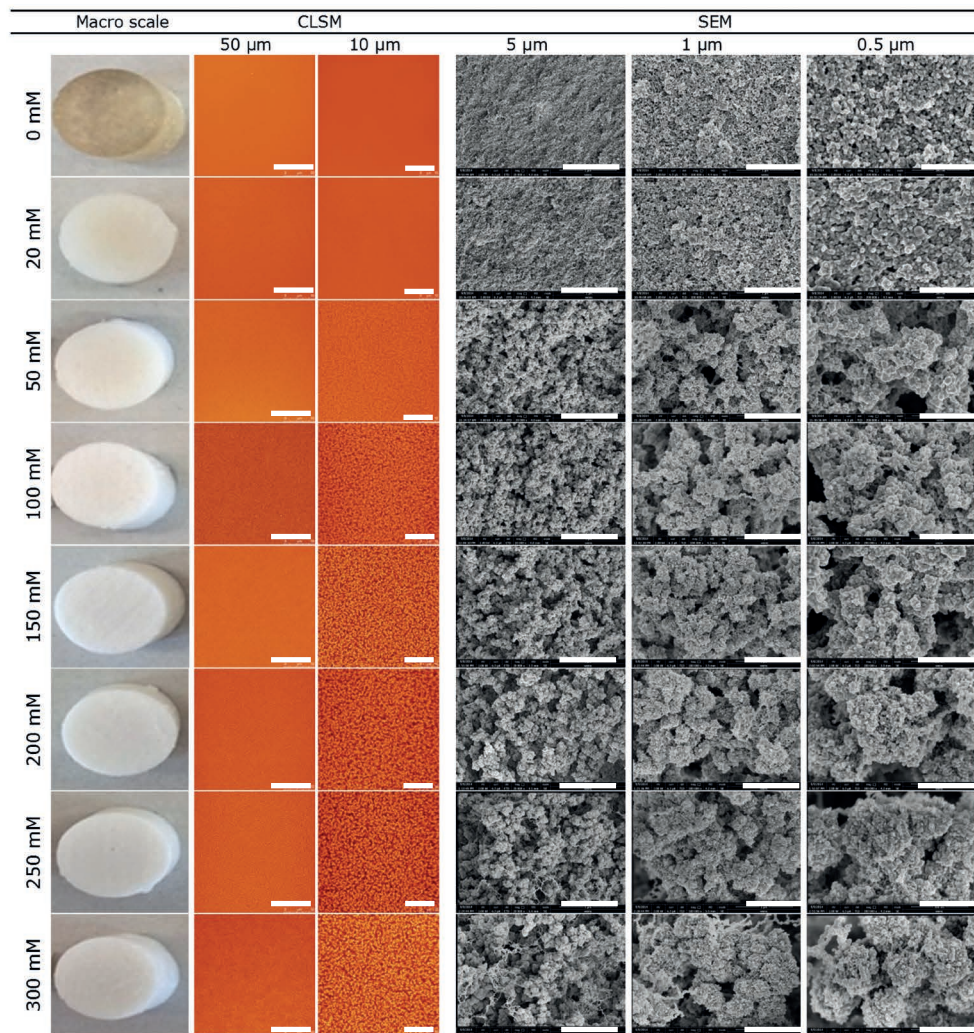
4

Figure 4.1 Microstructure of 12% w/w ovalbumin gels in the presence of 0-300 mM NaCl at different length scales. The indicated length scales corresponds to the bar in the image.
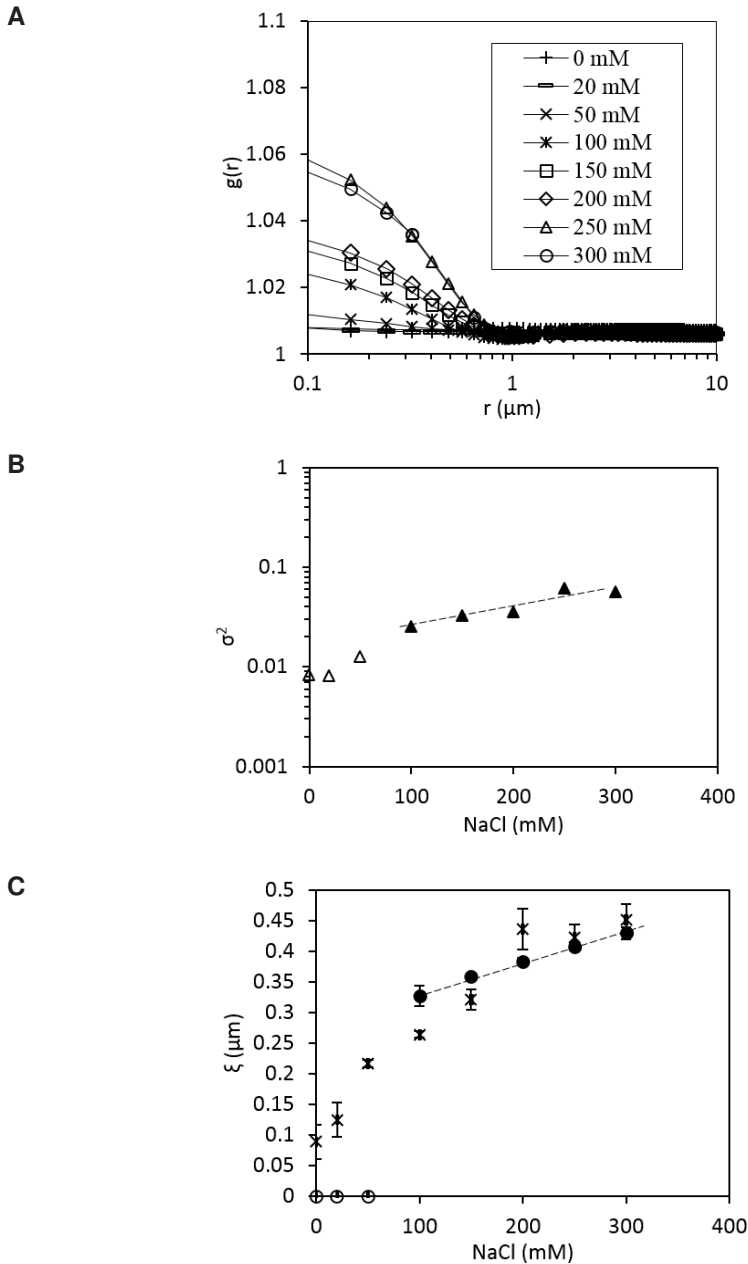
A

B

C

Figure 4.2 Image analysis. (A) Semi-logarithmic representation of the pair-correlation function of 12% w/w ovalbumin gels prepared in the presence of 0-300 mM NaCl. (B) A plot of σ^2 versus 0-300 mM salt of 12% w/w ovalbumin gels. (C) Correlation length (ξ) versus salt concentration obtained by (●) CLSM and (x) SEM image analysis. Open symbols in B and C panels represent data below the CLSM resolution limit.
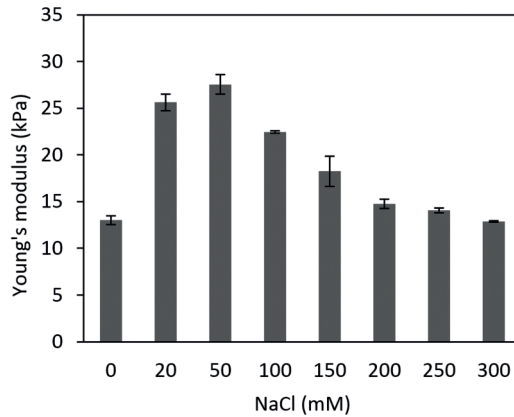
Figure 4.3 Young's modulus of 12% w/w ovalbumin gels prepared in the presence of 0-300 mM NaCl.

4.3.3 Water holding

The water holding results for 12% w/w ovalbumin gels containing 0-300 mM NaCl centrifuged for 10 min are shown in **Figure 4.4**. Exposing samples to 10 min centrifugation reflects a steady state between applied pressure and removed water. From the graph it can be observed that almost no water could be removed from the gels containing less or equal to 20 mM NaCl at all pressures applied. The gel with 50 mM NaCl had a water loss of maximally 25%, and gels containing 100-300 mM salt resulted in a comparable water loss of 50-55%. From these latter gels the majority of water was already removed at low applied pressures (5-20 kPa).
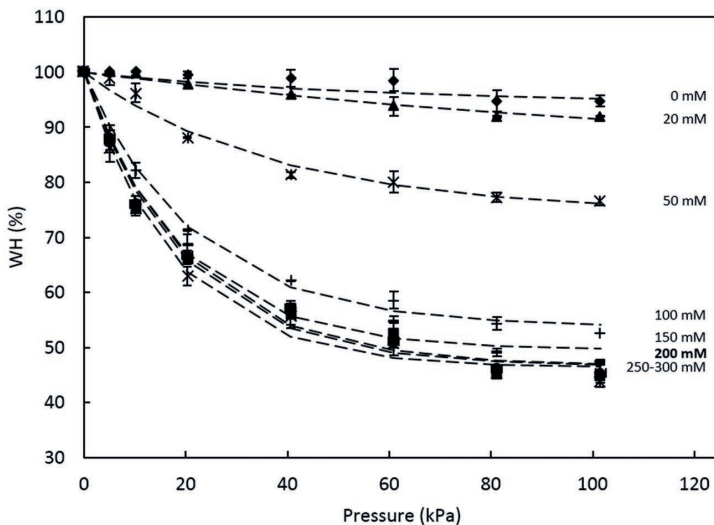

Figure 4.4 WH of 12% w/w ovalbumin gels containing 0-300 mM NaCl centrifuged for 10 min at different centrifugal forces. The dashed lines represent fits obtained using equation 4.3. The corresponding pressure (kPa) was calculated as described in **Material and Methods section 4.2.3**.

4.3.4 Water holding and gel morphology

Obtained WH data (**Figure 4.4**) were fitted using equation 4.3 to derive fitting parameter A_{max}, the maximum percentage of water which can leave the system. The A_{max} was plotted over gel coarseness (measured by SEM) and gel stiffness (Young's modulus), and is shown in **Figure 4.5**. From **Figure 4.5A** it can be seen that with increasing coarseness more water is removed from the gel. Up to length scales of 0.13 µm hardly any could be removed from the gel. This length scale is denoted as the lower limiting length scale (LL), at which no water can be removed from the gel by centrifugal forces up to 1000 RCF. Coarseness at length scales of 0.22-0.32 µm resulted in pronounced water loss upon applied pressure. Above 0.4 µm length scale gels resulted in the maximum removed water and was denoted as upper limiting length scale (UL). In comparison to reported values in literature, LL is likely to be generic for all type proteins [3, 8, 14], and UL is protein specific [14].
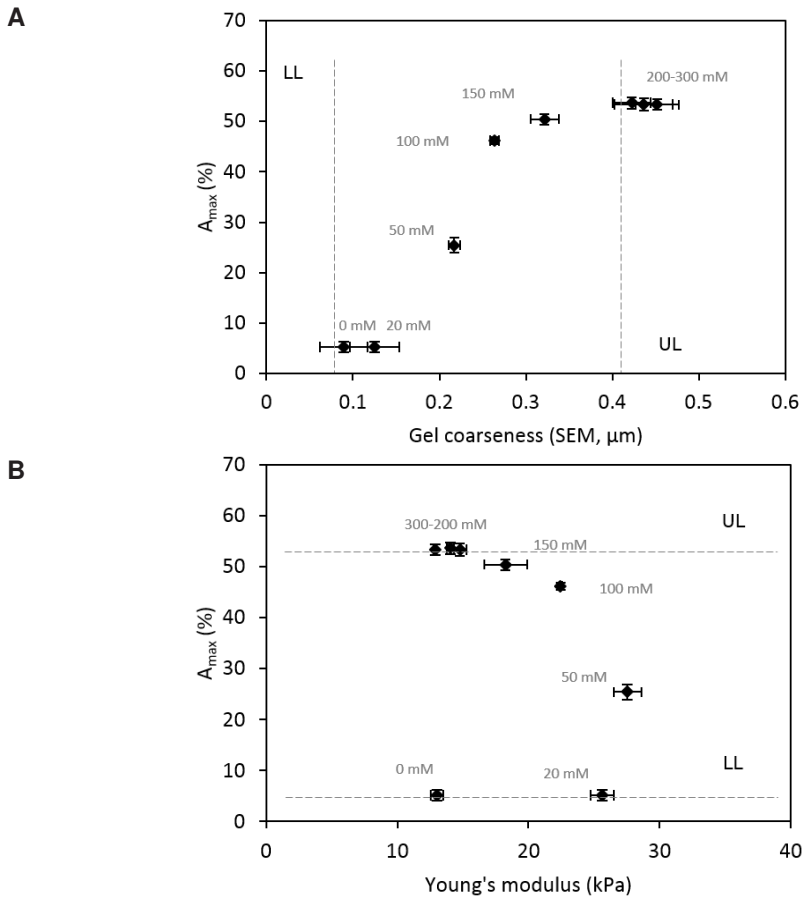

Figure 4.5 Maximum amount of removed water from the gel, A_{max}, over (A) gel coarseness obtained from SEM images, and (B) over Young's modulus. Dashed lines represent lower limiting length scales (LL), where no water can be removed from the gel and upper limiting length scales (UL), where no more water can be removed from the gel.

The effect of gel stiffness on A_{max}, as shown in **Figure 4.5B,** displayed no clear relationship between removable water and gel stiffness. This can be explained by the presence of UL and LL. Gels which fall in limiting scale regimes can differ in gel stiffness and coarseness, but will result in no water removal in the LL case, and similarly, water removal in the UL case. Apparent correlation of WH and Young's modulus is seen when focused on gels in between the two limiting scales, with pronounced water loss. It can be observed that stiffer gels had higher WH (or lower A_{max}) than less stiff gels. This observation is opposite to previously reported in **Chapter 2** for soy protein gels with magnesium salts [2], and suggests that the role of network stiffness and WH relation is protein specific.

4.3.5 Effective gel permeability coefficient

Effect of both gel coarseness and gel stiffness on WH of a gel once pressure is applied is shown in **Figure 4.6** for 12% w/w ovalbumin gel containing 200 mM NaCl centrifuged over a range of pressures at several fixed times. The differences observed in WH between 1 to 10 minutes centrifugation time is likely to represent the effect of gel microstructure deformation. Major changes in gel WH appeared up to 5 min centrifugation, and no observable changes were seen after 10 min centrifugation (**Figure 4.6**, solid line). No further changes indicate that steady state between applied force and removable water is reached. The magnitude of applied pressure (e.g. 40 kPa versus 100 kPa) shows different WH-time dependencies. In the range of 20-60 kPa change in WH was significant, whereas above or below this range change in WH was marginal. These results suggest an effect of gel deformability on water removal from the gel.
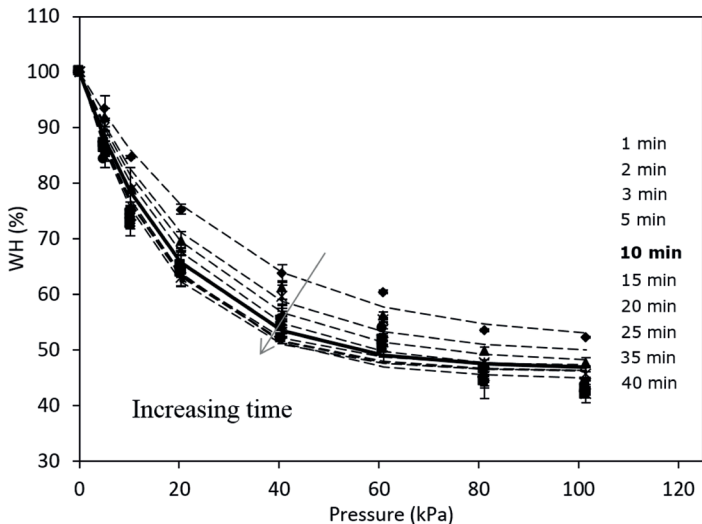

Figure 4.6 Example of 12% w/w ovalbumin gel with 200 mM NaCl centrifuged over a range of RCF for different times. Dashed lines stand for WH data measured after 1 to 40 min centrifugation, solid lines stands for WH data after 10 min centrifugation. The arrow indicates the direction of increase in centrifugation time.

WH data obtained by measuring WH over the range of applied pressures at different fixed times of gels in the presence of 0-300 mM NaCl were fitted to equation 4.3. Fitting parameter *k1*, denoted as effective gel permeability coefficient, was further used to compare changes in gel water holding under applied pressure in time. The effective gel permeability coefficients are shown in **Figure 4.7**. For clarity reasons, an example of the change in *k1* with time for the gel with 50 mM NaCl is shown in panel A, and *k1* as a function of salt concentration after 25 min centrifugation is displayed in panel B. All shown *k1* parameters were obtained at the same 5-100 kPa pressure range. It was noted that the effective permeability coefficient increased (stepwise) with increasing centrifugation time and increasing ionic strength. Generally, two effective permeability coefficient regimes were seen: (i) up to 5 minutes centrifugation and (ii) above 10 minutes (plateau) (**Figure 4.7A**). In the first regime, the stepwise increment in effective gel permeability coefficient represents viscoelastic behavior of the gel. Network ability to resist applied pressure is linked to a yielding phenomenon related to gel stiffness. The plateau regime represents gel microstructure after deformation, where fracture events and compression of the network have already appeared. Comparison of plateau values (**Figure 4.7B**) of gels with different NaCl concentrations indicates that increasing salt concentration results in higher effective gel permeability which could be accounted for increased gel coarseness, as shown by image analysis of CLSM and SEM images of gel microstructures.
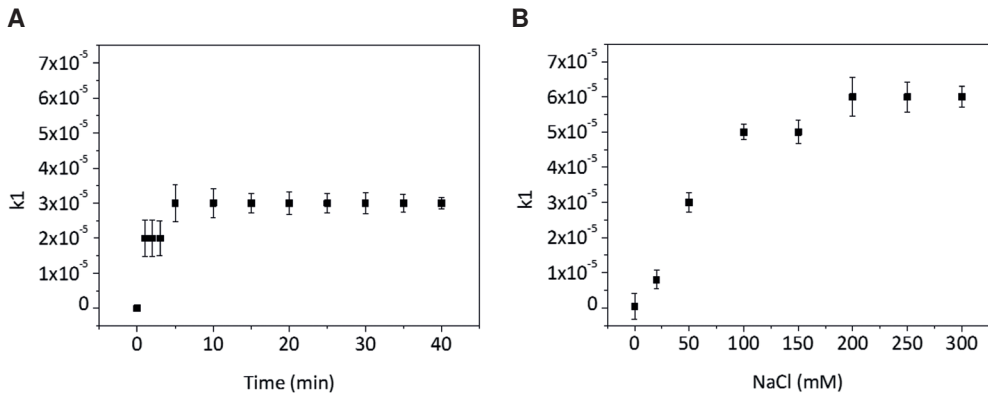
A

B

Figure 4.7 (A) Effective gel permeability coefficient (*k1*) change in time of 12% w/w ovalbumin gel with 50 mM NaCl. (B) Effective gel permeability coefficient (*k1*) as a function of salt concentration after 25 min centrifugation.

4.3.6 Effective gel permeability coefficient and gel morphology

The effective gel permeability coefficient (*k1*) is suggested to reflect changes in gel microstructure under applied pressure in time. To obtain insight in how effective gel permeability coefficient relates to gel morphology at (i) the yielding regime and (ii) the microstructure deformation regime, a 3D plot (**Figure 4.8**) was used to visualize the relation between *k1* and gel coarseness and stiffness.

From the graph it can be observed that gel coarseness and stiffness were related to each other in case of gels with 50-300 mM NaCl (with increasing building clock size from 0.2 to 0.4 µm). Coarser gels were less stiff gels and had higher effective gel permeability coefficients. Gels with 0 and 20 mM NaCl (building block size <0.13 µm) did not follow this dependence because of the LL (**Figure 4.5A**). Little or no water removal from these gels results in no pronounced differences in *k1* at any centrifugation time applied. Increment in *k1* for gels with increasing coarseness and decreasing stiffness was seen in both (i) yielding and (ii) microstructure deformation regimes. Based on the above described results it can be concluded, that the change in gel morphology in time under applied pressure is larger for coarse and more deformable gels, resulting in more water removal from the gel. Stiff and fine gels require more energy to deform the network, as well as higher force to overcome higher capillary forces to expel water.
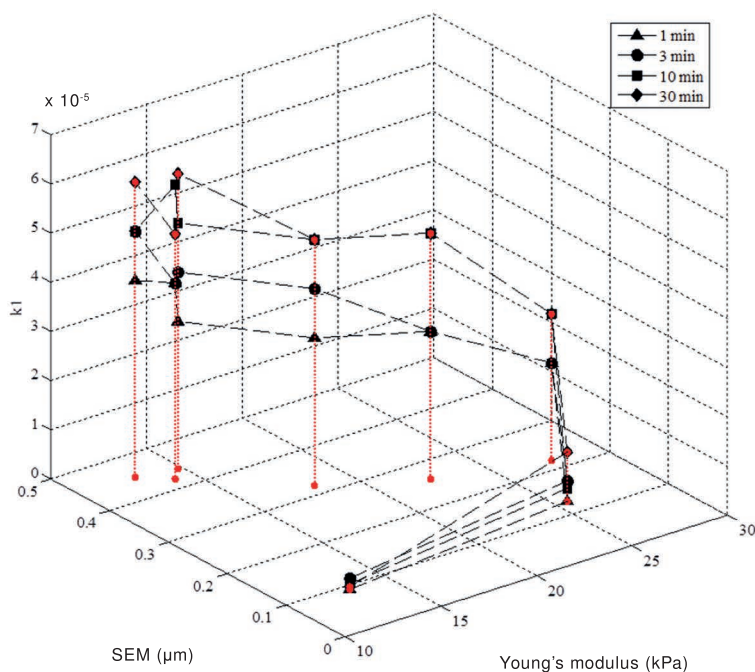

Figure 4.8 Change in effective gel permeability coefficient *k1* at (i) yielding regime (1 and 3 min) and (ii) gel microstructure deformation regime (10 and 30) min in relation to gel coarseness and stiffness.

4.3.7 Effective water flux coefficient

Both gel coarseness and stiffness were shown to affect the effective gel permeability coefficient in time under applied pressure. Coarseness was dominant in determining effective gel permeability, while the stiffness is expected to be dominant in determination of water flow kinetics from the gel. An example of a 12% w/w ovalbumin gel with 200 mM NaCl centrifuged over time at fixed different forces is shown in **Figure 4.9**. From the graph

it can be seen that major changes in WH appeared within the first 5 min of centrifugation, and no observable changes in WH were seen after 10 min centrifugation. The applied pressure is shown to be proportional to the quantity of water removed. Up to 40-60 kPa pronounced differences are seen in removed water, and at higher applied pressures the difference in WH becomes marginal, suggesting an effect of the network deformability on water removal from the gel.
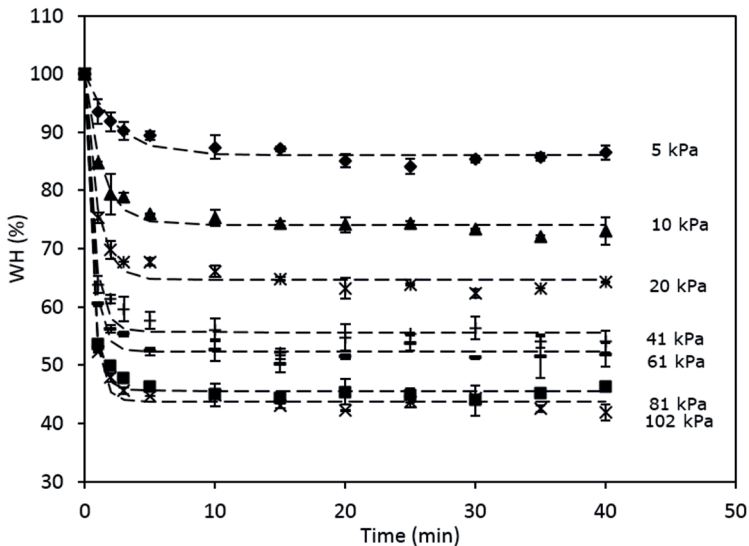

Figure 4.9 WH data as a function of time at fixed applied pressures of a 12% w/w ovalbumin gel with 200 mM NaCl.

To illustrate how deformability affects water flow kinetics from the gel once force is applied, WH data obtained by centrifugation of 0-300 mM NaCl gels over time at different fixed forces were fitted to equation 4.3. Fitting parameter $k2$, denoted as effective water flux coefficient, was further used to compare gels in water flow under applied force in time (**Figure 4.10**). From the graph it can be seen that higher applied pressures resulted in higher water flux coefficient, followed by the leveling-off of the curves. The velocity of the fluid in the stationary state is proportional to the applied pressure (linear relationship) [27]. In case of a rigid gel, which should be treated as a rigid porous medium, permeability does not depend on the magnitude of applied force. However, obtained results clearly indicate force-dependent structural changes. This behavior is attributed to gel morphological properties [28] and represents the effect of gel deformability. The leveling-off of the curve reflects compressibility of the gel.

The above discussed results show that gels with 100-300 mM NaCl differed in coarseness (**Figure 4.2C**), stiffness (**Figure 4.3**) and effective gel permeability coefficient (**Figure 4.7B**), but were comparable in maximum amount of removable water at steady state (**Figure 4.5A**). The results shown in **Figure 4.10**, however, show clear differences in the

effective water flux coefficient for the same gels. These results indicate that the kinetics at which water flows out of the gel is depending on the network stiffness. Accordingly, the ability to remove comparable amount of water from these gels could be ascribed to water flow kinetics from the gel dominated by network stiffness.
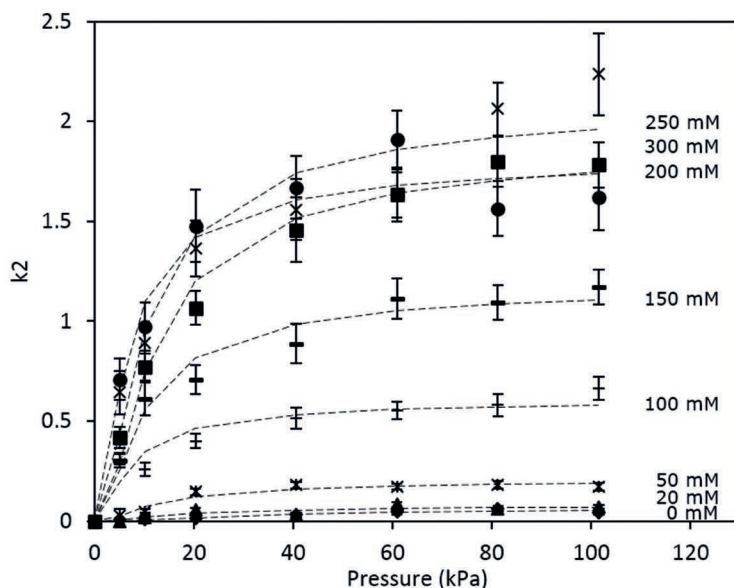

Figure 4.10 Effective water flux coefficient ($k2$) plotted over applied pressures for 12% ovalbumin gels with different NaCl concentrations.

4.3.8 Effective water flux coefficient and gel morphology

The effective water flux coefficients ($k2$) increased with increasing applied pressure and with increasing ionic strength. Slopes of $k2$ as a function of pressure differed in steepness. The slopes of $k2$ over the salt concentration are shown in **Figure 4.11**. Assuming, that in case of fine gels water removal is caused by network deformation, higher degree and easier network compression would result in higher effective water flux coefficient. Therefore, steeper slope would indicate easier (faster) gel network deformation. To illustrate the relation of change in $k2$ slope and gel deformability, Young's modulus data (**Figure 4.3**) were overlaid with a change in $k2$ slopes for the different gels (**Figure 4.11**). From the graph it can be observed that decreasing gel stiffness correlates to a change of the $k2$ slope. A change in the slope of $k2$, i.e. the easiness of gel network deformation, shows that less stiff gels are deformed easier. Easier and therefore faster network deformation results in quicker water removal from the gel.

The interplay between gel coarseness and gel stiffness shows a cooperative effect on gel WH measured under applied pressure. Increasing salt concentration resulted in coarser and less stiff gels (**Figure 4.8**). The 0 and 20 mM gels, as discussed earlier, fall in the

LL length scale region where gels could differ in stiffness, but because of the very fine morphology no water could be expulsed. Coarse gels in combination with decreased stiffness resulted in higher effective permeability coefficients and a higher effective water flux, but at the same time they were easier to deform resulting in higher water flux. Less coarse gels had lower effective water flux coefficient and were more resistant to deformation. To conclude, if all samples would have the same stiffness, flux over force would have a linear relationship and would be mainly dependent on gel coarseness.
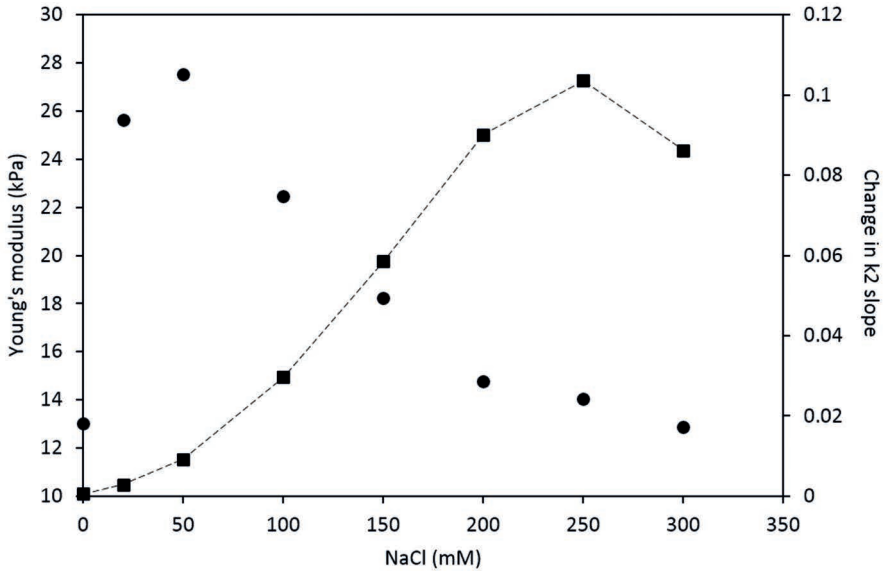

Figure 4.11 Young's modulus (●) and change in *k2* slope (-■-) of 12% w/w ovalbumin gels prepared in the presence of 0-300 mM NaCl.

4.4   Conclusions

To conclude, once pressure is applied on a gel, the microstructure of a semi-solid will deform, and gel permeability and water flow become dependent on both gel morphology and its deformability. To predict WH of a gel under applied deformation (i) gel coarseness, (ii) gel stiffness and (iii) interplay between both have to be considered. First of all, gel coarseness determines the final WH of a gel, where lower and upper limiting scales for water removal are present. In case of ovalbumin gels, below 0.1 μm length scale no water could be removed from the gel, and above 0.4 μm gels result in the same final WH. Secondly, gel stiffness defines the kinetics of water removal from the gel. In case of a stiff gel, applied energy first would go towards network deformation rather than water exudation, whereas less stiff gels would result in network compression and easier water removal from the gel. Finally, the interplay between gel coarseness and gel stiffness shows a cooperative effect on gel WH. Coarse and less stiff gels have higher effective

water flux, but are easier affected by applied pressure. Less coarse, but stiff gels have lower effective water flux coefficient, but are more resistant to deformation and require more energy to deform the network, as well as higher pressure to overcome high capillary forces to remove water. The cooperative effect of coarseness and stiffness allows one to make gels differing in coarseness and stiffness with the same final gel WH, but different in effective water flux (water removal kinetics).

4.5 Acknowledgements

4

References

1. Hermansson, A-M. and Lucisano, M., *Gel characteristics—water binding properties of blood plasma gels and methodological aspects on the waterbinding of gel systems.* Journal of Food Science, 1982. 47(6): p. 1955-1959.

2. Urbonaite, V., et al., *Origin of water loss from soy protein gels.* Journal of Agricultural and Food Chemistry, 2014. 62(30): p. 7550-7558.

3. Urbonaite, V., et al., *Water holding of soy protein gels is set by coarseness, modulated by calcium binding, rather than gel stiffness.* Food Hydrocolloids, 2015. 46: p. 103-111.

4. Molina, E., Defaye, A.B., and Ledward, D.A., *Soy protein pressure-induced gels.* Food Hydrocolloids, 2002. 16(6): p. 625-632.

5. Maltais, A., et al., *Formation of soy protein isolate cold-set gels: protein and salt effects.* Journal of Food Science, 2005. 70(1): p. 67-73.

6. Renkema, J.M.S. and van Vliet, T., *Heat-induced gel formation by soy proteins at neutral pH.* Journal of Agricultural and Food Chemistry, 2002. 50(6): p. 1569-1573.

7. Foegeding, E.A., Bowland, E.L., and Hardin C.C., *Factors that determine the fracture properties and microstructure of globular protein gels.* Food Hydrocolloids, 1995. 9(4): p. 237-249.

8. Hermansson, A-M., *Structuring water by gelation food materials science*, J.M. Aguilera and P.J. Lillford, Editors. 2008, Springer New York. p. 255-280.

9. Chantrapornchai, W. and McClements, D.J., *Influence of NaCl on optical properties, large-strain rheology and water holding capacity of heat-induced whey protein isolate gels.* Food Hydrocolloids, 2002. 16(5): p. 467-476.

10. Hermansson, A-M., *Gel characteristics—structure as related to texture and waterbinding of blood plasma gels.* Journal of Food Science, 1982. 47(6): p. 1965-1972.

11. Puppo, M.C. and Añón, M.C., *Structural properties of heat-Induced soy protein gels as affected by ionic strength and pH.* Journal of Agricultural and Food Chemistry, 1998. 46(9): p. 3583-3589.

12. Stevenson, C.D., Dykstra, M.J., and Lanier, T.C., *Capillary pressure as related to water holding in polyacrylamide and chicken protein gels.* Journal of Food Science, 2013. 78(2): p. 145-151.

13. Puppo, M.C., Lupano, C.E., and Anon, M.C., *Gelation of soybean protein isolates in acidic conditions. Effect of pH and protein concentration.* Journal of Agricultural and Food Chemistry, 1995. 43(9): p. 2356-2361.

14. Hermansson, A-M., *Fat and waterholding in functional properties of food macromolecules.* Functional Properties of Food Macromolecules, ed. J.R. Mitchell and D.A. Ledwards. 1986, London and New York: Elsevier Applied Science Publishers.

15. van den Berg, L., et al., *Serum release: The hidden quality in fracturing composites.* Food Hydrocolloids, 2007. 21(3): p. 420-432.

16. Walstra, P., *Physical Chemistry of Foods.* 2003: New York [etc.], US: Marcel Dekker.

17. Mellema, M., et al., *Structure and scaling behavior of aging rennet-induced casein gels examined by confocal microscopy and permeametry.* Langmuir, 2000. 16(17): p. 6847-6854.

18. Verheul, M. and Roefs, S.P.F.M., *Structure of whey protein gels, studied by permeability, scanning electron microscopy and rheology.* Food Hydrocolloids, 1998. 12(1): p. 17-24.

19. Kocher, P.N. and Foegeding, E.A., *Microcentrifuge-based method for measuring water-holding of protein gels.* Journal of Food Science, 1993. 58(5): p. 1040-1046.

20. Weijers, M., Visschers, R.W., and Nicolai, T., *Influence of the ionic strength on the structure of heat-set globular protein gels at pH 7. Ovalbumin.* Macromolecules, 2004. 37(23): p. 8709-8714.

21. Fischer, H., Polikarpov, I., and Craievich, A.F., *Average protein density is a molecular-weight-dependent function.* Protein science : a publication of the Protein Society, 2004. 13(10): p. 2825-2828.

22. Ako, K., et al., *Quantitative analysis of confocal laser scanning microscopy images of heat-set globular protein gels.* Food Hydrocolloids, 2009. 23(4): p. 1111-1119.

4

23.   Renkema, J.M.S., Knabben , J.H.M., and van Vliet, T., *Gel formation by β-conglycinin and glycinin and their mixtures.* Food Hydrocolloids, 2001. 15(4–6): p. 407-414.

24.   van Vliet, T., et al., *Colloidal aspects of texture perception.* Advances in Colloid and Interface Science, 2009. 150(1): p. 27-40.

25.   Srinivasan, G. and Shobha, G., *Statistical texture analysis.* Proceedings of World Academy of Science, Engineering and Technology 2008. 36: p. 1264-1269.

26.   Zayas, J.F., *Functionality of proteins in foods*. 1996: Berlin [etc.], US: Springer.

27.   Tokita, M. and Tanaka, T., *Friction coefficient of polymer networks of gels.* The Journal of Chemical Physics, 1991. 95(6): p. 4613-4619.

28.   Grattoni, C.A., et al., *Rheology and permeability of crosslinked polyacrylamide gel.* Journal of Colloid and Interface Science, 2001. 240(2): p. 601-607.

4

Chapter 5

Relation between gel stiffness and water holding for coarse and fine-stranded protein gels

The aim of this chapter was to investigate the relationship between gel water holding and stiffness for gels with different morphology. For this purpose, gels were prepared from whey protein isolate at varying ionic strength to create fine and coarse-stranded gels. These gels were characterized for their coarseness, stiffness and water holding. Water holding was measured both as a function of time and applied pressure. Increased gel coarseness in both fine and coarse gels resulted in a larger extent of network deformation. For fine gels, the coarseness of the gel was shown to be dominant in water removal. In the case of coarse gels, coarseness and stiffness had a counteracting effect, but coarseness was still dominant. These results show that the interplay of tuning coarseness of protein networks independent of stiffness provides a balanced tool to set the water holding in food gels.

Keywords: Young's modulus, gel coarseness, gel stiffness, water holding, WPI gels, effective gel permeability coefficient, effective water flux coefficient

5.1   Introduction

To better understand sensory perception of foods, studies of water exudation from protein-based gels are of high importance. Understanding the structural origins that determine water holding is therefore essential to allow design of food products with a predicted oral perception. The water exudation (water loss) from the gel is determined by the water holding capacity of the gel under applied pressure. Water holding (WH) of a gel has been reported to be determined by the gel microstructure [1-3] and gel stiffness [4].

Gel microstructure formation is directed by net repulsive forces among denatured proteins during aggregation [5]. Depending on these forces, globular proteins can form gels varying in microstructure from fine to coarse-stranded [6-8]. When electrostatic repulsion dominates, the network will be composed of fine strands with a diameter in the order of nanometers [5], for which the threshold is the size of the individual protein molecule of roughly 3-5 nm [9]. When attractive forces are more dominant, a coarser network is formed. Coarse-stranded networks are composed of relatively large particulate (spherical) aggregates with diameters in the range of 0.1 – 1 µm [6, 10], as determined by e.g. the type of protein, protein concentration, pH, ionic strength, type of salts etc. The different networks can be characterized by means of coarseness which is defined as the structural inhomogeneity pictured in the microscopy images.

The relation between gel coarseness and WH has been described for different protein systems and attempts to link WH to typical length scales in the network have been made [2, 3, 11-15]. When gels with different microstructures were studied, gel coarseness was dominant in determining WH [2, 3].

The length scale, at which no water can be removed from the gel, seems to be generic for globular proteins and is reported to be below 0.1µm [4, 16, 17]. The length scale where pronounced water loss is apparent is protein specific [3, 4]. Hermansson reported that pore sizes, as a representative for coarseness, in the range of 0.1 to 2 µm are relevant for whey protein gels WH [17]. More recently, for ovalbumin gels it was reported that pronounced water loss occurs at typical length scales in the network ranging from 0.1 to 0.45 µm [4], while for soy protein gels, length scales from 0.3 to 4.7 µm were identified [3].

Once WH is studied under applied deformation, not only gel coarseness, but also gel stiffness is said to become important. The extent by which a gel network deforms upon applied force is crucial for removal of water [16]. The impact of gel stiffness on water removal was reported for both ovalbumin and soy gels in **Chapters 2** and **4**. In the case of ovalbumin, an apparent positive correlation between WH and stiffness (represented by Young's modulus) was shown [4], while the opposite correlation was shown for soy protein gels [2]. These observations suggest that the role of network stiffness and WH relation is gel morphology specific, and the mechanism for water removal may be different for coarse and fine-stranded gels.

Coarse and less stiff gels have a higher effective water flux, and are easier affected by applied pressure [4] while less coarse and stiff gels have a lower effective water flux, and are more resistant to deformation. Less coarse and stiff gels require more energy for deformation of the network, as well as higher applied pressure to overcome high capillary forces to remove water. The cooperative effect of coarseness and stiffness allows one to tailor gels with similar WH, but different in effective water flux (water removal kinetics). An understanding of the interplay between the effect of coarseness and stiffness on WH in fine and coarse gels would in the end allow one to control and tune the perception of juiciness [18] and the release of tastants from food products.

Since the relation between gel morphology, stiffness and coarseness is still not well understood, the objective of this chapter was to investigate the relationship between WH and stiffness for fine-stranded and coarse gels to get insight in water removal mechanism from the gel. For this purpose, whey proteins were chosen for their ability to form stiff gels, and a variation in coarseness from nanometer to micrometer scales was obtained by varying ionic strength during network assembly. These gels were characterized for their microstructure, their stiffness and their water holding, as a function of time and pressure.

5.2   Material and Methods

5.2.1   Material

Whey protein isolate (WPI) Bipro was obtained from Davisco Foods International, Inc. (Le Sueur, USA) and contained about 94 % (w/w) whey protein, 5 % (w/w) moisture and 1 % (w/w) ash. Sodium chloride (NaCl) was purchased from Sigma-Aldrich (Steinhem, Germany). MilliQ water was used for preparing solutions. Reagents were of analytical grade and used without further purification.

5.2.2   Preparation of gels

WPI was dissolved in milliQ water to 14% (w/w) concentration at pH 7.2. The protein solution was stirred overnight at room temperature to achieve complete protein solubilisation. The protein solution was mixed with different NaCl concentrations ranging from 0 to 300 mM. The protein solution prior to gelling was de-aerated under vacuum for 5 min (vacuum pump MZ 2C NT, Vacuubrand, Wertheim, Germany). Gelation was performed in 20 ml syringes (20 mm in diameter), pre-lubricated with paraffin oil to facilitate removal of the gel, and closed airtight to reduce air bubble formation during heating. The samples were incubated at 95°C for 30 min in a water bath and subsequently cooled overnight at room temperature. Every sample was prepared at least in duplicate.

5.2.3   WH measurements at given time and pressure

The centrifugation procedure of gels was adapted from Kocher and Foegeding [19]. A microcentrifuge filtration unit was composed of an inner spin tube and a 2 ml Eppendof tube (Axygen Biosciences, Inc., Union City, USA). Gels were cut in 10 mm high and 4.8 mm

5

diameter cylinders using a cork borer and carefully placed on the bottom of the spin tube. The bottom of the spin tube was covered with a 5.5 mm diameter filter paper to reduce grid size. Centrifugation was performed at 20 – 3000 relative centrifugal forces (RCF) for 10 to 40 min at 20°C. Expulsed serum (water loss) from the gel was collected at the bottom of the Eppendorf tube. The WH was defined as the percentage of water in the gel remaining after centrifugation according to

$$WH = \frac{W_T - W_{RCF}}{W_T} \cdot 100 \quad (\%) \tag{5.1}$$

where W_T is the total initial amount of water in the sample and W_{RCF} denotes the amount of water removed from the sample at a given RCF. Measurements were performed in duplicate.

To evaluate the magnitude of pressure applied on the gel, RCF was converted to applied pressure (P) in Pascal (Pa) as follows:

$$P = \frac{(V_s \cdot \varnothing_{protein} \cdot \rho_{protein} + V_s \cdot \varnothing_{water} \cdot \rho_{water}) \cdot RCF \cdot g}{A} \tag{5.2}$$

where V_S is the volume of the sample (m³), $\varnothing$ is the volume fraction of proteins or water in the sample, $\rho_{protein}$ = 1350 kg/m³ [20], ρ_{water} = 1000 kg/m³, g is gravitational acceleration (9.8 m/s²), and A is the area of the cylinder top surface (m²). As an example, 100 RCF is equivalent to 10 kPa applied on the gel. Using above described experimental set-up, WH of gels was measured (i) as a function of applied pressure (P) for fixed time (1 min, 2 min, 3 min etc. up to 40 min), and (ii) as a function of time (t), for a fixed pressure (20 RCF, 50 RCF, 100 RCF up to 1000 RCF). Obtained WH versus applied pressure (P) at fixed times, and time (t) at fixed applied pressures were fitted using the following equation assuming a single exponential decay

$$WH = A_{max} \cdot exp^{-k_i f(P,t)} + B \tag{5.3}$$

from where the fitting parameters A_{max} represents the maximum percentage of water that can be removed from the system and B represents the percentage of water remaining in the gel. Determined parameter k_i describes the kinetics, either as a function of applied pressure or time. The fitting parameter k as a function of pressure at fixed different times is denoted as $k1$ and represents the gel permeability coefficient. The parameter k as a function of time at different applied pressures is denoted as $k2$ and reflects the water flux from the gel [4]. Plots of $k2$ over applied pressure (P) for different gels were used to obtain the slope (d$k2$/dP) using Origin60. The data for fine gels was fitted with a linear relation using simple linear regression. The data for coarse gels was fitted using

$$k2 = a \cdot e^{-\frac{b}{P}} \tag{5.4}$$

where b is taken as the slope (d$k2$/dP), which represents a pressure dependent flux from the gel determined by the morphology of the gel.

5.2.4 Confocal laser scanning microscopy (CLSM)

CLSM was used to obtain information about the microstructure. 12% (w/w) protein solution was mixed with fluorescent dye Rhodamine B to a final dye concentration of 0.001% (v/w). Samples for microstructural analysis were gelled in glass cuvettes using 125 μl Gene Frame adhesive system (Fisher Scientific, Loughborough, UK). Imaging of the samples was performed using a Leica TCS-SP5 confocal laser scanning microscope (Leica Microsystems (CMS) GmbH., Mannheim, Germany). Leica objective lenses HC PL APO 20x/0.70 IMM/ CORR CS and HCX PL APO 63x/1.20 W CORR CS were used. The excitation wavelength and emission spectral regime of Rhodamine B was 561 nm and 570-725 nm, respectively.

5.2.5 CLSM image analysis

The pair correlation function is used to obtain a value for the typical length scale within the system. CLSM images were analyzed to obtain a pair correlation function, $g(r)$, of the protein concentration as a function of the distance r using the procedure described by Ako et al. [21]. Pair correlation functions, $g(r)$, were fitted assuming a stretched exponential decay [21] according to

$$g(r) = B \cdot exp^{-\left(\frac{r}{\xi}\right)^{\beta}} + 1 \qquad (5.5)$$

where B, ξ and β are fitting parameters. The parameter ξ represents the correlation length, which can be seen as a representative of the typical length scale of the network. Theoretically, the minimum value of distance (r) that can be detected by CLSM is 0.3 μm (63x water immersion objective). σ^2, which is $g(r = 0.3$ μm) - 1) is used as an indication of the heterogeneity of the gels and is valid for the case where pictures imaged in the presence of constant protein and fluorescent dye concentrations are compared. The fitting parameter B represents σ^2 at $r = 0$.

5.2.6 Scanning electron microscopy (SEM)

Gels were cut in 1.3 cm high and 1 cm diameter cylinders using a gel slicer and a cork borer and placed for 8 h into an aqueous 2.5% (v/v) glutaraldehyde solution for crosslinking of the proteins. After crosslinking, excess of glutaraldehyde was removed by placing gel pieces in demineralized water overnight. Samples were gently rotated during the process. Demineralized water was subsequently replaced for acetone in a few steps. Gel pieces in acetone were dried by critical point drying (CPD), fractured and attached on sample holders with CCC Carbon Adhesive (Electron Microscopy Sciences, Washington, USA). After evaporation of the solvent from the adhesive the samples were sputter coated with a 15 nm thick layer of iridium (MED 020, Leica, Vienna, Austria) and analyzed in a field emission scanning electron microscope (Magellan 400, FEI, Eindhoven, the Netherlands) at a working distance of about 4 mm, with SE detection at 2 kV and 6.3 pA. The digital images were contrast optimized with Photoshop CS5.

5.2.7 SEM image analysis

ImageJ 1.49d was used as a tool to measure building block sizes (aggregate size) visualized in SEM images at magnifications of 20,000, 100,000 and 200,000. On average 15 images were analyzed per gel. Building block sizes were obtained by direct visual inspection of the gel and are representative numbers over the different magnifications and multiple spot analysis in each of the images. The derived building block sizes were averaged.

5.2.8 Large deformation rheology

14% (w/w) WPI gels were sliced with a gel slicer into cylinders of 20 mm in height and 20 mm in diameter. Fracture stress and fracture strain were measured by uniaxial compression with an AP-501 rheometer (Anton Paar, Graz, Austria) mounted with a 50 kg load cell. Paraffin oil was applied on top and bottom of the gel to prevent friction during compression. Gel samples were compressed to 90% of their initial height between two parallel plates at a constant deformation rate of 1 mm/s. Measurements were performed at 20°C in triplicate. The Young's modulus, E, was calculated from the linear part of the stress over strain curve within the region of 0.05-0.15 of true fracture strain, and the mean values of fracture stress and strain were calculated as described by Renkema et al. [22]. At a compression speed of 1 mm/s, the deformation needed to determine the Young's modulus is faster than the stress relaxation process of the material [23], and therefore the modulus is not influenced by changes in the network.

5.3 Results and discussion

5.3.1 Gel microstructure

To study the relation between gel stiffness and WH for fine-stranded and coarse protein gels, a range of gel morphologies was obtained by keeping protein volume fraction constant and varying ionic strength. Heat treatment of a 14% (w/w) WPI solution (pH 7.2) in the presence of 0-300 mM NaCl resulted in heat-set gels varying from transparent to opaque in their visual appearance. Obtained gel microstructures were visualized at different length scales ranging from centimeter to nanometer and are shown in **Figure 5.1**. In the images representing a length scale of 50 micrometer, no individual structural units can be distinguished in gels up to 100 mM NaCl additions. Above 100 mM NaCl, structural inhomogeneity became apparent. Differences in building block sizes and in their connectivity between gels containing 0-100 mM NaCl were best observable on 0.5 micrometer length scale (last column of **Figure 5.1**). Gels with NaCl concentration above 100 mM are composed of building blocks that were already observable on the 5 micron length scale. At these salt concentrations, aggregates composing the network became larger and more spherical (**Figure 5.1**, SEM images). Overall, 14 % (w/w) WPI gels prepared in the presence of up to 100 mM NaCl increased in coarseness on sub-micron length scale, and for salt additions above 100 mM on micrometer scale.
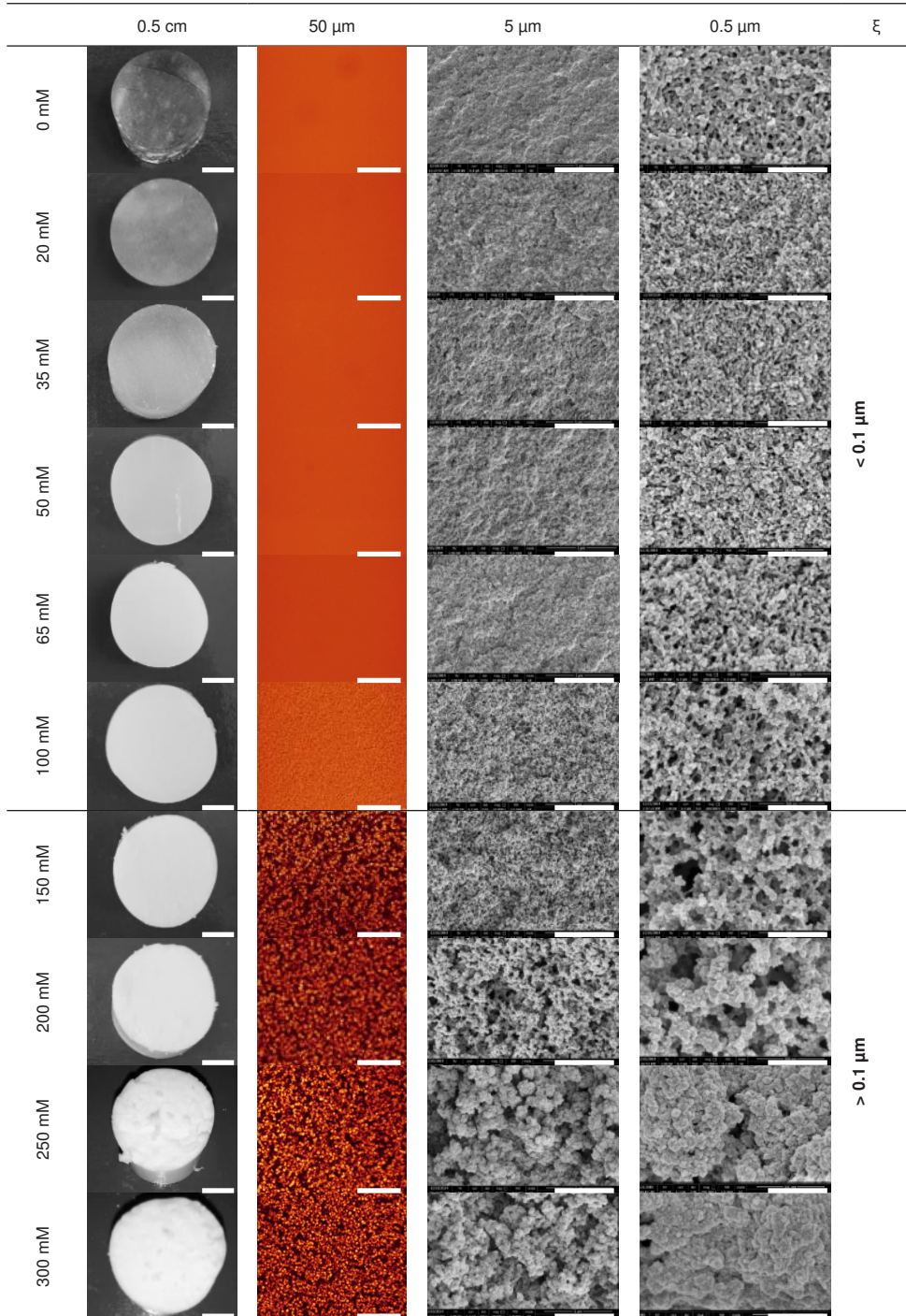
Figure 5.1 Microstructure of 14% (w/w) WPI gels at pH 7.2 in the presence of 0-300 mM NaCl at different magnifications. The indicated length scales correspond to the bar in the images.

To obtain a quantitative measure for gel coarseness, two different image analysis methods were used, depending on the length scales at which structural units could be seen. First, fine structures (0-100 mM NaCl gels) were analyzed manually for typical aggregate building block sizes visualized in SEM images. Second, the correlation length (ξ) of the structures seen in CLSM images (150-300 mM gels) was analyzed by means of the pair correlation function. A decrease of the correlation function is related to intensity fluctuations, reflecting the morphology of the gel [21]. Obtained coarseness parameter over increased salt concentration is shown in **Figure 5.2**. From the figure it can be seen that gel coarseness increased with increasing ionic strength. Gels in the presence of up to 100 mM NaCl increased in coarseness from 0.03 to 0.1 µm, which will be further referred to as fine-stranded gels. Increasing the salt concentration from 100 to 150 mM NaCl resulted in a large increment in the coarseness parameter from 0.1 to 1.6 µm. Gels prepared in the presence of 150-300 mM NaCl increased in coarseness from 1.6 to 2.0 µm, and will be referred to as coarse gels. A plateau in coarseness was observed for gels with 250-300 mM NaCl. In agreement with literature, a threshold in coarseness of 0.1 µm is used to differentiate between fine and coarse-stranded gels [5, 6, 11, 24, 25].
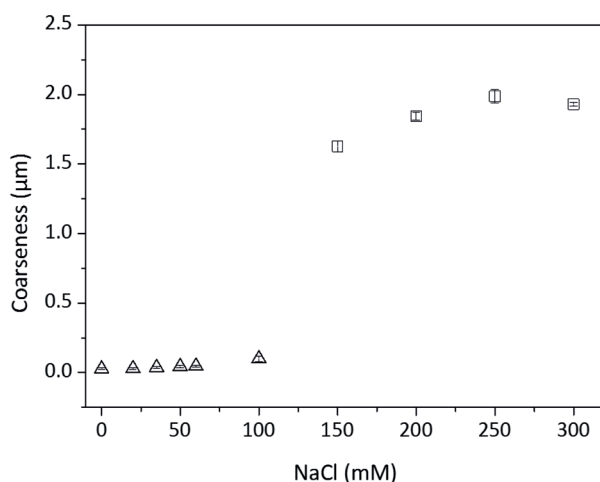

Figure 5.2 Gel coarseness of 14% (w/w) WPI gels at pH 7.2 prepared in the presence of 0-300 mM NaCl: (Δ) typical aggregate building block sizes analyzed manually from SEM images, and (□) correlation length (ξ) of gel microstructure visualized in CLSM images.

5.3.2 Mechanical responses

Large deformation rheology of the different 14% (w/w) WPI gels was performed to determine the Young's modulus. Young's modulus reflects the stiffness of the material and is presented in **Figure 5.3**. An optimum in the Young's modulus can be observed for the gel containing 150 mM NaCl. The increase in the Young's modulus with increasing NaCl concentration, followed by a decrease at higher NaCl concentrations, is in accordance

with literature [4, 26]. The addition of salt reduces electrostatic repulsion between proteins by screening of charges, leading to aggregation upon protein denaturation, and therefore coarser gel microstructures are formed. The optimum in the modulus can be explained by two opposing contributions. Increasing coarseness yields thicker strands and thereby an increase in the Young's modulus. However, when strands increase in thickness even further, this results in a lower number of connectivity points in the network (**Figure 5.1**, 0.5 µm scale). These microstructural changes are then reflected in a decrease in the Young's modulus. Accordingly, gels with 50 mM and 250 mM NaCl added are good examples of the interplay between these contributions, as they are comparable in Young's modulus (**Figure 5.3**) but differ largely in coarseness (**Figure 5.1**).
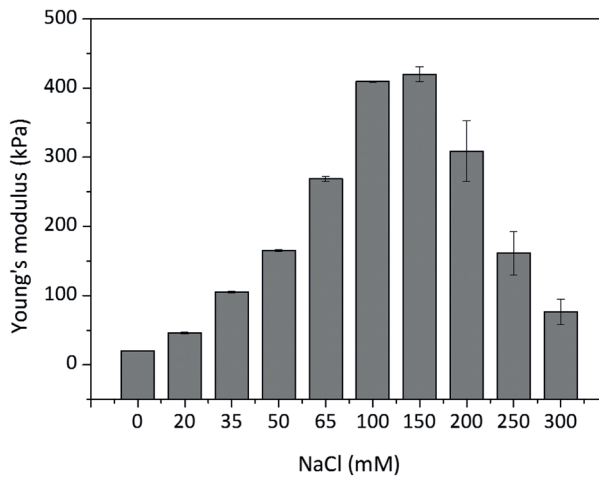

Figure 5.3 Young's modulus of 14% (w/w) WPI gels at pH 7.2 prepared in the presence of 0-300 mM NaCl.

5.3.3 Water holding

The water holding results for 14 % (w/w) WPI gels containing 0-300 mM NaCl centrifuged for 10 min to remove water are shown in **Figure 5.4**. Exposing samples to 10 min of centrifugation reflects the equilibrium state between applied pressure and removed water [4]. From the graph it can be seen that almost no water could be removed from the gel containing no salt. Increasing salt concentrations up to 300 mM decreased WH from 95% to 50 %. Gels prepared in the presence of 0-150 mM NaCl have a more linear dependence between measured WH and applied pressure but differed in the final WH measured at maximum forced applied (300 kPa). Gels above 150 mM NaCl addition have a more exponential relationship between measured WH and applied pressure, and resulted in comparable final WH at maximum pressure applied.

5.3.4 WH and gel morphology

The obtained WH data (**Figure 5.4**) were fitted using equation 5.3 to derive A_{max}, the

maximum amount (%) of water that can be removed from the gel (equals 100% - WH). A_{max} was plotted over gel coarseness (**Figure 5.2**) and gel stiffness (**Figure 5.3**), and is presented in **Figure 5.5**. From **Figure 5.5A** it can be observed that with increasing coarseness more water is removed from the gel. A clear distinction between fine gels with correlation length below 0.1 µm and coarse gels with a correlation length above 0.1 µm can be noted. The increase in correlation lengths of imaged gels from 0.03 to 0.1 µm resulted in a pronounced water loss from 5 up to 30%. Gels with higher correlation lengths of 1.6-2.0 µm had a water loss of 40-50%. From the graph it can be seen that above a coarseness of 1.9-2.0 µm no more water can be removed from the gel, which can be referred to as the upper limiting length scale, as reported earlier in **Chapter 4**.
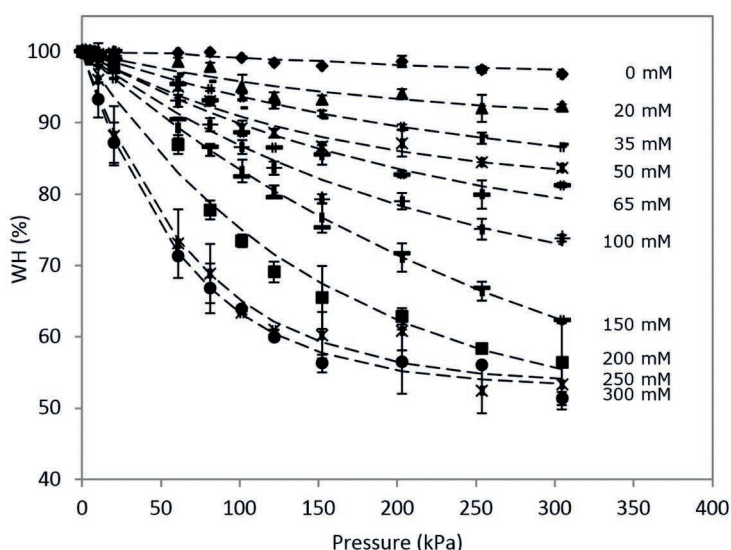

Figure 5.4 WH of 14% (w/w) WPI gels containing 0-300 mM NaCl centrifuged for 10 min at different centrifugal forces. The corresponding pressure (kPa) has been calculated as described in **Material and Methods section 5.2.3**. The dashed lines represent the fittings obtained using equation 5.3.

How A_{max} is affected by gel stiffness (Young's modulus) is shown in **Figure 5.5B.** The results display two distinct regimes. From the graph it can be seen, that fine-stranded WPI gels with length scale below 0.1 µm had a positive correlation between removed water and gel stiffness, while coarser gels with a correlation length above 0.1 µm had a negative correlation; both relations appear linear. In different coarse protein gels ($\xi > 0.1$ µm), both positive and negative correlations between stiffness and A_{max} have been observed, but the nature of this phenomenon is not clarified [2-4]. A positive correlation between removed water (A_{max}) and gel stiffness was reported for 10% (w/w) heat-set soy protein gels prepared in the presence of 0-100 mM $MgSO_4$ and $MgCl_2$ salts, as discussed in **Chapter 2**. A negative correlation between A_{max} and gel stiffness was indicated for 12% (w/w) heat-set ovalbumin gels prepared in the presence of 0-300 mM NaCl (**Chapter 4**), and for 10%

(w/w) succinylated soy protein gels prepared in the presence of 100 mM $CaCl_2$ or $CaSO_4$, in which the coarseness was varied by the degree of protein succinylation (**Chapter 3**). From literature, it could be suggested that the observed correlations are protein specific, but the results presented in **Figure 5.5B** suggests that the relation between removed water and stiffness is not protein specific, but morphology dependent.

A

B
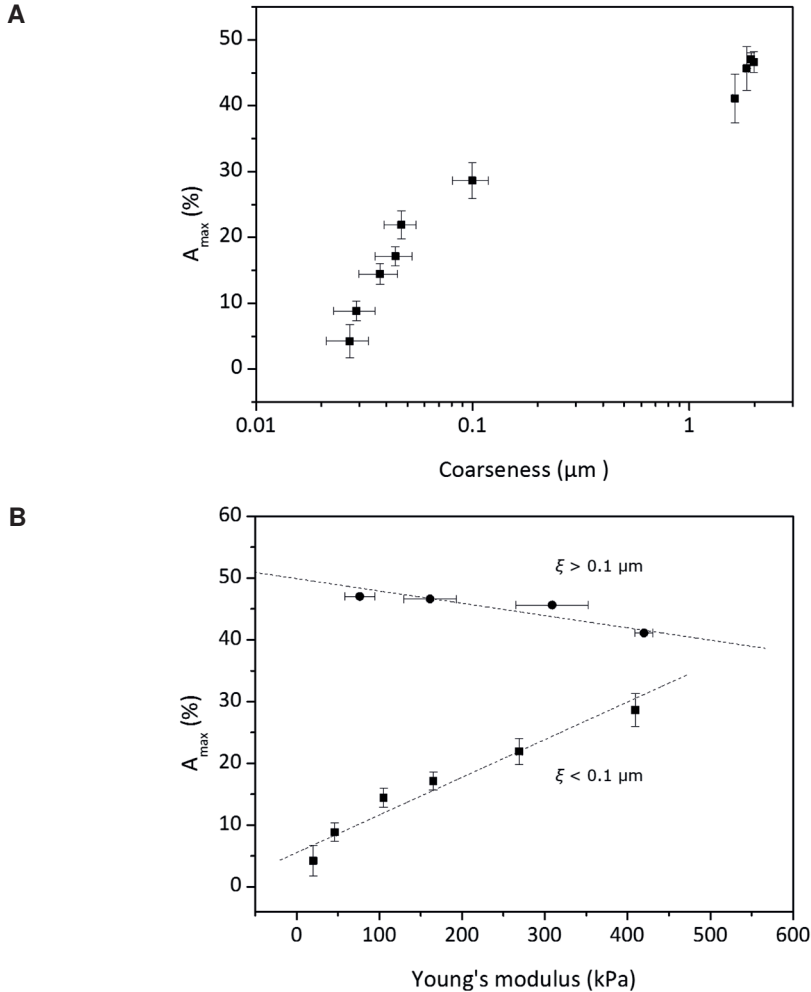
Figure 5.5 Panel A shows maximum removed water A_{max} (%) over coarseness for 14% (w/w) WPI gels prepared in the presence of 0-300 mM NaCl. Panel B shows A_{max} (%) over Young's modulus (kPa) for fine ($\xi < 0.1$ μm) and coarse ($\xi > 0.1$ μm) gels, shown in **Figure 5.1**.

5.3.5 Effective gel permeability coefficient for fine and coarse gels

Measuring WH over a range of applied pressures at different fixed times of the different gels allows one to obtain the fitting parameter k using equation 5.3. Fitting parameter $k1$,

denoted as the effective gel permeability coefficient, was further used to compare changes in gel WH under applied pressure in time. The effective gel permeability coefficients are shown in **Figure 5.6**, where panel A shows $k1$ for fine gels with coarseness below 0.1 µm, and panel B $k1$ for coarse gels with length scale above 0.1 µm. In both coarseness regimes $k1$ increased with increasing centrifugation time, indicating morphology changes with increasing applied force. The $k1$ increment in time was exponential, for which the steady state (plateau value) was reached after 5-10 min. Such a change in permeability has been observed before for other protein gels. For example, for 12% (w/w) ovalbumin gels the increment in $k1$ in time was shown to be stepwise, which was linked to a yielding phenomenon of the gel network [4].
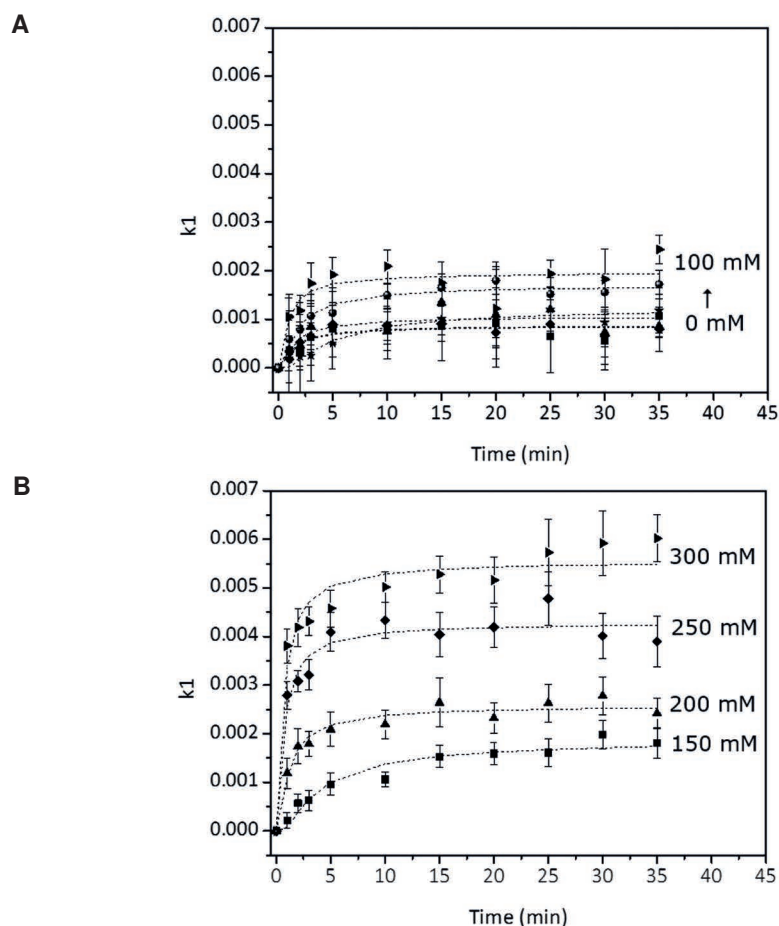

Figure 5.6 Effective gel permeability coefficient ($k1$) as a function of time for 14% (w/w) WPI gels prepared in the presence of 0-300 mM NaCl: (A) fine gels with length scale < 0.1 µm and (B) coarse gels with length scale > 0.1 µm. Dotted lines represent fitting obtained using equation 5.4.

In the steady state regime (10 min centrifugation), compression of the network has been completed and microstructural rearrangements and perhaps fracture events have taken place [4]. Comparison of plateau values of gels with different coarseness's suggests that increasing coarseness results in higher effective gel permeability. Effective gel permeability ($k1$) at 10 min (steady state) plotted over coarseness of the gels for both coarseness regimes, below 0.1 µm (**Figure 5.7A**) and above 0.1 µm (**Figure 5.7B**), show a positive correlation, where coarser gels had higher effective permeability coefficient. For both regimes, $k1$ is in the range between 0.0005 and 0.005. These values for permeability are much higher than those found for other protein gels, such as $k1$ values reported for 12% (w/w) ovalbumin gels (**Chapter 4**), which are 100 times lower compared to those obtained for WPI gels [4]. The lower $k1$ values for the ovalbumin gels cannot be explained by coarseness only, since the coarseness of the gels (0.09-0.45 µm) fall within the range of the coarseness of the WPI gels. Based on these observations it is expected that the magnitude of $k1$ is defined not only by coarseness, but also by gel stiffness and by the connectivity of pores. Higher connectivity between neighboring pores could lead to a more effective channeling of the water phase and therefore higher permeability.

To illustrate the effect of gel stiffness on $k1$ for both fine and coarse gels, $k1$ measured at 10 min (steady state) was plotted over the Young's modulus as presented in **Figure 5.7C** and **D**. From **Figure 5.7C** it can be observed that in fine gels, $k1$ appears to slightly increase with increasing gel stiffness, however the standard deviations of $k1$ is too large to substantiate this. An increase in $k1$ with increased gel coarseness as shown in **Figure 5.7C** suggests that permeability in fine gels is dominated by coarseness and not by stiffness. In coarse gels (**Figure 5.7D**) a negative correlation between $k1$ and gel stiffness was found. Less stiff gels had higher effective gel permeability. A decrease in $k1$ in coarser and more deformable gels could be caused by decreased porosity or network densification caused by gel deformation. At the same time, these results could indicate that energy is used for deformation of the gel, and therefore not for water removal.

5.3.6 Effective water flux coefficient for fine and coarse gels

WH data obtained by measuring WH over the range of different times at different fixed pressures of gels in the presence of 0-300 mM NaCl were fitted to equation 5.3. $k2$, denoted as effective water flux coefficient, was further used to compare the water flow in gels under applied pressure in time (**Figure 5.8**). From the graphs it can be observed that the trend of $k2$ in fine (**Figure 5.8A**) and in coarse gels (**Figure 5.8B**) is very different. In fine gels, $k2$ values are low (up to 0.1) and show a linear relation with pressure, whereas in coarse gels, $k2$ values are much higher (between 0.1 and 1.0) and a non-linear relation with pressure is apparent. In fine gels (**Figure 5.8A**), a minimum pressure of 500 kPa was needed to initiate water flux. The linear relation that is apparent above this pressure threshold, suggests that the gel behaves as a rigid porous medium, where the velocity of the fluid in the stationary state is linearly proportional to the applied pressure [27]. In rigid materials, no energy is used for deformation of the gels, and therefore all energy can be used for water removal.

5

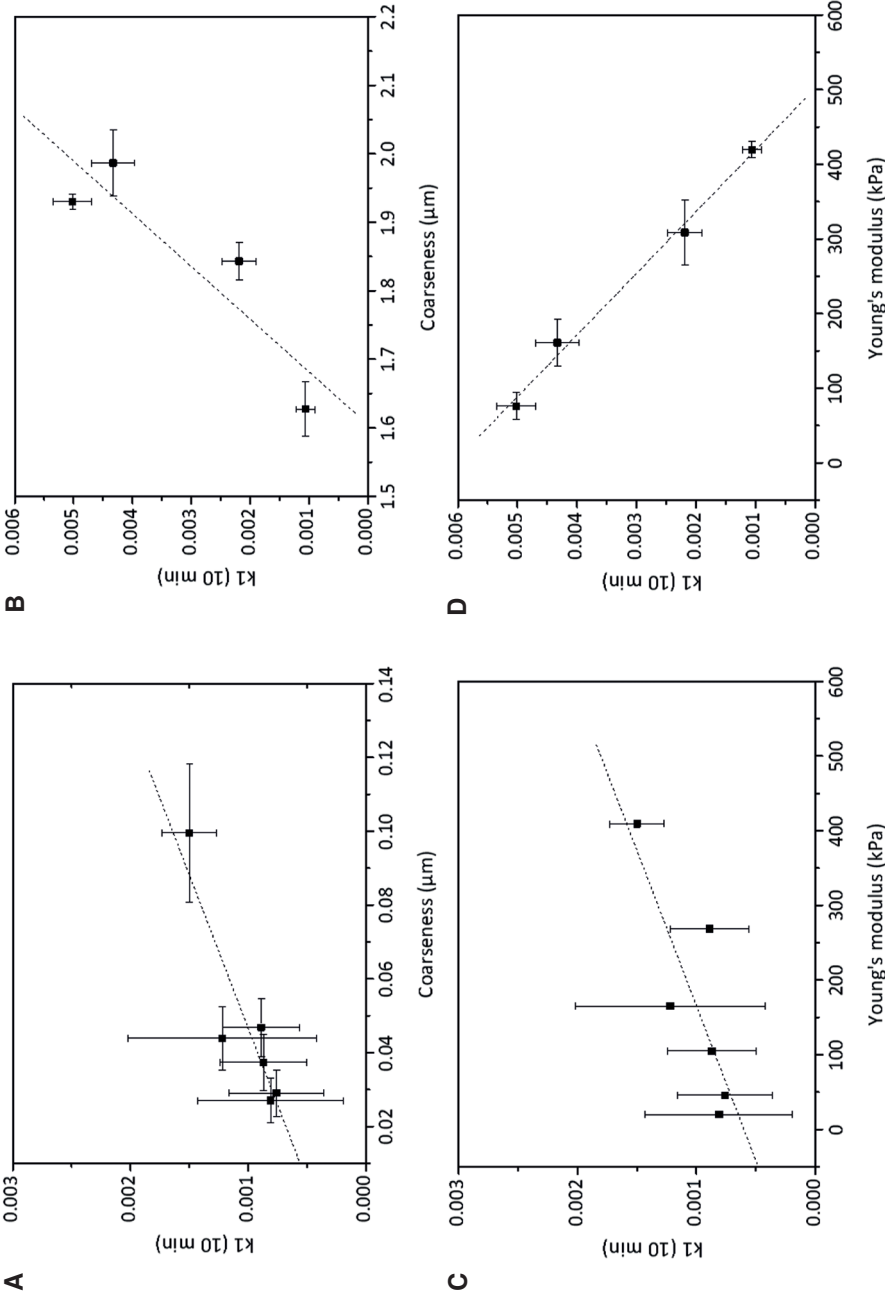**Figure 5.7** A plot of gel permeability coefficient (*k1*) over coarseness measured at 10 min (steady state) for (A) gels with coarseness > 0.1 μm. A plot of *k1* over Young's modulus measured at 10 min (steady state) for gels with coarseness < 0.1 μm and (B) gels with measured correlation length (C) below 0.1 μm, and (D) with correlation length above 0.1 μm. In all plots the dotted lines are added to guide the eye.

Figure 5.8 Effective water flux coefficient ($k2$) as a function of pressure for 14% (w/w) WPI gels prepared in the presence of 0-300 mM NaCl: (A) gels with coarseness < 0.1 μm and (B) gels with coarseness > 0.1 μm. Dotted lines represent fitting obtained using equation 5.4.

For coarse gels (**Figure 5.8B**), it can be observed that higher applied pressures resulted in an increase in water flux ($k2$), followed by a leveling-off of the curves to a constant value for $k2$. The non-linear relation between the water flux and applied pressure indicate that force-dependent structural changes occur in these coarse gels. Such behavior has been discussed before [28] and was suggested to represent gel deformability [4]. The contribution of coarseness to the effective water flux coefficient ($k2$) is shown in **Figure 5.9A** and **B**. A similar dependence is observed for both fine and coarse gels, where higher coarseness leads to higher $k2$, in agreement with above discussed results (coarseness relation to $k1$).

5

Figure 5.9 A plot of $k2$ over coarseness measured at 1000 kPa (steady state) for (A) gels with coarseness < 0.1 μm and (B) gels with coarseness > 0.1 μm. A plot of $k2$ over Young's modulus measured at 10 min (steady state) for gels with measured correlation length (C) below 0.1 μm, and (D) with correlation length above 0.1 μm. In all plots the dotted lines are added to guide the eye.

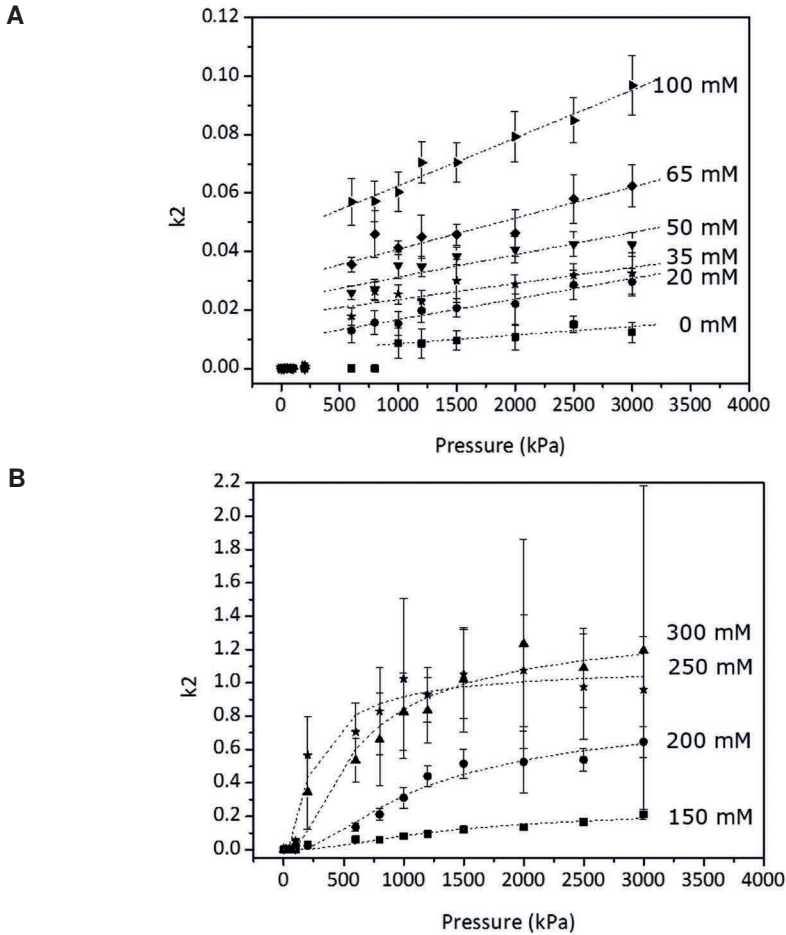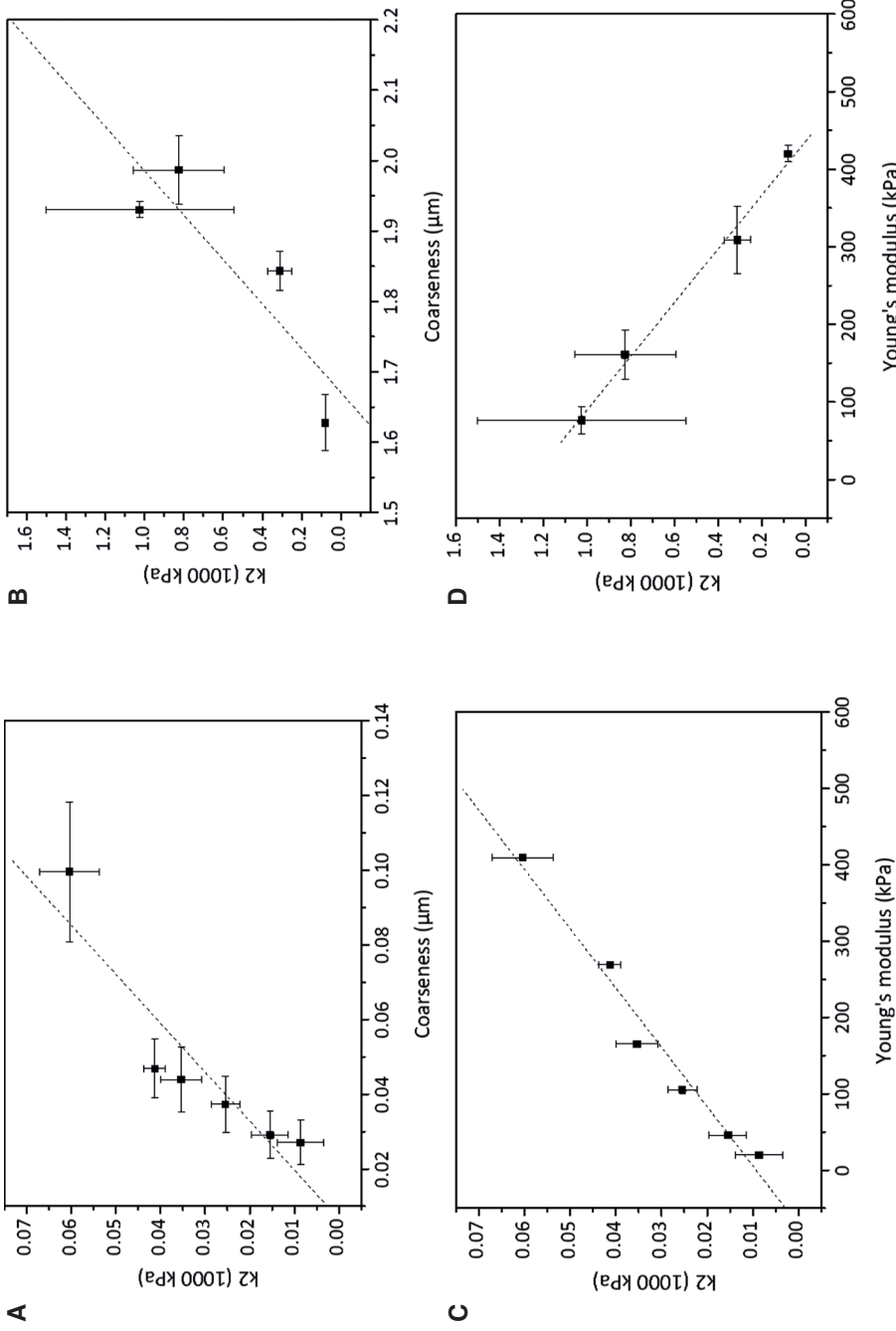The effect of gel stiffness on the effective water flux coefficient ($k2$) is presented in **Figures 5.9C** and **D**. From these graphs it can be seen that in the case of fine gels (**Figure 5.9C**), a higher water flux coefficient is seen for an increase in gel stiffness. In fine gels, small changes in gel permeability occur (**Figure 5.7C**), while the water flux significantly increases (**Figure 5.9C**). An increase in water flux with applied pressure, while permeability remains similar, indicates that coarseness is a dominant parameter in water removal from the fine gels. The applied energy is used for water removal rather than for network deformation.

In the case of coarse gels (**Figure 5.9D**), stiffness yields a lower water flux coefficient, i.e. for stiffer gels water removal becomes more difficult. An increasing stiffness leads to a decrease in gel permeability and decreased water flux from the gels. Decreased water flux in stiff gels indicates that removal of water is more difficult even though more energy is applied. In this case, the energy applied is directed to network deformation, and thus less energy can be used for water removal.

5.3.7 Effect of gel deformability in fine and coarse gels

From the above it follows that for coarse gels, the energy exerted is partly used for the deformation of the gel instead of water removal. Depending on the amount of pressure applied, the deformation of the gel will be different, which will also affect the ease of water removal. Therefore, the pressure-dependent water flux, defined as the change in water flux over pressure ($dk2/dP$), also represents the deformation of the network. This deformation is represented by the slopes in **Figures 5.8A** and **B**. For fine gels, the slope (> 500kPa) is constant for the entire pressure range used, but for coarse gels, the slope is pressure-dependent. To illustrate the extent of deformation (deformability) for these coarse gels, equation 5.4 can be applied. The $dk2/dP$ values are plotted in **Figure 5.10** as a function of the coarseness and the stiffness of the gels. For fine gels, it can be observed that the values for $dk2/dP$ are small, indicating a limited extent of deformation. However, for coarse gels, values for $dk2/dP$ are much higher.

When evaluating the effect of gel coarseness on the deformability of the gel, more coarse gels are deformed to a larger extent in both fine (**Figure 5.10A**) and coarse gels (**Figure 5.10B**). The extent of deformation in fine gels is smaller compared to coarse gels, as is evident from the lower (by almost a factor 20.000) values for $dk2/dP$ over coarseness, as indicated in **Table 5.1**.

When evaluating the contribution of gel stiffness to the deformability of the gels (**Figures 5.10C** and **D**), it can be observed that in fine gels $dk2/dP$ has a positive correlation with gel stiffness, while for coarse gels there is a negative correlation. For coarse gels, the extent of gel deformation decreases with increased gel stiffness, i.e. less stiff gels are easier and more deformable compared to more stiff gels. As more energy is used for the deformation of the gel, less energy is available for water removal. For the fine gels, a small increase in the extent of deformation can be noted with respect to the coarseness. $dk2/dP$ over the Young's modulus (increased stiffness) for fine gels is almost a factor of 1000 lower as compared to coarse gels (**Table 5.1**).
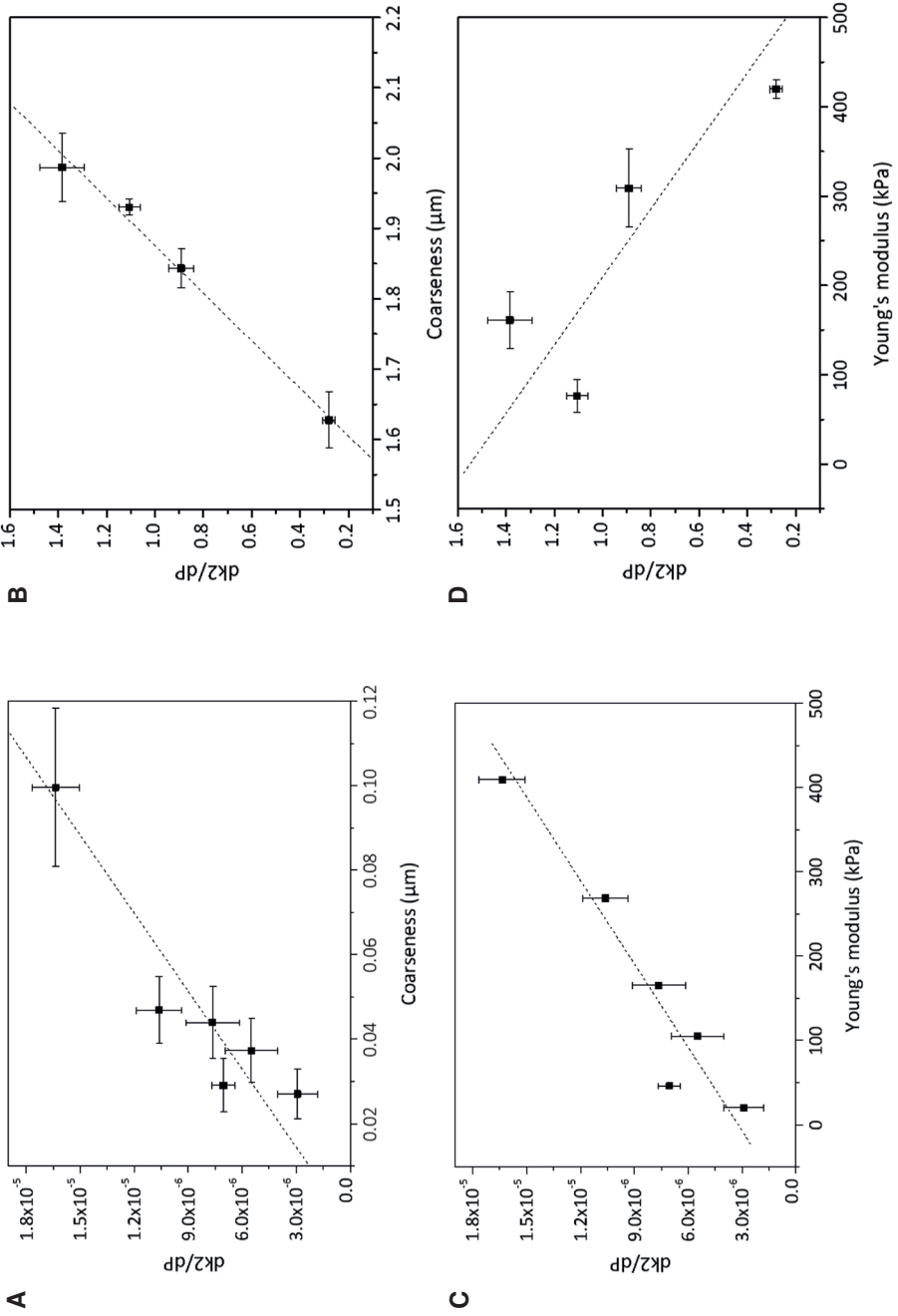
5

Figure 5.10 The extent of deformation (deformability), represented by d*k2*/d*P*, over coarseness for fine gels (panel A) and coarse gels (panel B), and Young's modulus for fine gels (panel C) and coarse gels (panel D).

Table 5.1 Slopes of linear fitted data in **Figure 5.10**, where *C* stands for the coarseness and *E* for the Young's modulus.

	d(d$k2$/dP)/ dC	d(d$k2$/dP)/ dE
Fine gels	$1.6 \cdot 10^{-4}$	$3.2 \cdot 10^{-6}$
Coarse gels	3.0	$-2.6 \cdot 10^{-3}$

These results suggest that in the case of fine gels, gel network deformability has a negligible role and therefore also the stiffness of the gels is of minor importance. For these gels, the coarseness of the gel is dominant in water removal. In coarse gels, the extent of deformation and therefore also the stiffness does contribute to water removal from the gel. For coarse gels with increased stiffness, the lower extent of deformation leads to an increase in the water removal, while an accompanying decrease in the coarseness leads to a decrease in the water removal. For the coarser gels, the contributions of stiffness and coarseness have a counteracting effect. As there is still a positive relation between water removal and coarseness (**Figure 5.5**), it can be concluded that in this case coarseness is still dominant.

5.4   Conclusions

Water removal is dependent on the morphology of gels, which is defined by both the coarseness and the stiffness of the gel network. The amount of pressure applied affects the deformation of the gel and thereby the ease of water removal. In the case of fine-stranded gels, deformation of the gel was found to be negligible and therefore also the stiffness of the gels is of minor importance for water removal. For fine gels, the coarseness of the gel is the dominant parameter. In the case of coarse gels, gels with increasing coarseness (less stiff gels) have a much larger extent of deformation compared to fine gels. Therefore, in coarse gels, the extent of deformation (deformability) and the stiffness of the network are important parameters in water removal from the gel. For gels with increased stiffness, the lower extent of deformation leads to an increase in the water removal, while an accompanying decrease in the coarseness leads at the same time to a decrease in the water removal. In the case of coarse gels, the contributions of stiffness and coarseness have a counteracting effect, but coarseness was found to be still dominant in water removal. These insights could be exploited in product development to predict and tune water holding or oral processing and sensory perception of (new) products.

5.5   Acknowledgements

5

References

1.   Hermansson, A-M. and Lucisano, M., *Gel characteristics—water binding properties of blood plasma gels and methodological aspects on the waterbinding of gel systems.* Journal of Food Science, 1982. 47(6): p. 1955-1959.

2.   Urbonaite, V., et al., *Origin of water loss from soy protein gels.* Journal of Agricultural and Food Chemistry, 2014. 62(30): p. 7550-7558.

3.   Urbonaite, V., et al., *Water holding of soy protein gels is set by coarseness, modulated by calcium binding, rather than gel stiffness.* Food Hydrocolloids, 2015. 46: p. 103-111.

4.   Urbonaite, V., et al., *Permeability of gels is set by the impulse applied on the gel.* Food Hydrocolloids, 2015. http://dx.doi.org/10.1016/j.foodhyd.2015.03.024

5.   Ikeda, S. and Morris, V.J., *Fine-stranded and particulate aggregates of heat-denatured whey proteins visualized by atomic force microscopy.* Biomacromolecules, 2002. 3(2): p. 382-389.

6.   Langton, M. and Hermansson, A.-M., *Fine-stranded and particulate gels of β-lactoglobulin and whey protein at varying pH.* Food Hydrocolloids, 1992. 5(6): p. 523-539.

7.   Clark, A. and Ross-Murphy, S., *Structural and mechanical properties of biopolymer gels*, in Biopolymers. 1987, Springer Berlin Heidelberg. p. 57-192.

8.   Lefèvre, T. and Subirade, M., *Molecular differences in the formation and structure of fine-stranded and particulate β-lactoglobulin gels.* Biopolymers, 2000. 54(7): p. 578-586.

9.   Richards, F.M., *The interpretation of protein structures: total volume, group volume distributions and packing density.* Journal of Molecular Biology, 1974. 82(1): p. 1-14.

10.   Stading, M. and Hermansson, A.-M., *Large deformation properties of β-lactoglobulin gel structures.* Food Hydrocolloids, 1991. 5(4): p. 339-352.

11.   Chantrapornchai, W. and McClements, D.J., *Influence of NaCl on optical properties, large-strain rheology and water holding capacity of heat-induced whey protein isolate gels.* Food Hydrocolloids, 2002. 16(5): p. 467-476.

12.   Hermansson, A-M., *Gel characteristics—structure as related to texture and waterbinding of blood plasma gels.* Journal of Food Science, 1982. 47(6): p. 1965-1972.

13.   Puppo, M.C. and Añón, M.C., *Structural properties of heat-Induced soy protein gels as affected by ionic strength and pH.* Journal of Agricultural and Food Chemistry, 1998. 46(9): p. 3583-3589.

14.   Stevenson, C.D., Dykstra, M.J., and Lanier, T.C., *Capillary pressure as related to water holding in polyacrylamide and chicken protein gels.* Journal of Food Science, 2013. 78(2): p. 145-151.

15.   Puppo, M.C., Lupano, C.E. and Anon, M.C., *Gelation of soybean protein isolates in acidic conditions. Effect of pH and protein concentration.* Journal of Agricultural and Food Chemistry, 1995. 43(9): p. 2356-2361.

16.   Hermansson, A.M., *Structuring water by gelation food materials science*, J.M. Aguilera and P.J. Lillford, Editors. 2008, Springer New York. p. 255-280.

17.   Hermansson, A-M., *Fat and waterholding in functional properties of food macromolecules.* Functional Properties of Food Macromolecules, ed. J.R. Mitchell and D.A. Ledwards. 1986, London and New York: Elsevier Applied Science Publishers.

18.   Northcutt, J.K., Foegeding, E.A., and Edens, F.W., *Water-holding properties of thermally preconditioned chicken breast and leg meat.* Poultry Science, 1994. 73(2): p. 308-316.

19.   Kocher, P.N. and Foegeding, E.A., *Microcentrifuge-based method for measuring water-holding of protein gels.* Journal of Food Science, 1993. 58(5): p. 1040-1046.

20.   Fischer, H., Polikarpov, I., and Craievich, A.F., *Average protein density is a molecular-weight-dependent function.* Protein science : a publication of the Protein Society, 2004. 13(10): p. 2825-2828.

21.   Ako, K., et al., *Quantitative analysis of confocal laser scanning microscopy images of heat-set globular protein gels.* Food Hydrocolloids, 2009. 23(4): p. 1111-1119.

5

22.   Renkema, J.M.S., Knabben, J.H.M., and van Vliet, T., *Gel formation by β-conglycinin and glycinin and their mixtures.* Food Hydrocolloids, 2001. 15(4–6): p. 407-414.

23.   de Jong, S., van Vliet, T., and de Jongh, H.H.J., *The contribution of time-dependent stress relaxation in protein gels to the recoverable energy that is used as tool to describe food texture.* Submitted, 2015.

24.   Baussay, K., et al., *Influence of the ionic strength on the heat-induced aggregation of the globular protein β-lactoglobulin at pH 7.* International Journal of Biological Macromolecules, 2004. 34(1–2): p. 21-28.

25.   Stading, M., Langton, M., and Hermansson, A.-M., *Microstructure and rheological behaviour of particulate β-lactoglobulin gels.* Food Hydrocolloids, 1993. 7(3): p. 195-212.

26.   Zayas, J.F., *Functionality of proteins in foods*. 1996: Berlin [etc.], US: Springer.

27.   Tokita, M. and Tanaka, T., *Friction coefficient of polymer networks of gels.* The Journal of Chemical Physics, 1991. 95(6): p. 4613-4619.

28.   Grattoni, C.A., et al., *Rheology and permeability of crosslinked polyacrylamide gel.* Journal of Colloid and Interface Science, 2001. 240(2): p. 601-607.

5

Chapter 6

Protein aggregates may differ in water entrapment but are comparable in water confinement

In the context of the water distribution in complex food systems, in this study it was aimed to investigate whether protein aggregates varying in size and density differ in entrapped and confined water. Soy protein aggregates (1% v/v) prepared in the presence of 3.5 mM divalent salts increased in size and decreased in apparent density following the salt type order $MgSO_4$, $MgCl_2$, $CaSO_4$ and $CaCl_2$. In the absence of applied (centrifugal) forces, larger and less dense aggregates entrap more water. Entrapped water of ~ 8 to 13 g water/ g protein is associated to (pelleted) aggregates and is not constrained in exchangeability with the solvent. When force is applied, more water can be displaced from the larger and more deformable aggregates. The amount of confined water within aggregates was independent of aggregate density and accounted for ~ 3.5 g water per gram of protein. Confined water in aggregates is hindered in its diffusion because of physical structure hindrance, and therefore not directly exchangeable with the solvent. These insights in protein aggregate size and deformability of the aggregates can be used to tune water holding on larger length scales.

Keywords: soy protein aggregates, aggregate size, aggregate density, entrapped water, confined water

6.1   Introduction

To better understand sensory perception of foods, water exudation studies on protein-based gels are of a high importance. Water holding (WH) is defined as a sum of five different contributions retaining water in the gel network originating at different length scales ranging from molecular to macro scales [1]. The WH property of a gel is determined by the two gel characteristics coarseness and stiffness [1-3]. Gel coarseness determines the maximum amount of water removed from the gel at defined conditions, where lower and upper limiting length scales for water removal are identified [1, 3, 4]. Gel stiffness is the major determinant for the water removal kinetics from the gel [4]. The combination of gel coarseness and gel stiffness has a cooperative effect on gel WH.

The macroscopic properties of the gel, such as the WH and the water removal kinetics are determined by the gel network structure and its properties, originating from specific protein interactions and protein-protein interactions [5]. The mechanism by which protein aggregates cluster and develop into a space-filling network is expected to play a role in the microstructure and stiffness of a gel [6] and subsequently its WH [2, 7, 8]. Aggregate size and density are closely linked to gel microstructure [9], gel stiffness and hence to WH [10]. Nieuwland and co-workers have shown that larger and denser ovalbumin aggregates lead to coarser and less stiff gels with lower WH, while small and open aggregates contained more water because of a higher apparent connectivity leading to gels with a fine structure [10].

In **Chapter 2**, our study on WH of soy protein gels prepared in the presence of $MgSO_4$ and $MgCl_2$ showed that increasing the salt concentration yielded aggregates larger in size as well as coarser gels with lower WH capacity. Differences in aggregate sizes obtained by different types of salt was not reflected in the maximum amount of water removed from the gel but did affect water removal kinetics (**Chapter 2**). Similarly, Peters et al. (2015) showed that the crosslink density of whey protein particles also did not affect the overall WH of the particle. No information, however, was provided on water removal kinetics [11].

Although a number of studies have been performed to evaluate sub-micron and microstructure contributions to gel WH [1, 3, 4], it is unclear what the contribution of water associated to the protein aggregate is. Understanding whether aggregates should simply be seen as initial building blocks to obtain different gel microstructures to tune WH, or as structural elements which, depending on size and structure, differ in confined water, would allow one to better control and tune WH properties of food products. Insights in protein aggregate size and deformability of the aggregates could be used to control WH on larger length scales. Within this study we aim to modulate aggregate morphology using different types of salt and to investigate whether aggregates different in size and density differ in quantity of free diffusible and confined water (non-free diffusible) within the aggregate structure.

6.2 Material and Methods

6.2.1 Material

Defatted soy flour was provided by Cargill BV (Amsterdam, The Netherlands). Micellar casein isolate was kindly provided by Friesland Campina in a concentration of 14.6 % (w/w). Anhydrous magnesium sulfate ($MgSO_4$), anhydrous magnesium chloride ($MgCl_2$), calcium sulphate dihydrate ($CaSO_4 \cdot 2H_2O$), calcium chloride dihydrate ($CaCl_2 \cdot 2H_2O$) and deuterium oxide (D_2O) with a purity of 99.9 atom % D were obtained from Sigma-Aldrich (Steinheim, Germany). Reagents were of analytical grade and used without further purification.

6.2.2 Preparation of (soy) protein solutions

Soy protein solution, further denoted as SP, was prepared as described before in **Chapter 2**. The protein content of SP was determined by Kjeldahl (calculated using N x 6.25), where the protein isolation yielded typical 11-12% (w/w) stock-solutions. The ratio of the predominant proteins glycinin:β-conglycinin was estimated to be 50:50 by gel electrophoresis and reversed phase high-performance liquid chromatography (results are not shown). SP solution was stored at 4°C in the presence of 0.02% sodium azide and used within a month after preparation. The enthalpy change, indicative for the protein nativity, was 15.2 J/g protein as measured by differential scanning calorimetry (DSC) (Q1000, TA Instrument, New Castle, USA).

As a reference material, a casein micelle stock solution, depleted of whey proteins, was prepared as described by Nieuwland et al. (2014) [12], diluted to 12% (w/w) and stored at -20°C until further use. The casein micelle stock solution further denoted as CM was defrosted overnight in the refrigerator and equilibrated at room temperature for 2 h at 20 °C before usage.

6.2.3 Preparation and characterization of soy protein aggregates (0.1% v/v protein)

6.2.3.1 Preparation of SP aggregates

Stock solutions of SP and CM were diluted to 2% (w/w) protein and 20 mM salt solutions with $MgSO_4$, $MgCl_2$, $CaSO_4$ and $CaCl_2$ were prepared. A 40 mM MOPS buffer was prepared at pH 7.0. All solutions were filtered with disposable syringe filters (Machery-Nagel Chromafil RC-20/25, pore size 0.45 μm). The protein stock solutions were mixed with salt solutions to a final protein concentration of 0.1% (v/v), a salt concentration of 0.35 mM and 20 mM MOPS buffer in a total volume of 2 ml. Prepared solutions were heated at 95°C for 30 min to allow aggregation of the proteins and the solution was left to cool to 25°C. When other protein or salt concentrations were used, it is accordingly indicated in the text.

6

6.2.3.2 Characterization of the SP aggregates

Dynamic light scattering (DLS)

The size of the protein aggregates prepared as described above was determined using dynamic light scattering (Zetasizer Nano ZS, Malvern Instruments Ltd, Worcestershire, United Kingdom) by 173° angle backward scattering. Measurements were performed at 20°C and repeated five times per sample. The data were analyzed using a non-negative least square analysis (general purpose model).

Static light scattering (SLS)

To obtain a structure factor of the protein aggregates, static light scattering measurements were performed. Samples were prepared at a protein concentration from 0.001 to 0.3% protein (v/v) in a 20 mM MOPS buffer (pH 7.0) in the presence of salt as described above while keeping the protein to salt ratio constant. Measurements were performed using an ALV Compact Goniometer System with four detector units (ALV/CGS-4, Langen, Germany) and two ALV-5000/E multiple tau digital correlators. A Coherent Verdi V2 diode-pumped laser was used operating with vertically linearly polarized light with wavelength $\lambda = 532$ nm. The range of scattering wave vectors covered $4.65 \times 10^{-3} < q < 3.09 \times 10^{-2}$ nm^{-1} ($q = 4\pi \cdot n_s \cdot sin(\theta/2)/\lambda$), with n_s the refractive index of the solution and θ the angle of observation). The temperature of the cuvette holder was controlled by a thermostat bath at 20±0.1°C. If necessary the solutions were diluted to exclude inter-particle interactions.

Asymmetric flow field flow fractionation (AF4)

AF4 was used to fractionate polydisperse SP aggregates followed by an online multi-angle static laser light scattering (MALLS) detection and concentration measurement using UV and RI to determine the particle size and mass. The AF4 instrumentation comprised of a HPLC unit (Ultimate 3000, Dionex/Thermo Fisher Scientific, Sunnyvale, USA), MALLS (Dawn Heleos-II, λ=658 nm, 130 mW Laser, vertically polarized) and a RI detector (Optilab T-rEX, B) (Whyatt Technology, Santa Barbara, USA). A separation channel (HF5 cartridge, Wyatt Technology, Dernbach, Germany), was comprised of polyethersulphone hollow-fiber with a nominal molecular weight cut-off of 10 kDa, corresponding to an average pore size of 5 nm (Fiber type FUS 0181, Microdyn-Nadir, Wiesbaden, Germany). Data collection and analysis was done using Astra-6 software.

Protein aggregates of 0.1% protein (v/v) in a 20 mM MOPS buffer at pH 7.0, in the presence of 0.35 mM divalent salt were measured. The sample injection volume was 20 µl using a 60 µl loop in partial inject mode. The detector flow rate was kept constant at 0.5 ml min^{-1}. The sample was injected at a flow rate of 0.2 ml min^{-1} and focused for 8 min. Elution was performed under varying cross flow rate (V_x). At the start of elution, V_x was kept constant at 0.5 ml min^{-1} for 10 min followed by a decay in 3 steps: from 0.5 to 0.35 ml min^{-1} in 1 min, from 0.35 to 0.2 ml min^{-1} in 2 min and from 0.2 to 0 ml min^{-1} in 8 min. Then, V_x was kept at zero-velocity for 10 min. Light scattering signals from 53° to 100° were used for the data extrapolation using a 1st order Zimm plot fit. From the fitted weight averaged molar masses of the aggregates (M_m) and z-averaged radius of gyration (R_g), the apparent

density (ρ_{app}) was calculated using the following equation

$$\rho_{app} = \frac{M_m}{N_A \frac{4}{3} \pi R_g^3} \tag{6.1}$$

where N_A is the Avogadro's number.

6.2.4 Preparation and characterization of SP aggregates for confined and entrapped water measurements (1% v/v protein)

6.2.4.1 Preparation of SP aggregates

The prerequisite for aggregates used for measurements for confined free diffusible water (equal to entrapped minus confined) and non-free diffusible (confined) is that they need to be large and dense enough to be pelleted upon centrifugation (at 20,000 RCF). For this reason, aggregates were prepared at 1% (v/v) protein by keeping the protein to salt ratio the same as for aggregates prepared for the structural characterization as described above. Protein stock solutions were mixed with salt solutions to a final protein concentration of 1% (v/v) and a salt concentration of 3.5 mM as described in paragraph 6.2.3. Solutions were heated at 95°C for 30 min to allow aggregation of the proteins to occur and the solution was then left to cool at room temperature to 25°C. When other protein or salt concentrations were used, it is accordingly indicated in the text.

6.2.4.2 Characterization of the SP aggregates
Scanning electron microscopy (SEM)

Aggregates prepared at 1% (v/v) protein concentration at pH 7.0 in the presence of 3.5 mM $MgSO_4$, $MgCl_2$, $CaSO_4$ and $CaCl_2$ salts were imaged by SEM. Circular glass cover-slips of 8 mm (Menzel, Brauschweig, Germany) were cleaned by dipping twice in alcohol. Excess of remaining alcohol on the edge of the glass was carefully tipped to a filter paper. A piece of parafilm was spread on the table, using a few droplets of water for better sticking capacity, to obtain a clean hydrophobic surface. Poly-L-lysine of 0.2% (w/v) was pipetted in 100 µl quantities on the parafilm surface to obtain single droplets. Each cover-slip was placed on top of the droplet, carefully turned around and left for 5 min to ensure both sides were completely covered with poly-L-lysine. Treated cover-slips were dipped in MilliQ water twice, and excess of remaining water was carefully tipped to a filter paper. Rinsed cover-slips were placed in the holder and left to dry overnight at room temperature. Finished cover-slips were placed for 30 minutes in 1 ml Eppendorf tubes filled with the 0.3% (v/v) aggregate dispersions for aggregate attachment. Cover-slips with attached aggregates were washed twice in MilliQ water, placed in a 2.5 % (v/v) glutaraldehyde solution for 30 min for cross-linking of the proteins and later washed in MilliQ water again to rinse off the gluteraldehyde. The samples were dehydrated in a series of acetone (10, 30, 50, 70, 100 %) for 10 minutes per step and critical point dried (CPD) with carbon dioxide (CPD 030, BalTec, Liechtenstein, Germany). The cover slips were fitted on a sample holder by carbon adhesive tabs (Electron Microscopy Sciences, Washington, USA) and subsequently sputter coated with a 10 nm

thick layer of iridium (MED 020, Leica, Vienna, Austria). Samples were analyzed in a field emission scanning electron microscope (Magellan 400, FEI, Eindhoven, The Netherlands) at a working distance of approximately 4 mm, with SE detection at 2 kV and 6.3 pA. The digital images were contrast-optimized with Photoshop CS5.

ImageJ 1.49d was used as a tool to evaluate bead sizes visualized in SEM images at magnifications of 100,000. On average 3 spots were analyzed per gel. Bead sizes were obtained by direct visual inspection of the gel image and averaged.

6.2.4.3   Pelleting aggregates using centrifugation

Prepared 1% (v/v) protein aggregate solutions at pH 7.0 in the presence of 3.5 mM $MgSO_4$, $MgCl_2$, $CaSO_4$ and $CaCl_2$ were centrifuged at 20,000 RCF for 10 min at 20°C (Centrifuge 5430R - Eppendorf AG, Hamburg, Germany). The protein content in the pellet was determined by measuring the protein content in the supernatant after addition of 8 M urea as a powder (0.755 g urea/ g supernatant). To optimize protein solubilization in 8 M urea, the supernatant was heated at 70°C for 10 min. The protein content was determined by measuring absorbance at 280 nm with a Cary 50 Bio UV-Visible spectrophotometer (Agilent Technologies, Amstelveen, The Netherlands). A linear calibration curve for proteins was obtained by measuring the absorbance of 0.005-1% (v/v) soy protein solutions in the presence of 8 M urea. Using these calibration curves, the protein content (g) in the supernatant was obtained. The difference between total protein content of the sample and measured in the supernatant phase was taken as the protein content of the pellet (g) ($m_{protein}$). For all 4 different salts, approximately 37% non-pelleted aggregates remained in the supernatant and thus it was assumed that 63% was present in the pellet.

Alternatively, the non-filtrated and filtrated supernatants (Machery-Nagel Chromafil RC-20/25, pore size 0.45 μm) were analyzed by SDS-Page and DLS (results not shown). The results confirmed that non-pelleted proteins were actually small aggregates that did not sediment during centrifugation at 20,000 RFC for 10 min.

Pellet density by X-ray computer tomography (XRT)

The pellet volume was measured by X-ray tomography (XRT). Pelleted 1% (v/v) aggregates in the presence of 3.5 mM $MgSO_4$, $MgCl_2$, $CaSO_4$ and $CaCl_2$ salts were measured non-invasively as a three-dimensional (3D) structure with a spatial resolution of 10 μm by XRT, GE Phoenix v|tome|x m 180kV transmission tube (Windstorm, Germany). The transmission of the conical X-ray beam through the sample was recorded by a digital GE DXR detector array with 2024 × 2024 pixels (pixel size 200 μm). Samples were imaged at distance of 40.8 mm. Power setting of 100 kV and 135 μA were used. The 3D density map was obtained after tomographical reconstruction of images acquired under 1200 rotations over 360 degrees with a step size of 0.3 degrees. The acquisition time for one projection was 250 ms. Averaging 3 projections results in a total acquisition and read-out time of about 20 min.

6.2.4.4   Water entrapped in the pellet

1% (v/v) protein aggregate solutions prepared in the presence of 3.5 mM $MgSO_4$, $MgCl_2$, $CaSO_4$ and $CaCl_2$ salts were centrifuged at 20,000 RCF for 10 min at 20°C (Centrifuge 5430R - Eppendorf AG, Hamburg, Germany). The supernatant was carefully removed using a pipette, and the remaining serum was drained by leaving the Eppendorf tubes upside-down on the filter paper for 15 min. The tubes containing the protein aggregate pellets were weighted. Water entrapped in the pellet (EWP) was calculated as water remaining in the pellet after centrifugation according to equation 6.2 and expressed as g water/ g protein retained by the pellet.

$$EWP = \frac{W_{total} - W_{removed}}{m_{protein}} \qquad (6.2)$$

In this equation, W_{total} is water present in the sample (g), $W_{removed}$ is water drained from the tube after centrifugation (g) and $m_{protein}$ is the mass of the pelleted proteins (g). When other salt concentrations were used, it is accordingly indicated in the text. Measurements were performed at least in duplicate.

Free-diffusible water determined by proton nuclear magnetic resonance (^{1}H-NMR)

Free-diffusible water is defined as the sum of free diffusible water entrapped by aggregates (EWA_{FD}), and water present in between pelleted aggregates (EWI_{FD}). Free diffusible water ($EWA_{FD} + EWI_{FD}$) was measured by ^{1}H-NMR. To confirm that all free diffusible water is accounted for at the first re-dispersion step, the pellets were subsequently re-dispersed in 2 ml D_2O using a 1 ml pipette tip by gentle manipulation with the pipette tip. Dispersions in D_2O were left for 30 min to allow H_2O present in the aggregates to exchange with D_2O to form HDO and subsequently the samples were centrifuged again at 20,000 RCF for 10 min at 20°C (Centrifuge 5430R - Eppendorf AG, Hamburg, Germany). This procedure was repeated for 3 times and is further denoted as consecutive washing steps. HDO present in the collected supernatant was quantified by Nuclear Magnetic Resonance (NMR). ^{1}H NMR spectra of D_2O samples containing HDO were recorded at a probe temperature of 300K on a Bruker Avance-III-500 spectrometer at the Wageningen NMR Centre (WNMRC), Wageningen, The Netherlands. For each spectrum 8 scans were recorded with a relaxation delay of 10 s.

Non free diffusible water confined within aggregates

Non free diffusible water confined within aggregates (g water/ g protein), CWA_{NFD}, was calculated as follows:

$$CWA_{NFD} = \frac{EWP - \left(EWA_{FD} + EWI_{FD}\right)}{m_{protein}} \qquad (6.3)$$

in which the sum of EWA_{FD} and EWI_{FD} was measured by ^{1}H-NMR, as described earlier.

6

To demonstrate if (partial) aggregate dissociation would release an additional amount of water, pellets were dispersed in D_2O containing 8 M deuterated urea. Deutarated urea was obtained by dissolving urea up to 10 M in D_2O and freeze-dried (repeated for 3 times). Pellets in the presence of urea were heated at 70ºC for 10 min in the water bath allow aggregates to dissociate.

Definitions

From the experimental setup described above, entrapped water by the aggregate (EWA_{FD}) is associated to the aggregates and is not constrained in exchangeability with the solvent. The total amount of entrapped water by the pellet (EWP) is the sum of water entrapped within the aggregate (EWA_{FD}) and water present in between the pelleted aggregates (EWI_{FD}). Confined water within the aggregate (CWA_{NFD}) is defined as water that is hindered in its diffusion because of the physical aggregate structure. This is not free diffusible water on the time scales measurement were performed (15 min).

6.3 Results and discussion

6.3.1 Aggregate size

In this study it was aimed to obtain protein aggregates different in size and density and to show if the acquired structures account for different amount of entrapped and confined water present within the aggregate. The sizes of the aggregates prepared in a 0.1% (v/v) SP solution in the presence of 0.35 mM $MgSO_4$, $MgCl_2$, $CaSO_4$ and $CaCl_2$ salt were measured using DLS and are shown in **Figure 6.1.** The z-averaged diameter of these aggregates increased in size from 94 to 130 nm going from the addition of $MgSO_4$ to $MgCl_2$, $CaSO_4$ and $CaCl_2$.
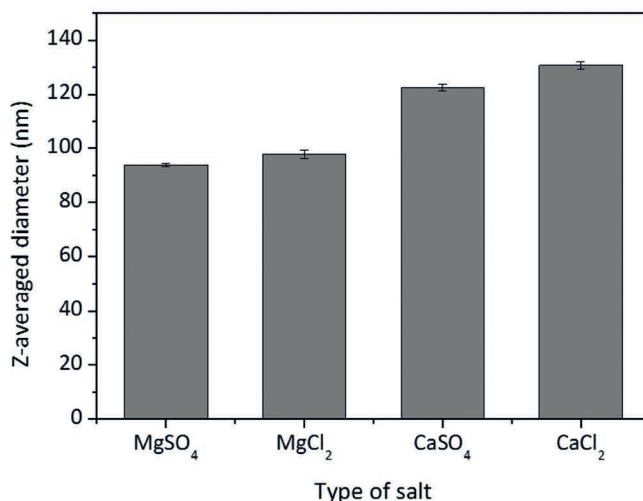

Figure 6.1 Z-averaged diameter of aggregates prepared in 0.1% (v/v) SP solution in 20 mM MOPS buffer, pH 7.0, in the presence of 0.35 mM $MgSO_4$, $MgCl_2$, $CaSO_4$ and $CaCl_2$ salts.

6.3.2 Aggregate density

Information on the aggregate structure was further obtained using AF4 fractograms yielding a so-called conformation plot (**Figure 6.2A)** showing the scaling of the size (R_g) and the averaged molar mass (M_m). Although the conformation plot of SP aggregates shows similar curves for the different salts indicating alike aggregate "build-up", it can be seen that aggregates formed in the presence of $MgSO_4$ are the smallest and aggregates formed in the presence of $CaCl_2$ are the largest in size, in agreement with DLS data. In agreement with **Figure 6.1**, aggregates prepared in the presence of magnesium salts had lower averaged molar mass compared to aggregates prepared in the presence of calcium salts.

Assuming that R_g and M_m of aggregates have a power law relationship as $R_g \sim M_m^{1/df}$, the exponent of such a curve provides a fractal dimension (d_f), [13]. On a log-log plot, this relation should result a straight line, from which the fractal dimension is represented by the slope. The fractal dimension directly relates to the openness of aggregates, where a lower d_f represents a more open aggregate structure [14-16]. From **Figure 6.2A** it can be seen that measured SP aggregates had 1 order of magnitude variation in M_m, and that the curve of R_g over M_m obtained is not linear. Based on these results, the fractal dimension (d_f) could not be obtained for measured SP aggregates, but the results still provide an indication of the internal density of the aggregates. From the curve, two regimes can be observed. These curves show that the fractal dimension for smaller sized aggregates is larger (steeper slope) than for larger aggregates. The beginning of the curve indicates a range of aggregates increasing in size, but having the same molar mass, and the second part of the curve shows aggregates increased in size and density. As soy proteins have an affinity for divalent cations, the addition of these salts may cause instantaneous protein clustering (nucleation). A fast initial clustering could yield inefficiently-formed aggregates that serve as a nucleus for denatured proteins to form a dense cover during heating. As a result a more open aggregate structure inside the aggregate could be formed in comparison to the outer structure.

The densities of above mentioned aggregates were derived from aggregate size (R_g) and average mass of the aggregate (M_m) measured using AF4 [13, 17]. The apparent aggregate density of different SP aggregates was calculated using equation 6.1 and is shown in **Figure 6.2B**. **Figure 6.2B** shows the fractogram depicting the Rayleigh ratio (scattering light intensity) and the calculated apparent densities. From the graph it can be seen that aggregates decrease in apparent density following this order of $MgSO_4$, $MgCl_2$, $CaSO_4$ and $CaCl_2$. To conclude, soy protein aggregates increased in size and decreased in density following the salt type order $MgSO_4$, $MgCl_2$, $CaSO_4$ and $CaCl_2$.
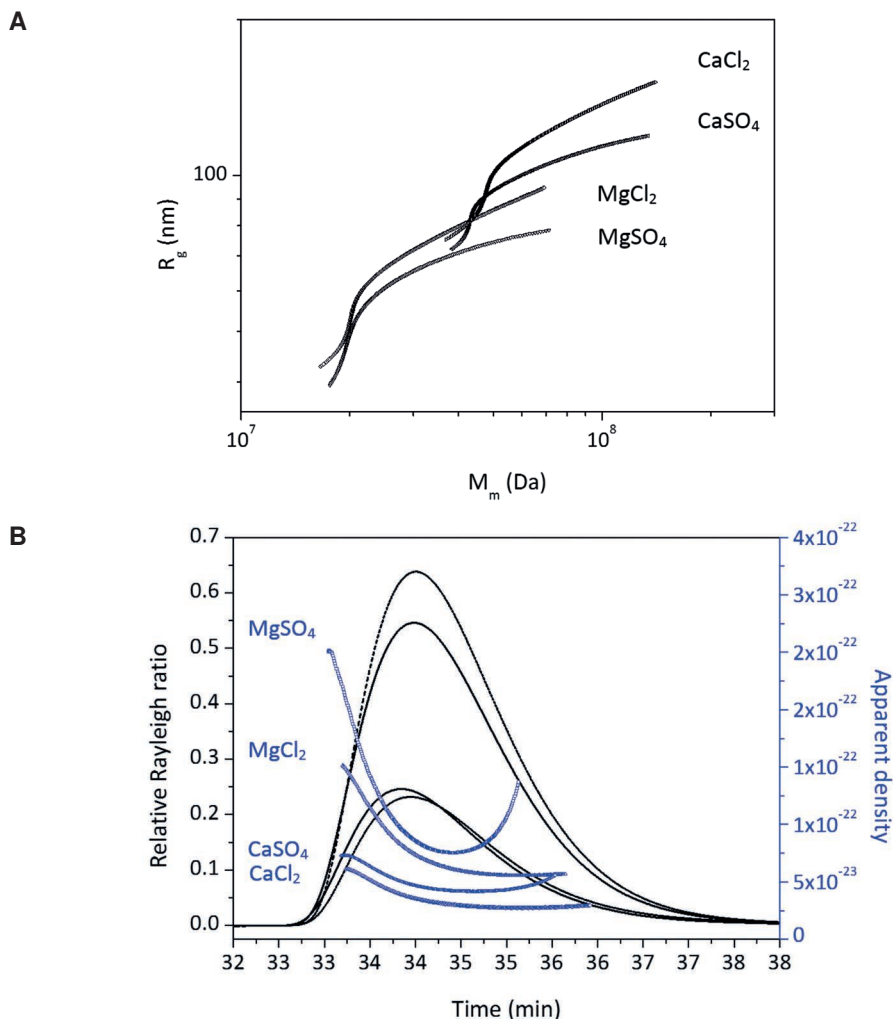
6

A

B

Figure 6.2 Panel A shows conformation plot indicating the scaling of size (R_g) to molar mass (M_m). Panel B shows the Rayleigh ratio (lower peaks for magnesium salts and higher peaks for calcium salts) and the calculated apparent density of aggregates using equation 6.1 SP aggregates in 20 mM MOPS buffer, pH 7.0, in the presence of 0.35 mM $MgSO_4$, $MgCl_2$, $CaSO_4$ and $CaCl_2$ salts.

6.3.3 Aggregate morphology

In order to determine the amount of water associated with the aggregate, the aggregates had to be collected as a pellet. Aggregates used for the determination of free diffusible water and non-free diffusible water (confined) within the aggregate were prepared at 1% (v/v) protein concentration in the presence of 3.5 mM $MgSO_4$, $MgCl_2$, $CaSO_4$ and $CaCl_2$ salts. To translate the measured aggregate characteristics (differences in size and density) of aggregates prepared at 0.1% (v/v) protein to aggregates prepared at 1% (v/v) protein, static light scattering (SLS) experiments were performed to obtain the size of aggregates

prepared at concentrations of 0.001 to 0.3% (v/v) protein in the presence of salts, while keeping protein to salt ratio constant to obtain a structure factor for the different protein aggregates. For all salts, the size of the aggregates increased with increasing protein concentration (results not shown). As these aggregates were too large at all concentrations prepared, it was not possible to obtain a structure factor.

To verify whether differences in size and density are apparent in 1% (v/v) SP aggregates in the presence of the various salts, SEM imaging of these aggregates was performed. Aggregates depicted at different length scales are shown in **Figure 6.3**.
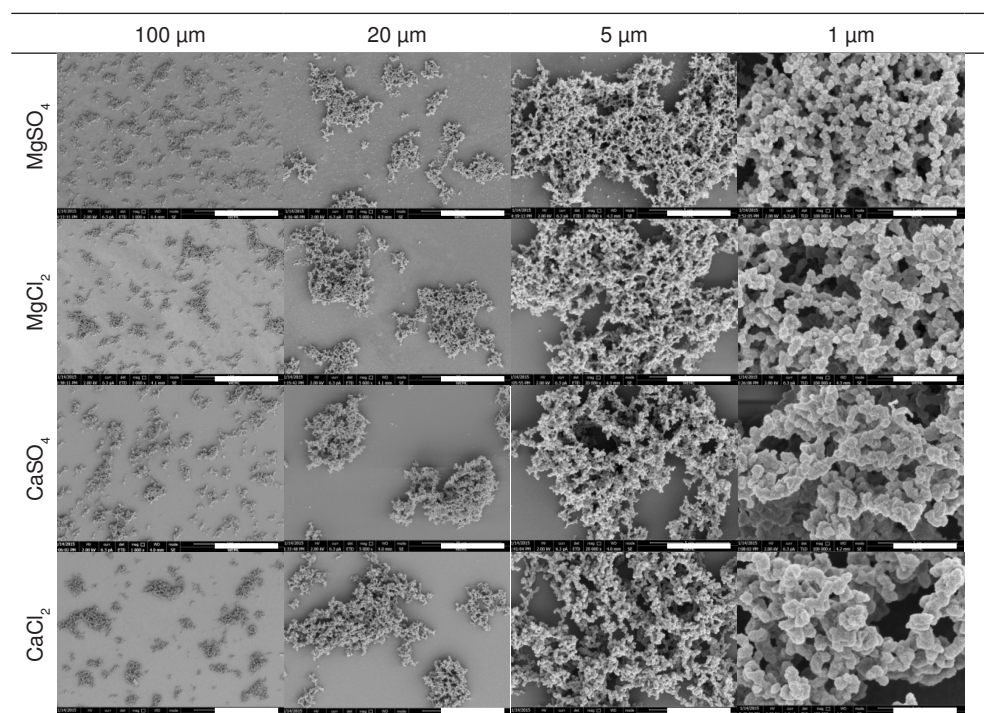

Figure 6.3 SEM images of 1% (v/v) SP aggregates prepared in 20mM MOPS buffer, pH 7.0, in the presence of 3.5 mM $MgSO_4$, $MgCl_2$, $CaSO_4$ and $CaCl_2$ salt over different length scales. The indicated length scales corresponds to the bar in the images.

From images with the lowest magnification it can be observed that the aggregates differ in size; aggregates prepared in the presence of $MgSO_4$ were the smallest and in the presence of $CaCl_2$ were the largest in size, in agreement with the results above. The aggregates formed had an irregular shape and were polydisperse in nature. In the presence of magnesium salts, aggregates varied from approximately 5 to 20 µm. In the presence of $CaSO_4$, the aggregates varied between 5 and 25 µm, and in the presence of $CaCl_2$ aggregates up to 30 µm were found. Differences in aggregate microstructure in the presence of different salts were seen on 1 µm scale images (images on the

right) in the bead size, and in thickness of the strands, which were composed from these beads. The beads were fairly regular spherical particles and increased in size as measured by image analysis from 0.1 to 0.3 μm (**Figure 6.4**) following the salt addition in the order of $MgSO_4$, $MgCl_2$, $CaSO_4$ and $CaCl_2$. The increment in size and more open structures observed in **Figure 6.3** are in agreement with aggregate size and density results shown in **Figures 6.2** of aggregates prepared at 0.1% (v/v) protein concentration.
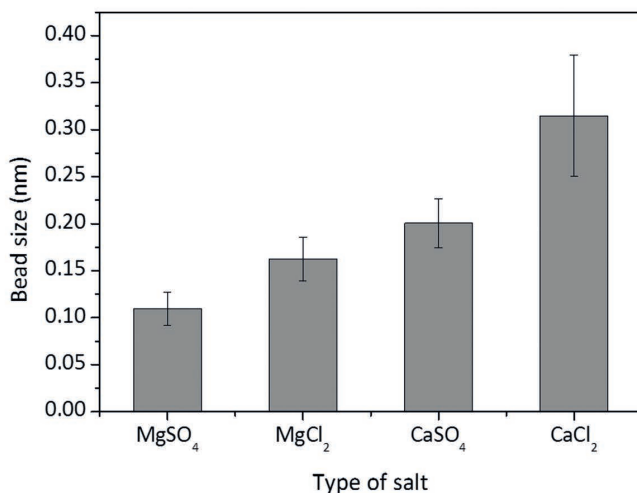

Figure 6.4 Bead sizes of 1% (v/v) SP aggregates prepared at pH 7.0 in the presence of 3.5 mM $MgSO_4$, $MgCl_2$, $CaSO_4$ and $CaCl_2$ salt imaged by SEM.

6.3.4 Water entrapped by the pelleted aggregates

Protein aggregates prepared at 1% (v/v) in the presence of 3.5 mM or 8.0 mM $MgSO_4$, $MgCl_2$, $CaSO_4$ and $CaCl_2$ salts were centrifuged at 20,000 RCF for 10 min at 20°C. The quantity of water entrapped by the pelleted aggregates, *EWP* (water in between and within the aggregates), is shown in **Figure 6.5**. From the figure it can be observed that water entrapped by the pelleted aggregates prepared in the presence of 3.5 mM salts increased from approximately 8 to 13 g of water per g of protein for salts in the following order of $MgSO_4$, $MgCl_2$, $CaSO_4$ and $CaCl_2$. No significant difference was found between water entrapped by the pelleted aggregates prepared in the presence of $MgSO_4$ and $MgCl_2$ salts (~ 8 g water/g protein). Aggregates prepared in the presence of $CaSO_4$ entrapped slightly more water compared to aggregates prepared in the presence of magnesium salts (~ 8.5 g water/g protein), while in the presence of $CaCl_2$ this difference became much larger (~ 13 g water/ g protein). Pellet densities measured using XRT (**Table 6.1**) showed complementary results to the measured entrapped water presented in **Figure 6.5**. Pellets with higher amount of entrapped water had higher densities suggesting that, indeed, larger and less dense aggregates entrap higher amounts of water. This finding is in agreement with the results reported by Nieuwland and colleagues, where larger and

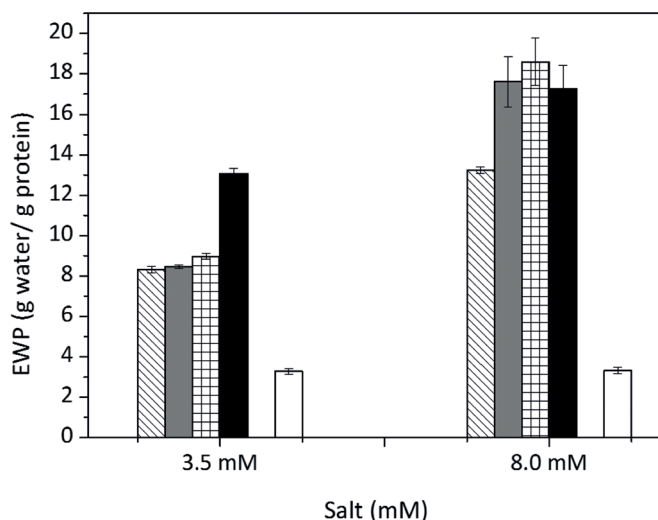denser aggregates in the gel measured on larger length scales by SESANS resulted in lower gel WH [10].

Figure 6.5 Water entrapped by the pelleted 1% (v/v) SP aggregates (EWP) prepared in the presence of 3.5 mM and 8.0 mM $MgSO_4$ (striped), $MgCl_2$ (grey), $CaSO_4$ (grid), $CaCl_2$ (black). White columns stand for a control sample containing 1% (v/v) CM aggregates prepared in the presence of 3.5 mM and 8.0 mM $CaCl_2$.

Table 6.1 Densities of pelleted 1% (v/v) SP aggregates prepared in the presence of 3.5 mM salts at pH 7.0.

	Pellet (g)	Volume (mm³)*	Density (g/cm³)
$MgSO_4$	0.118±0.002	114	1.035
$MgCl_2$	0.123±0.002	111	1.106
$CaSO_4$	0.134±0.002	121	1.105
$CaCl_2$	0.186±0.002	159	1.171

*Single measurement

To illustrate whether higher salt concentrations would affect the size of the aggregate and the accompanying amount of water entrapped, an additional set of aggregates was prepared from a 1% (v/v) protein solution in the presence of 8.0 mM of salt. The pelleted 1% (v/v) aggregates (**Figure 6.5**) entrapped approximately double the amount of water ranging from approximately 13 to 19 g of water per g of protein compared to aggregates prepared in the presence of 3.5 mM salts. Obtained results on aggregate size confirmed that pelleted aggregates prepared at higher salt concentration are larger and thereby entrap more water.

6.3.5 Aggregate compressibility

To compare the amount of entrapped water in pelleted aggregates to water entrapped by the aggregates in the solution, the apparent density, ρ_{app} (g/cm³), of 0.1% (v/v) SP aggregates was calculated using the radius of gyration (R_g) and averaged molar mass (M_m) obtained from AF4 measurements (see equation 6.1). The quantity of water entrapped by aggregates was calculated as $1/\rho_{app}$ (g water/ g protein) and is presented in **Table 6.2**. Values for entrapped water calculated for 0.1% (v/v) aggregates and measured values for 1% aggregates are shown in **Table 6.2** and expressed as g of water per g of protein. From the calculated values of entrapped water by aggregates in the solution it can be seen that aggregates larger in size and lower in density (for CaCl$_2$) entrap more water. The difference in water entrapped by the aggregates in the solution and those compressed in a pellet could be explained by aggregate compressibility at the centrifugation force used. The compressibility factor, taken as the ratio between *EWP* and water entrapped by the aggregates in solution (**Table 6.2**), shows that smaller and denser prepared aggregates, like those in the presence of magnesium salts, entrap less water, and are also less compressible. Larger and more open aggregates, as in the presence of calcium salts, entrap more water and are more compressible. In agreement with our findings, Bell and colleagues suggested that aggregate strength, determined by the structure of the aggregate (based on density-size relationship), decrease with increasing aggregate size [18].

Table 6.2 Water entrapped by aggregates in the solution (calculated) versus pelleted aggregates (measured).

	Aggregates in solution (g water/ g protein)	*EWP* (g water/ g protein)	Compresssibility factor
MgSO$_4$	20.78	8.21	2.53
MgCl$_2$	27.58	8.47	3.26
CaSO$_4$	41.26	8.97	4.60
CaCl$_2$	57.56	13.07	4.40

6.3.6 Repetitive forces applied on aggregates

To differentiate between entrapped and confined water by aggregates, pellets were re-dispersed in D$_2$O, to allow water between the aggregates to diffuse from the aggregates and exchange with the solvent, giving HDO that is quantified by ^{1}H-NMR (see paragraph 6.3.7). A number of pellet re-dispersion steps followed by centrifugation, further denoted as subsequent washing steps, were applied to the pellets to assure that all diffusible water was accounted for.

Pelleted protein aggregates were consecutively washed 3 times in D$_2$O. At each washing step pelleted aggregates were re-dispersed in the same amount of D$_2$O. Changes in water entrapment by the pelleted aggregates over washing steps are shown in **Figure 6.6A**. From the graph it can be observed that with each additional washing step water entrapped by the pelleted aggregates decreased by approximately 12-15%. The decreased amount

of entrapped water with additional re-dispersion and centrifugation steps is suggested to represent compressibility of the pelleted aggregates as described above. To verify that the decrease of water entrapment is caused by pellet compressibility and not by aggregate disassembly caused by depletion of divalent ions during the washing-step, a control experiment was performed where pelleted aggregates were washed in D_2O in the presence of $CaCl_2$. Obtained results did not show any significant effect on water entrapped by pelleted aggregates (data not shown).
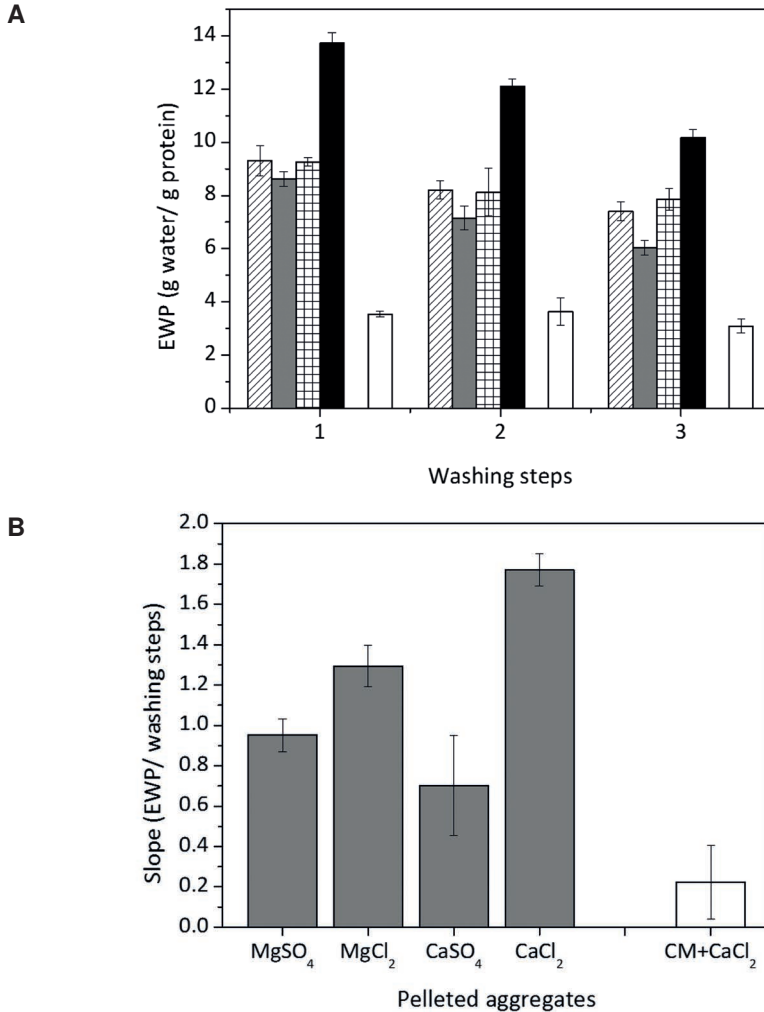
A

B

Figure 6.6 Panel A shows a change in D_2O entrapment by 1% (v/v) SP aggregates prepared in the presence of 3.5 mM $MgSO_4$ (striped), $MgCl_2$ (grey), $CaSO_4$ (grid), $CaCl_2$ (black) over washing steps in D_2O. Panel B shows the rate of change in quantity of entrapped water by pelleted aggregates prepared in the presence of 3.5 mM salt affected by 3 washing steps. In both panels white columns stand for a control sample, 1% (v/v) CM aggregates prepared in the presence of $CaCl_2$.

The change in the amount of entrapped water retrieved from the aggregates by the subsequent washing steps was evaluated by taking the slope of entrapped water over three washing steps as shown in **Figure 6.6A**, and presented in **Figure 6.6B** for the different salts. From the graph it can be seen that $MgCl_2$ and $CaCl_2$ aggregates were more affected by each washing step compared to $MgSO_4$ and $CaSO_4$ aggregates. To conclude, once pelleted aggregates are evaluated, larger and less dense SP aggregates are more compressible compared to smaller and denser aggregates. When reoccurring compression appears (e.g. washing steps), aggregates prepared in the presence of chloride salts (less dense) are compressed more than aggregates prepared in the presence of sulfate salts (more dense).

6.3.7 Water between aggregates and diffusible water

1% (v/v) SP aggregate pellets were re-dispersed in D_2O, and water free to diffuse from ibetween aggregates (EWI_{FD}) and from within the aggregates (EWA_{FD}) (HDO) was quantified by[1]H-NMR. The amount of HDO from the aggregates (in between and within) prepared in the presence of 3.5 mM salt is shown in **Figure 6.7A**. More water had diffused from aggregates larger in size and lower in density ($CaSO_4$, $CaCl_2$). This correlates positively with the results found for water entrapped by pelleted aggregates (**Figure 6.6**); the more water is retained by pelleted aggregates, the more water is free to diffuse from these aggregates. Three consecutive washing steps were performed and the results confirmed that almost all water free to diffuse from within and in-between the aggregates already diffused in the first washing step, as almost no additional water has diffused in the second and third washing step. This shows that indifferent to aggregate size or density all diffusible water is exchanged with D_2O on the minutes timescale.

In a parallel experiment, pelleted aggregates were re-dispersed in D_2O in the presence of 8 M deuterated urea to allow aggregate dissociation. It was aimed to evaluate if in the case destabilization of the aggregates would be induced, a larger amount of water, in addition to the regular washing, could be released (**Figure 6.7B**). From the graph it can be seen that addition of urea released not more than 0.5 g of water per gram of protein independent on aggregate structure. The amount of additionally released water was marginal compared to the free diffusible water measured.

As a reference sample to SP aggregates, CM aggregates, prepared from a 1% (v/v) solution in the presence of 3.5 mM $CaCl_2$, were used. Casein micelles are known for their loose packing and high porosity [19]. They have a voluminosity in milk of about 3-4 g water per g of dry casein [20, 21], where only a relatively small proportion, around 0.5 g H_2O per g dry casein, is directly bound to the casein [20]. Because of the sponge-like colloidal casein micelle structure, obtained particles were expected to have a high amount of water displaced from the (pelleted) material when force is applied. CM particles visualized by SEM had very coarse open structures up to 50 µm in size (data not shown). Entrapped water measurements of pelleted CM particles showed ~ 4 times lower amount

of entrapped water compared to pelleted SP (CaCl$_2$) aggregates (**Figure 6.5**, white columns). Although CM particles were larger in size compared to the soy aggregates, they entrap less water, indicating high aggregate compressibility. The small change in water entrapment as affected by re-occurring compression (washing steps) indicates a small degree of compression at re-occurring forces, as the maximum compression of the structures already have occurred in the first centrifugation step (**Figure 6.6B**). Compared to SP aggregates, as expected, CM particles had lowest amount of water entrapped. The large size, open structure and large compressibility of CM particles lead to high water displacement from the aggregate when external force is applied.
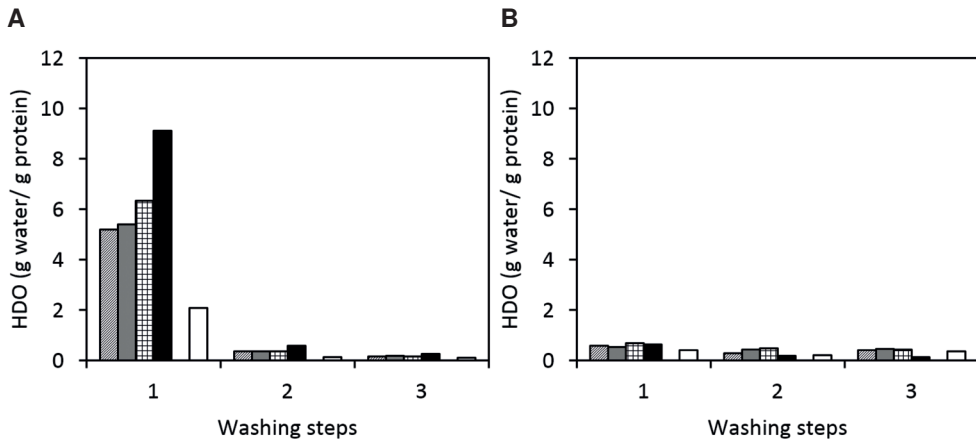

Figure 6.7 Panel A shows quantity of measured HDO diffused from aggregates (in between and within) prepared in the presence of 3.5 mM MgSO$_4$ (striped), MgCl$_2$ (grey), CaSO$_4$ (grid), CaCl$_2$ (black) salts. Panels B stands for additionally released non-free diffusible water measured in the presence of 8 M deuterated urea. In both panels white columns stand for the reference, 1% (v/v) CM aggregates prepared in the presence of CaCl$_2$.

6.3.8 Confined water within aggregate structure

Confined water within the aggregate (CWA_{NFD}) is defined as water that is hindered in its diffusion because of the physical aggregate structure. The results for calculated CWA_{NFD} (equation 6.3) for different aggregates are shown in **Figure 6.8**. From the graph it can be observed that in case of SP aggregates, the amount of confined water within aggregates is independent of the aggregate structure (size and density) and accounts for approximately 3.5 g of water per gram of protein. The reference material accounted for approximately 2 g of water per gram of protein and suggests that this quantity is protein specific.

From the above results it can be concluded that water entrapped by pelleted aggregates depends on aggregate size, density and compressibility, whereas confined water within aggregates is aggregate structure independent, but seems to be protein specific.
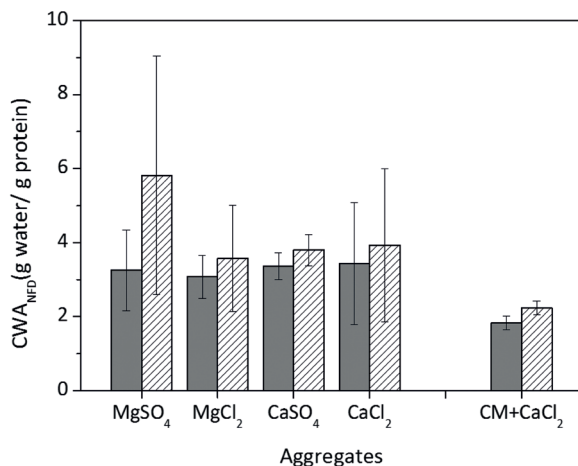
Figure 6.8 Confined water within aggregates: 3.5 mM (light grey color) versus 8.0 mM (striped).

6.3.9 Modulation of entrapped water

Different types of salts can be used to obtain different aggregate structures. To evaluate to what extent these different aggregates can be tuned for the amount of entrapped and confined water, different salt concentrations (3.5-10 mM) were tested. The obtained aggregates were measured for water entrapped by pelleted aggregates (*EWP*) and water confined within aggregates (CWA_{NFD}). The results for water entrapped by the pellet are shown in **Figure 6.9A**. From the graph, a transition-like behavior can be observed that decreases in salt concentration in the order of $CaCl_2 > CaSO_4 > MgCl_2 > MgSO_4$. Varied salt concentration yielded aggregates different in size and density, and as a result, the amount of water entrapped in the pellet varied from approximately 10 to 25 g of water per g of protein. The same aggregates measured for confined water (**Figure 6.9B**) resulted in 2 to 4 g of water per gram of protein and was aggregate structure independent in agreement with the results presented above.
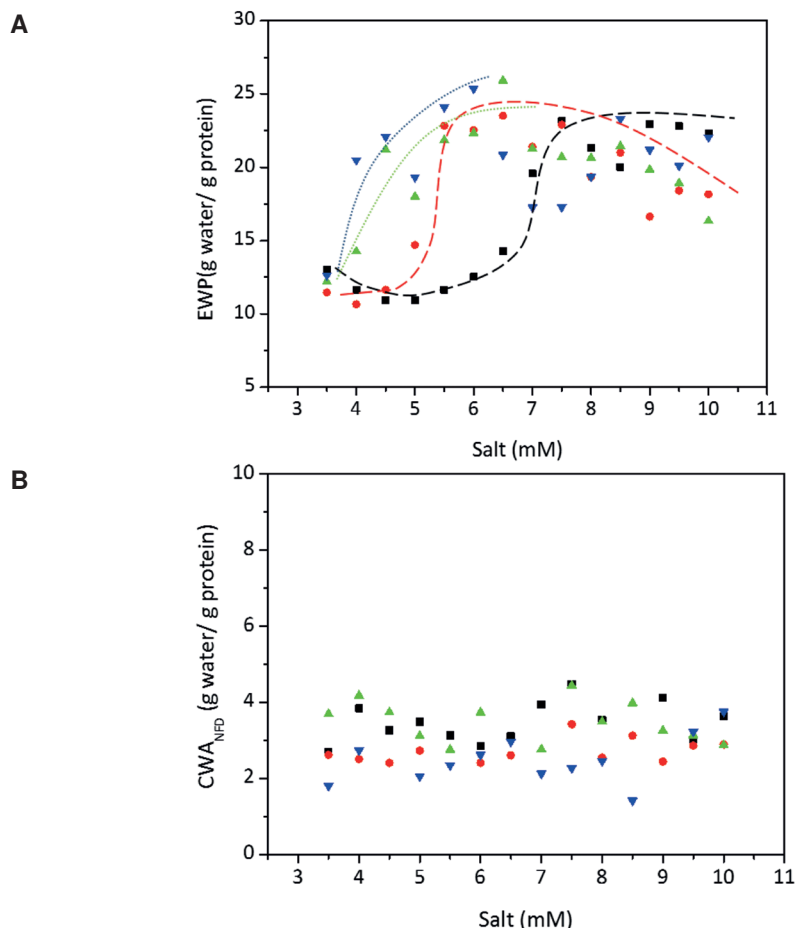
Figure 6.9 Panel A shows water entrapped by 1% (v/v) SP aggregates prepared in the presence of 3.5-10 mM (■) $MgSO_4$, (●) $MgCl_2$, (▲) $CaSO_4$ and (▼) $CaCl_2$. To guide the eye, dashed lines are added for magnesium salts and dotted lines for calcium salts. Panel B shows water confined within aggregate structures (CWA_{NFD}).

6.4 Conclusions

From this work two types of water within aggregate have been distinguished: (i) entrapped water and (ii) confined water. Entrapped water is associated to (pelleted) aggregates and is not constrained in the exchangeability with a solvent. Confined water in aggregates is hindered in its diffusion because of physical hindrance. This work aimed to show whether aggregates different in structure differ in these two types of water. Prepared aggregates increased in size and decreased in apparent density following the salt type order $MgSO_4$, $MgCl_2$, $CaSO_4$ and $CaCl_2$. Calculations based on AF4 data of water entrapped by aggregates in solution resulted in 21 g of water per g of protein for $MgSO_4$ aggregates (smallest and most dense) and 58 g of water per g of protein for $CaCl_2$ aggregates

(largest, least dense). The amount of water entrapped by the pelleted aggregates was ~ 2 to 4 times lower; the difference in entrapped water by the aggregates in the solution and the pelleted aggregates was accounted for by aggregate compressibility. Smaller and denser aggregates prepared in the presence of magnesium salts were about twice less compressible compared to larger and less dense aggregates prepared in the presence of calcium salts. When consecutive compression was applied (e.g. washing steps), aggregates prepared in the presence of sulfate salts (smaller and more dense structures) were less deformable as reflected by the quantity of entrapped D_2O compared to aggregates prepared in the presence of chloride salts (larger and less dense structures). Diffusible water measurements showed that irrespective of the aggregate size or density all diffusible water is instantly exchanged with D_2O. The larger and less dense aggregates entrap more water, and the amount of entrapped water is proportional to the amount of diffusible water. In case of soy protein aggregates, the amount of confined water within aggregates is aggregate structure independent and approximately 3.5 g of water is confined per gram of protein. Variation in aggregate structure by varying salt concentration showed that indeed a broad range of the amount of water entrapped in the pellet can be obtained. However, confined water remained independent of aggregate structure and only varied between 2 to 4 g of water per gram of protein, in agreement with the results of 3.5 and 8 mM $MgSO_4$ $MgCl_2$, $CaSO_4$ and $CaCl_2$ aggregates. To conclude, in the case where no forces are applied, larger and less dense aggregates entrap more water. When an external force is applied, more water can be displaced from these aggregates. The aggregate structural aspects do not affect quantity of confined water within aggregate structure. Insights in aggregate size and deformability can be used to better tune water holding on the larger length scales.

6.5   Acknowledgements

6

References

1. Urbonaite, V., et al., *Origin of water loss from soy protein gels.* Journal of Agricultural and Food Chemistry, 2014. 62(30): p. 7550-7558.
2. Hermansson, A-M. and Lucisano, M., *Gel characteristics—water binding properties of blood plasma gels and methodological aspects on the waterbinding of gel systems.* Journal of Food Science, 1982. 47(6): p. 1955-1959.
3. Urbonaite, V., et al., *Water holding of soy protein gels is set by coarseness, modulated by calcium binding, rather than gel stiffness.* Food Hydrocolloids, 2015. 46: p. 103-111.
4. Urbonaite, V., et al., *Permeability of gels is set by the impulse applied on the gel.* Food Hydrocolloids, 2015. http://dx.doi.org/10.1016/j.foodhyd.2015.03.024
5. Ikeda, S. and Morris, V.J., *Fine-stranded and particulate aggregates of heat-denatured whey proteins visualized by atomic force microscopy.* Biomacromolecules, 2002. 3(2): p. 382-389.
6. Alting, A.C., et al., *Number of thiol groups rather than the size of the aggregates determines the hardness of cold set whey protein gels.* Food Hydrocolloids, 2003. 17(4): p. 469-479.
7. Hermansson, A-M., *Gel characteristics—structure as related to texture and waterbinding of blood plasma gels.* Journal of Food Science, 1982. 47(6): p. 1965-1972.
8. Hermansson, A.M., *Structuring water by gelation food materials science*, J.M. Aguilera and P.J. Lillford, Editors. 2008, Springer New York. p. 255-280.
9. Walstra, P., *Physical Chemistry of Foods.* 2003: New York [etc.], US: Marcel Dekker.
10. Nieuwland, M., et al., *Relating water holding of ovalbumin gels to aggregate structure.* Submitted, 2015.
11. Peters, J.P.C.M., et al., *Effect of crosslink density on the water-binding capacity of whey protein microparticles.* Food Hydrocolloids, 2015. 44: p. 277-284.
12. Nieuwland, M., et al., *Characterizing length scales that determine the mechanical behavior of gels from crosslinked casein micelles.* Accepted for publication in Food Biophysics, 2015.
13. Aymard, P., et al., *Fractality of Globular Protein Aggregates: From the Molecular to the Microscopic Level.* Fractals, 1997. 05(2): p. 23-43.
14. Pouzot, M., et al., *Structure factor and elasticity of a heat-set globular protein gel.* Macromolecules, 2004. 37(2): p. 614-620.
15. Weijers, M., Visschers, R.W., and Nicolai, T., *Influence of the ionic strength on the structure of heat-set globular protein gels at pH 7. Ovalbumin.* Macromolecules, 2004. 37(23): p. 8709-8714.
16. Mehalebi, S., Nicolai, T., and Durand, D., *Light scattering study of heat-denatured globular protein aggregates.* International Journal of Biological Macromolecules, 2008. 43(2): p. 129-135.
17. Dhayal, S.K., et al., *Controlled formation of protein nanoparticles by enzymatic cross-linking of α-lactalbumin with horseradish peroxidase.* Food Hydrocolloids, 2014. 36(0): p. 53-59.
18. Bell, D.J., et al., *The density of protein precipitates and its effect on centrifugal sedimentation.* Biotechnology and Bioengineering, 1982. 24(1): p. 127-141.
19. Walstra, P., *The voluminosity of bovine casein micelles and some of its implications.* Journal of Dairy Research, 1979. 46(2): p. 317-323.
20. McMahon, D.J. and Brown, R.J., *Composition, Structure, and Integrity of Casein Micelles: A Review1.* Journal of Dairy Science, 1984. 67(3): p. 499-512.
21. Dalgleish, D.G., *On the structural models of bovine casein micelles-review and possible improvements.* Soft Matter, 2011. 7(6): p. 2265-2272.

6

Chapter 7

General discussion

7.1 Introduction

In this chapter, findings from this thesis are put in perspective to clarify water holding (WH) of globular protein gels (from animal and plant origin) at different length scales. In **Figure 7.1** a general concept of gel WH resulting from this thesis is presented in a schematic way. Different protein sources were used to obtain gels, i.e. soy protein (SP), ovalbumin (OVA) and whey protein isolate (WPI), and yielded inherently different gel morphologies, resulting from different microstructural building blocks of the gel network. To tune this gel morphology a number of approaches were taken to vary the building blocks of the network: (i) chemical protein modification (**Chapter 3**), (ii) protein complexation using divalent salts (**Chapters 3** and **4**) or (iii) varying ionic strength (**Chapters 4** and **5**). When the building blocks (aggregates) vary in size and (or) structure, network coarseness as well as gel stiffness is changed. Gel network coarseness and stiffness are therefore interrelated characteristics. From the scheme (**Figure 7.1**) it can be seen that obtained gels can be comparable in coarseness, but different in WH. In this case, it is expected that either initial building blocks (aggregate structure) (**Chapter 6**) or network stiffness (**Chapters 4** and **5**) cause differences in WH.

The discussion of the main results obtained in this thesis will follow the definition of WH as given in the introduction of this thesis. Shortly, WH is defined as sum of five contributions starting at the (sub-)nm length scale for molecularly bound water to that of the mm length scale, describing the contribution of rupture events to gel WH. A special focus will be given to the gel morphology contribution, where the effect of gel coarseness, gel stiffness and their interplay on water removal from the gel will be evaluated and generalized. Additionally, the relation between energy dissipation and water holding upon applied mechanical deformation will be discussed, followed by the relevance of these findings regarding applications and possible future research.

7.2 Molecularly bound water

In this thesis, the amount of molecularly bound water has been assumed to be constant and was not further investigated. A typical characteristic of molecularly bound water is that it is not in exchange with the solvent. Globular proteins are comparable in the amount of bound water, where 0.067 g/ g protein is reported for β-lactoglobulin, 0.057 g/ g protein for ovalbumin, and 0.058 g/ g protein for soy proteins [1]. At a water activity (A_w) <0.3, water is selectively hydrogen bonded to charged and polar amino acid residues to form a single-molecule bound water layer [2]. Molecularly bound water to the globular protein (0.06-0.07 g of water/ g protein) occupies the high-energy surface sites and ionic sites [3]. Half of this water, typically 0.03-0.04 g water/ g protein is required to hydrate peptide bonds [1], and approximately 0.006 g water/ g protein is engaged in hydrogen bonding between different polar groups of the peptide and is involved in stabilizing the structure of the protein in its native form [1].
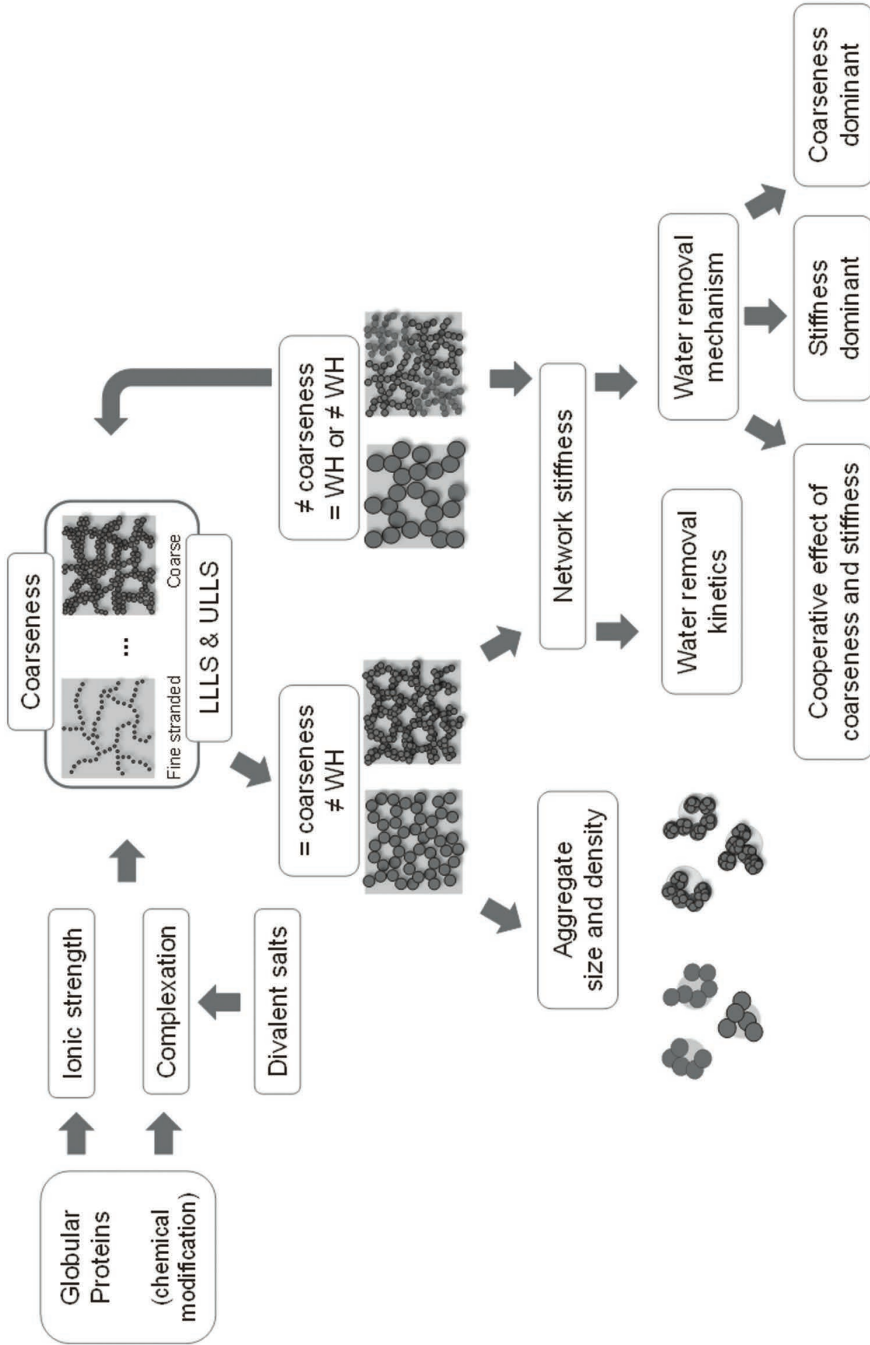
Figure 7.1 General concept of gel WH

7.3   Water entrapped by aggregates

Protein gels are build up from microstructural building blocks. Besides molecularly bound water, these building blocks have the ability to hold water. To better understand WH on the microstructural level, the contribution of individual building blocks (aggregates) to WH was evaluated (**Chapter 6**). In **Chapter 6** we could discriminate two types of water within the aggregates: (i) entrapped water and (ii) confined water (**Figure 7.2**). Entrapped water by the aggregate is associated to the (pelleted) aggregates and is not constrained in its exchangeability with a solvent. Confined water within the aggregate is defined as water that is hindered in its diffusion because of the physical aggregate structure and is not free-diffusible.
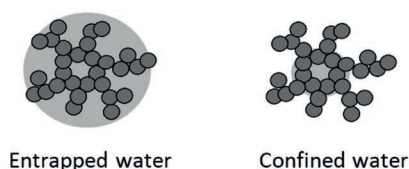

Entrapped water   Confined water

Figure 7.2 Schematic representation of the water associated with the aggregates: entrapped and confined water.

In this work, we created a broad range of soy protein aggregates, which varied in size and density. We have shown that entrapped water could be modulated by the aggregate size and its density. Larger and less dense aggregates entrap more water, but at the same time these aggregates are more deformable and result in higher water displacement from the aggregate structure when force is applied (e.g. centrifugation). Confined water within aggregates is independent on deformation and is comparable for the different aggregates prepared. In the case of soy protein aggregates, the amount of confined water is approximately 3.5 g of water per gram of protein. This is 10-100 times more than the amount of molecularly bound water. As we have studied a single protein system only, we cannot conclude on protein specificity regarding entrapped and confined water.

7.4   Water retained by gel microstructure

7.4.1   Coarseness contribution to gel WH

In literature, it is often discussed that WH of a protein-based gel is predominantly defined by the gel morphology on micrometer scale [4-7]. However, due to inconsistent methodology used and different protein systems studied no direct comparisons between gels and conclusions on the length scales dictating WH could be made. A consistent study of gel microstructure relation to gel WH was needed to provide clarity in coarseness contribution to WH. The different networks were characterized by means of coarseness, which is defined as the structural inhomogeneity pictured in the microscopy images.

Imaged (CSLM/SEM) gel microstructures were analyzed using image analysis, from which a coarseness parameter representing a typical length scale of the gel network was obtained. In agreement with literature, a threshold in coarseness of 0.1 μm in this work was used to differentiate between fine and coarse-stranded gels [8-12].

We observed that WH of protein gels depends on the coarseness of the gel, but the range of the coarseness is limited. In this work, we have identified lower limiting length scales (LL), upper limiting length scales (UL) and a regime for pronounced water loss, denoted as intermediate length scales (IL) for different protein systems studied (**Chapter 4**), and are presented in **Table 7.1**. The LL represents gel coarseness from which no water can be removed from the gel at the maximum external force applied. This length scale was shown to depend on the type of protein used to make the gels. For the different proteins, these LL were identified as: < 0.03 μm for 14% (w/w) WPI gels (**Chapter 5**), < 0.1 μm for 12% (w/w) ovalbumin gels (**Chapter 4**) and < 0.3 μm for 10 % (w/w) (modified) SP gels (**Chapter 3**). In addition to these differences in LL, these three different systems studied showed a large variation in their mechanical properties: WPI gels were 100 times stiffer than ovalbumin and SP gels.

Table 7.1 Lower (LL) and upper (UL) limiting length scales for different protein gels studied.

	LL (μm)	UL (μm)
14% WPI	< 0.03	> 1.8
12% OVA	< 0.1	> 0.42
10% (modified) SP	< 0.3	> 4.7

Differences between gels in LL and network stiffness indicate that the lower limiting length scale may be related to the stiffness of the gels. Therefore, the Young's modulus of the different gels was plotted versus the LL for the different protein systems. As can be observed in **Figure 7.3**, the parameters are linked via a power law relationship between Young's modulus and LL (**Figure 7.3**). This relation offers opportunities to predict a limiting length scale based on the stiffness of the gels. Munialo and colleagues have studied 10% (w/w) PPI gels at different pHs. These gels varied in stiffness form 1 to 11 kPa [13]. Assuming that the 10% (w/w) PPI gel would have a stiffness of 1 kPa, extrapolation of the curve in **Figure 7.3** leads to a LL of ~ 1.5 μm. This seems to be a realistic number for PPI gels, as the least coarse PPI gel studied had a coarseness parameter of 3.3 μm [13], much larger than the coarseness parameters of the other protein systems.

Besides the LL also an upper limiting length scale (UL) for the different protein gels was found. Above this length scale, an additional increased in coarseness does not change water holding not anymore. The UL were found to be: >1.8 μm for 14% (w/w) WPI gels (**Chapter 5**), > 0.42 μm for 12% (w/w) OVA gels (**Chapter 4**) and > 4.7 μm for 10% (w/w) (modified) SP gels (**Chapter 3**).
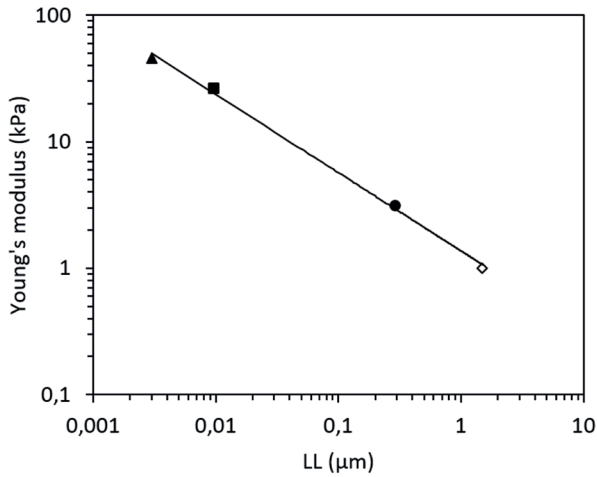
7

Figure 7.3 Relation between Young's modulus and LL, where ■ refers to 12% (w/w) ovalbumin gels, ● refers to 10% (w/w) (modified) SP gels, ▲ refers to14% (w/w) WPI gels, and ◇ refers to 10% PPI gels.

Between the lower and upper limiting length scales, a region is identified where pronounced water loss is apparent. This region is referred to as the intermediate length scale (IL).To show whether IL is protein or network specific, both coarseness and the maximum amount of removed water (A_{max}) were normalized. To normalize these parameters, coarseness was divided over LL, and A_{max} of each gel was divided over highest A_{max}, the amount of water removed from the gel when UL is reached. For the 10% PPI gels, the LL obtained from the extrapolation in **Figure 7.3** was used. The normalized water removal was plotted against the normalized coarseness and plotted in **Figure 7.4**. Surprisingly, all data now fall on a single master curve (**Figure 7.4**).
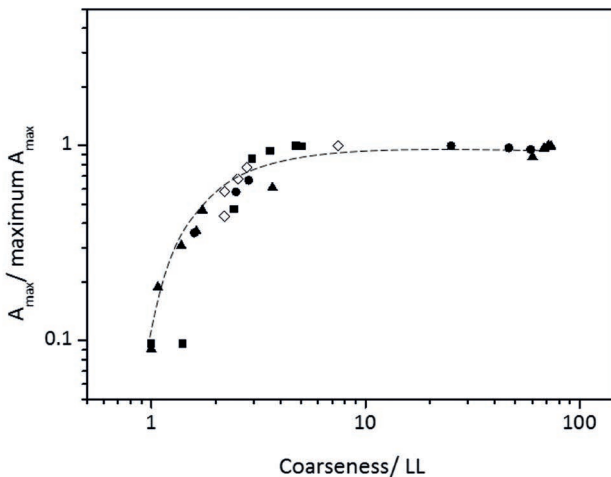

Figure 7.4 Normalized A_{max} (maximum amount of water removed from the gel) plotted versus the normalized gel coarseness, where ■ refers to 12% (w/w) ovalbumin gels, ● refers to 10% (w/w) (modified) SP gels, ▲ refers to14% (w/w) WPI gels, and ◇ refers to 10% PPI gels. The dotted line is added to guide the eye.

This result suggests that water removal, and obviously thus WH, is network morphology specific, and not protein specific. As the type of protein used to obtain a gel defines the gel morphology, it consequently indirectly affects and determines WH. Most importantly, this result implies that WH can be tuned by controlling the gel network properties, and the WH of a specific protein gel can be varied as long as the gel morphology can be changed.

7.4.2 Stiffness contribution to gel WH

Once gel water holding (WH) is studied under applied deformation, not only gel coarseness, but also gel stiffness becomes important if the coarseness is above the LL. The extent by which a gel structure deforms upon applied force is crucial for exudation of water, i.e. water removal [14]. In **Chapters 4** and **5** it was shown that gel stiffness defines the water removal kinetics from the gel within the IL length scales. In general, less stiff gels have higher water flux, but at the same time are quicker compressed (densified) by applied force, which could impair water removal [15, 16].

Stiffness of the gel and the magnitude of applied pressure will determine the total amount of water removal and the kinetics of the water removal from the gel. In case of fine gels, high capillary forces will keep the water within the gel, and a minimal pressure is needed to overcome the capillary force to initiate water flow from the narrow pores. The remaining pressure can be used to deform the network and will determine how much water can be removed.

Every type of protein will generate gels with different characteristics, and as the network morphology is altered also the stiffness of the network changes. How coarseness of different protein gels is linked to stiffness is illustrated in **Figure 7.5**. For a single protein type, the modulation of the network morphology by e.g. varying pH or salt concentration will result in a gradual increment in gel coarseness and therefore increased amount of water removed from the gel (A_{max}). In a broad range of coarseness values, typically a maximum in gel stiffness is present (**Chapters 2**, **3, 4** and **5**). The presence of such a maximum in gel stiffness is explained by two opposing contributions. First, increasing coarseness yields thicker strands, and therefore an increase in stiffness. Second, strands increasing in thickness result in a lower number of connectivity points in the network, and thereby a decrease in stiffness. As a result of the interplay between the two parameters, two distinct regimes regarding coarseness and stiffness are apparent: (i) increasing in coarseness and increasing in stiffness and (ii) increasing in coarseness and decreasing in stiffness (**Figure 7.4**). The change in coarseness and gel stiffness is protein specific (**Chapters 2**, **3, 4** and **5**). Some protein gels change to a larger extent in coarseness but limited in stiffness and other proteins change more in stiffness than in coarseness. From **Figure 7.6** (first column) it can be seen that for WPI gels, the gel stiffness increases with increasing coarseness (positive relation), while for OVA and SP gels, stiffness decreases with increasing coarseness (negative relation). The relative changes in coarseness and gel stiffness for the gels are given in **Table 7.1** as dC/dE (change in coarseness over

7

change in stiffness). The higher value for the (modified) SP gels indicate that for these gels the coarseness changes more than the stiffness (**Table 7.2**).

The water holding (WH) or water removal (A_{max}) can be presented as a function of both the coarseness and the stiffness. In **Chapter 5** we have shown that stiffness and coarseness can have a counteracting effect on the water removal from gels. For the different proteins studied, i.e. (modified) SP, OVA and WPI, increased gels coarseness leads to a higher A_{max} (**Figure 7.4**) and this relation seems to be very similar for all protein gels. How A_{max} is affected by the stiffness is shown in **Figure 7.6** (middle column). Also here, positive and negative correlations between A_{max} and gel stiffness are seen, which is the result of similar or opposing relations between coarseness and stiffness. The relation between water holding (WH) or water removal (A_{max}) and gel stiffness is thus not similar for the different protein gels.
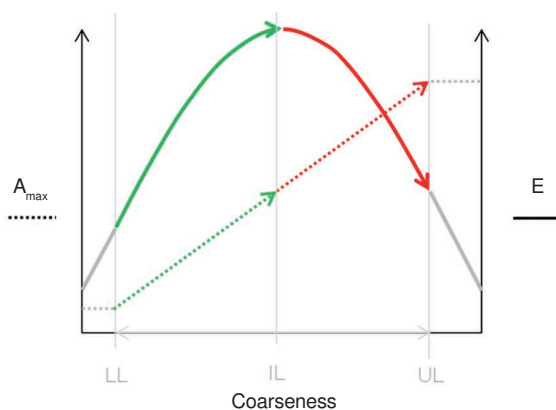

Figure 7.5 General concept of gel coarseness in relation to A_{max} and to Young's modulus (E).

To illustrate the effect of gel stiffness on the different aspects in WH, the coarseness, the maximum amount of removed water (A_{max}) and the water flux ($k2$) is plotted versus the Young's modulus for the three different gel systems studied in this thesis, namely WPI, OVA and (modified) SP (**Figure 7.6**). Only gels within the IL are used, and the gels with coarseness below the LL or above the UL length scale were omitted. From **Figure 7.6** it can be observed that 14% (w/w) WPI gels have a positive relation of coarseness, A_{max} and $k2$ to the Young's modulus. The other two systems, 12% (w/w) OVA and 10% (w/w) (modified) SP gels have a negative relation to gel stiffness. The relationship between the different parameters seems to be influenced by how the parameters change in relation to the others, which is reflected by the slope of the curves. The obtained data were fitted using a linear function to obtain the values for these slopes; this yields the slopes of dC/dE, dA_{max}/dE and d$k2$/dE (**Table 7.2,** left column), where dC stands for the change in coarseness, dA_{max} for change in maximum amount of removed water, d$k2$ for change in effective water flux coefficient and dE for change in Young's modulus. These slopes

represent how coarseness of the gel, A_{max} and the water flux changes as a function of the Young's modulus. As already discussed, water removal depends both on the stiffness and the coarseness of the gels. The effect of the stiffness is reflected in the values of dA_{max}/dE. In a similar way, the coarseness and the water removal can be linked by dA_{max}/dC, which represents the changes in water removal with respect to the change in coarseness. This relation can be obtained by dividing dC/dE by dA_{max}/dE, and is given in **Table 7.2** as the ratio. In a similar way, the relation between water removal and water flux ($dA_{max}/dk2$) is given, by dividing dA_{max}/dE by $dk2/dE$.
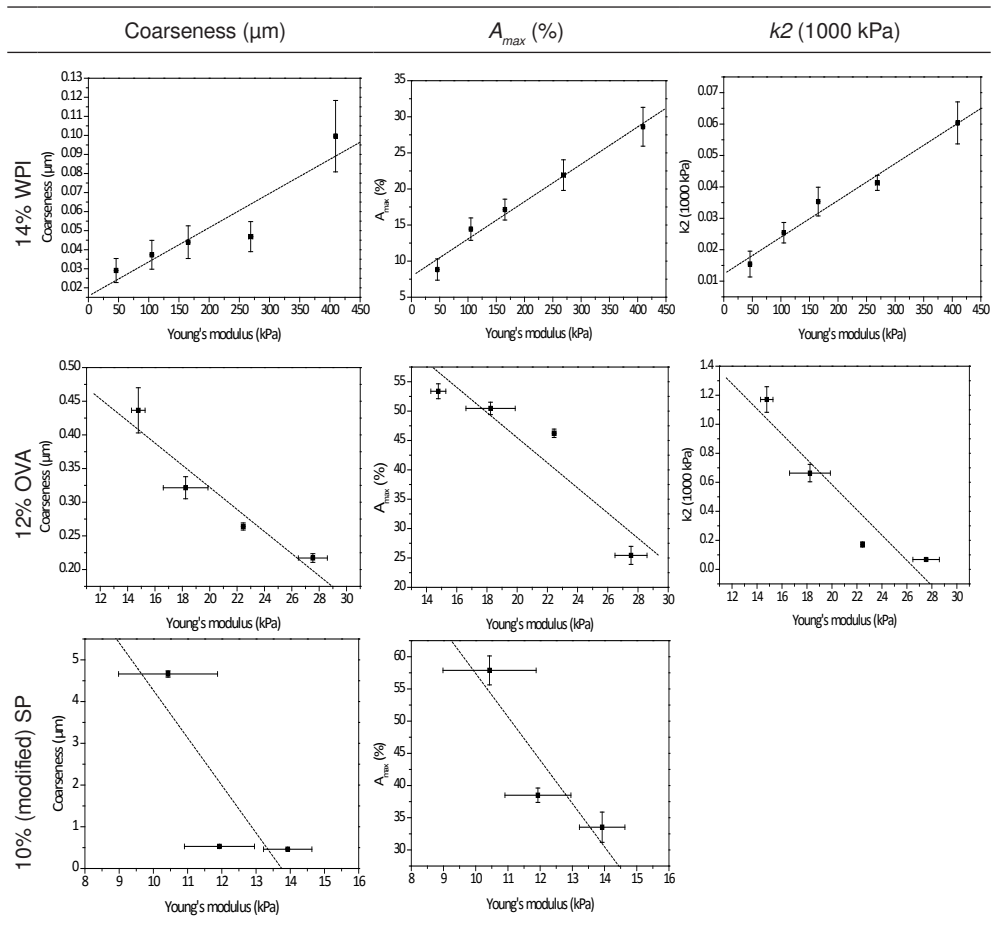
Figure 7.6 Effect of Young's modulus on A_{max} and $k2$ in pronounced water loss region (IL).

The values presented in **Table 7.2** give an indication in how much the parameters change in relation to another. For example, for different gels dC/dE is different. 14% (w/w) WPI gels have the smallest value for dC/dE, which indicates that these gels change the most in stiffness and the least in coarseness. In this case, the coarseness

and stiffness correlation is positive. 12% (w/w) OVA and 10% (w/w) (modified) SP gels have a larger value for dC/dE, so a larger change in the coarseness and a smaller change in the stiffness. However, in this case they have a negative coarseness – stiffness relation (increased coarseness yields decreased stiffness). When dA_{max}/dE is evaluated for the different systems, similar results are found as observed for the dC/dE. Obviously, for gels with higher dC/dE also higher dA_{max}/dE values are found, and the values for dA_{max}/dC are obtained for the three different gels (**Table 7.2**). For WPI gels we find the highest value. High values for dA_{max}/dC represent a large change in removed water from the gel with increased coarseness. At the same time, we also see that the change in removed water with respect to the change in Young's modulus (dA_{max}/dE) is very small. This means that coarseness is dominant in water removal from WPI gels and the stiffness is less relevant. For OVA and (modified) SP gels the gels have lower dA_{max}/dC values and negative correlations for coarseness and A_{max} with respect to the stiffness of the gel. For these gels, we see that the values for dA_{max}/dE are larger than in the case of WPI gels. The combined lower values for dA_{max}/dC and higher values for dA_{max}/dE indicate that the stiffness of the gels becomes more important and partially contributes to the water removal from the gel. In the case of gels with increasing coarseness and decreasing stiffness, the contributions of the stiffness and the coarseness have a counteracting effect. When the contribution of the stiffness is more dominant, this could limit water removal from the gel. However, in our protein gels, coarseness still remains dominant in A_{max} (**Chapter 5**). The lowest value for dA_{max}/dC and dA_{max}/dE for (modified) SP gels illustrates that stiffness becomes even more important, and could suggest that water removal is more dominated by gel stiffness.

Table 7.2 Effect of Young's modulus on gel WH.

Gels	Slopes (data from **Figure 7.5**)			Water removal	
	dC/dE	dA_{max}/dE	$dk2/dE$	dA_{max}/dC	$dA_{max}/dk2$
14% WPI	$1.8*10^{-4}$	$5.2*10^{-2}$	$1.2*10^{-4}$	289	442
12% OVA	$-1.6*10^{-2}$	-2.1	$-8.7*10^{-2}$	130	25
10% (modified) SP	-1.1	-6.7	-	6	-

The water flux from the gel is determined by the extent of deformation of the gels, and $k2$ can therefore be seen as the extent of the deformation. The deformation depends on the stiffness of the network and the pressure that is applied. As the stiffness is related to the gel network and therefore protein type, the water flux is not expected to be similar for the different protein gels. For stiffer gels a limited deformation is effectuated, and therefore the water removal mechanism may resemble that of rigid gels. For less stiff gels, the gels deform easier, leading to larger network deformation. Upon gel compression by an applied force, the extent of network deformation will affect the pore size and connectivity between

the pores. Lower connectivity between neighboring pores as a result of such compression could lead to a lower channeling propensity and thereby to lower gel permeability.

When comparing d$k2$/dE values for different gels (**Table 2**), it can be observed that d$k2$/dE is much lower for WPI gels compared to OVA gels. Lower d$k2$/dE values for WPI gels indicate that water flux from the gel is less affected by gel stiffness compared to OVA gels. The large value of dA_{max}/dE of WPI gels (**Table 2**) compared to d$k2$/dE shows that the change in amount of water removed from the gel is larger compared to the change in water flux as affected by gel stiffness, represented by a high value of dA_{max}/d$k2$. If stiffness is less relevant, it suggests that the water flux in WPI gels is more coarseness dominated. In the case of OVA gels, the value of dA_{max}/d$k2$ is much lower than for WPI, and therefore stiffness becomes more relevant. In the OVA gels, water removal is more dominated by stiffness, in line with the conclusion drawn from the relation of the water removal versus coarseness and stiffness.

To conclude, the results described in this thesis show that for water removal from gels, three regimes can be identified: (i) stiffness dominant, (ii) interplay between coarseness and stiffness and (iii) coarseness dominant. In the case of fine (but above the LL) and very stiff gels, the applied force acts on water removal rather than on network deformation, and in this case water removal is coarseness dominated. In the case of coarse gels, coarseness and stiffness have a cooperative effect on water removal. Applied force acts both on network deformation and water removal. Finally, in the case of gels low in stiffness and high in coarseness, coarseness will be dominant in the process of water removal.

7.5   Relation between WH and energy dissipation

From the above it can be concluded that the ability of a protein gel to deform upon applied mechanical forces is important for WH of protein gels. In **Chapters 2** and **3** we have shown that WH is linearly and positively correlated to the energy stored in the system when deformation is applied. The more generic correlation between RE and WH of gels with different microstructure and responses to mechanical deformation, was evaluated for different protein sources (**Figure 7.7**) [17]. For each of these protein gels, the recoverable energy (RE) was determined from a mechanical deformation test and **Figure 7.7** shows the results of RE as a function of the WH for various types of globular proteins. In all cases a positive and linear correlation can be observed with a distinct protein specificity in their intercept and slope of the correlation (**Table 7.3)**.
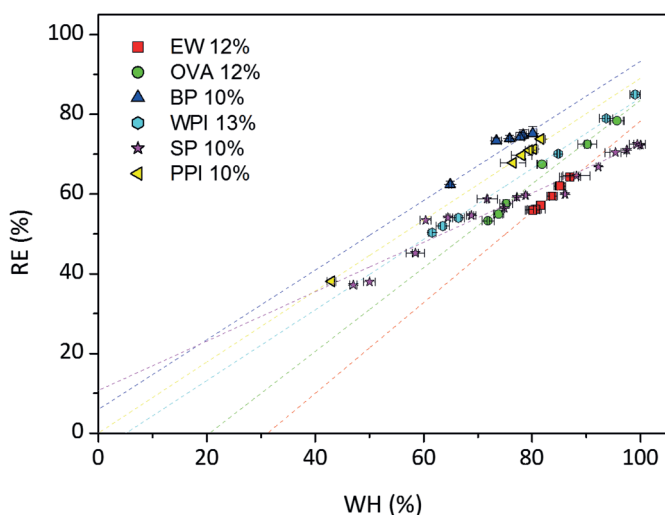
7

Figure 7.7 Relationship between WH and RE of globular protein heat set gels, where SP stands for soy proteins, BP for blood plasma proteins, OVA for ovalbumin, EW for egg white proteins, WPI for whey proteins and PPI for pea proteins.

Table 7.3 Slope and intercept of the correlation plot between RE and WH (**Figure 7.7**).

(w/w) gels	Slope (dRE/ dWH)	Intercept (y-axis)
10% SP	0.62	10.7
10% BP	0.88	5.9
13% WP	0.88	-4.5
10% PP	0.89	0.0
12% OVA	1.05	-21.5
12% EW	1.14	-35.5
10% EW	1.09	-27.2

7.5.1 The origin of the slope

Table 7.3 shows that for all protein systems studied the slope of RE over WH varies between 0.88 and 1.14, except that for soy, which was considerably lower (0.62). A lower slope would imply that in soy protein gels the loss of energy caused by friction flow is smaller than for the other type of protein gels. As discussed above in **Section 7.4**, the coarseness and the stiffness of the protein network are two key factors determining WH of protein gels. Consequently, the origin of the slope of RE as a function of WH was hypothesized to be related either to the gel coarseness or to the stiffness.

To investigate a possible relation between the slope and the two parameters, both the coarseness and the gel stiffness are plotted versus the slope (dRE/dWH) in **Figure 7.8**. **Figure 7.8A** shows that blood plasma protein and pea protein gels have a comparable slope (**Table 7.3**), but differ significantly in coarseness. Alternatively, the coarse soy and pea protein gels are comparable in coarseness, but differ in slope. These results illustrate that the origin of the slope does not solely originate from differences in coarseness. Similarly, when the relation between the slope and the Young's modulus is evaluated (**Figure 7.8B**), it can be observed that for the soy and pea protein gels with a different slope, next to a similar coarseness, the gels also have a comparable stiffness. And for pea proteins and blood plasma proteins with a similar slope, the gels differed in stiffness. Therefore the differences in slope cannot be explained by differences in gel stiffness. Similar to the water holding of the gels, the two parameters may have a counteracting effect, but are both important. Alternatively, it could be suggested that the smoothness of the network by means of the surface properties of the pores and channels, and the connectivity between neighboring pores could lead to less or more effective energy dissipation and thereby affect the slope.

In a recent study, the dissipated energy (1-RE) was dissected into six contributions, including fracture, debonding, microstructural friction, viscous flow, plastic deformation and stress relaxation [18]. Stress relaxation, a most profound dissipation mode, was found to be protein specific and not depending on the gel morphology. Therefore, we assume that stress relaxation will not affect the slope of the relation between WH and RE. However, there are two contributions that may affect the slope; the formation of micro-cracks during deformation and plastic deformation of the gel. Although the WH and RE measurements are performed in such way that macro-cracks are avoided, the occurrence of micro-cracks cannot be excluded. The presence of micro cracks would lower the RE. The role of serum as dampening of this dissipation mode has been reported in literature [19]. Unfortunately, up to now, these micro cracks or the energy dissipated via this phenomenon are difficult to quantify. Plastic deformation of a gel is another mode in which energy can be dissipated when deformation is applied and it relates to irreversible changes in microstructure occurring during deformation under the time scale of the RE measurements. Data on this phenomenon is lacking for the gels studied here and in general its contribution to the recoverable energy is unclear.
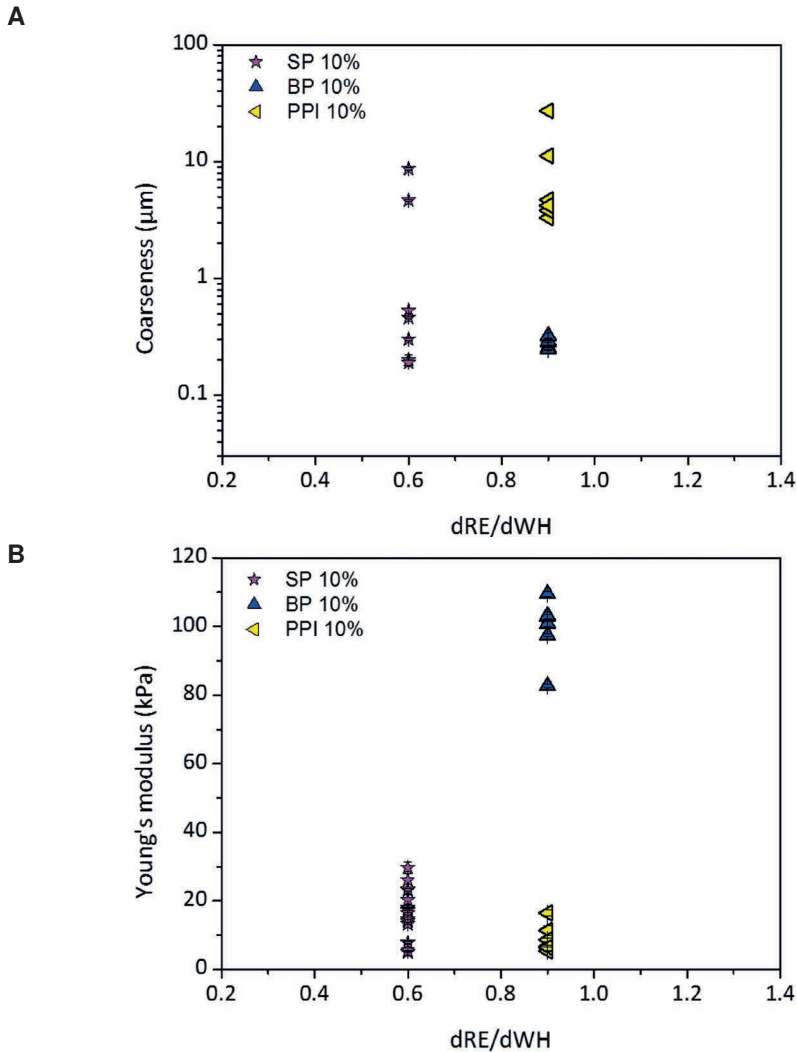
7

Figure 7.8 (A) Coarseness (µm) of the protein gels as a function of the slope for three different systems and (B) Young's modulus (kPa) as a function of the slope, where SP stands for soy proteins, BP for blood plasma proteins and PPI for pea proteins.

7.5.2 The origin of the intercept

Intercepts of the WH-axis are presented in **Table 7.3**. Negative values for these intercepts have no physical meaning and only imply that the recoverable energy of the material would be reduced to zero whereas these gels would still have a significant water holding. Two other groups of protein systems can be distinguished: the group for which the intercept is close to 0 and a group (consisting of OVA and egg white (EW) protein gels) for which the intercept is significantly negative. An intercept close to zero may indicate that when a protein gel would not be able to retain water during mechanical deformation, it would also not be capable to store

energy in the gel. EW and OVA gels clearly differ in their intercept compared to the other type of protein gels studied. The negative intercept would indicate that despite that a gel can hold water, the RE could diminish already to zero: this would indicate that the water flow is not the only dissipation mode that acts on the gel, and at least one other dissipation contribution plays a role.

To evaluate whether this intercept is related to either coarseness or stiffness of the gel **Figure 7.9** presents the coarseness and stiffness of different protein systems as a function of the intercept of the correlation curve between RE and WH.
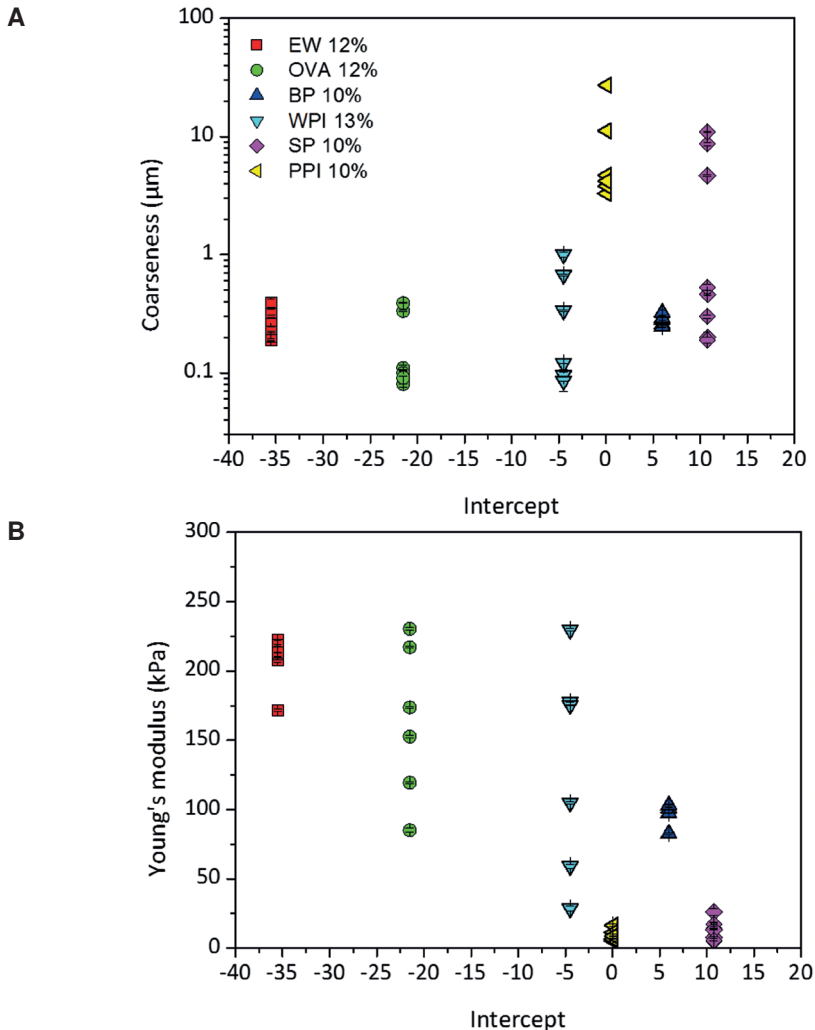

Figure 7.9 (A) Coarseness as a function of intercept of the relation between WH and RE and (B) Young's modulus (kPa) as a function of the intercept of the relation between WH and RE, where SP stands for soy proteins, BP for blood plasma proteins, OVA for ovalbumin, EW for egg white proteins, WPI for whey proteins and PPI for pea proteins.

In **Figure 7.9A**, it can be seen that the coarseness of ovalbumin, egg white and blood plasma protein gels are similar and changes occur in a narrow range of length scales, but their intercepts are different. On the other hand, whey, pea and soy protein have significantly higher coarseness, but their intercepts are similar. Gel stiffness also did not show a clear relation to the intercept (**Figure 7.9B**). Therefore, we can conclude that the origin of the intercept does not solely originate from differences in morphology (coarseness) and stiffness. These parameters may again have a counteractive effect, or the intercept is determined by other properties of the gel. As was already discussed for the slopes, the differences could possibly be indications for the occurrence of micro-cracks during deformation and to plastic deformation. Determination of the origin of the slope and intercept for a globular protein will allow better understanding and more precise tuning of WH impact onto the mechanical deformation of protein based gels.

7.6   Effect of macrofracture on gel WH

When pressure is applied on the gel network, eventually the gel will rupture, and may influence water removal, as these fracture event will lead to energy dissipation. In **Chapter 2** we have shown that fracture characteristics obtained from large deformation measurements as fracture stress and strain, have no correlation with the amount of expulsed water (A_{max}) from the gel network. To show the effect of controlled macro-destruction of the gel on A_{max} (water removal) and water flux from the gel ($k2$), 12% (w/w) ovalbumin gels were cut in a number of pieces or completely smashed (referred as "S" in **Figure 7.10**) and measured for their WH.
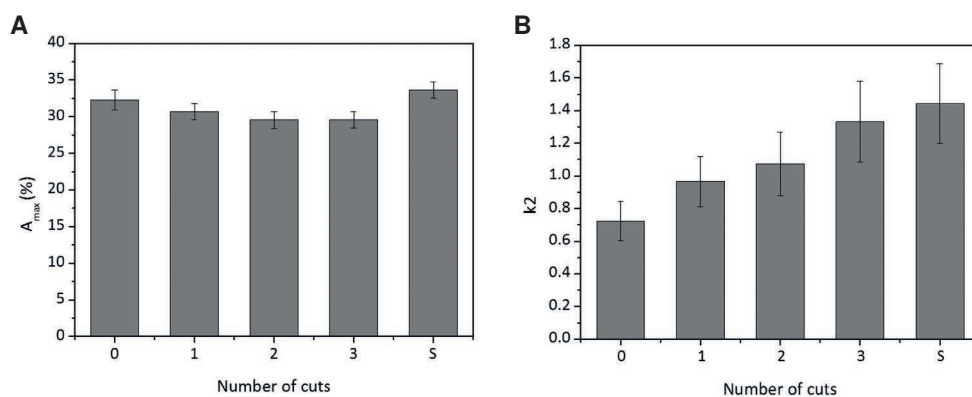

Figure 7.10 Effect of gel disruption (S stands for smashed) on (A) A_{max} and (B) $k2$ in 12% (w/w) ovalbumin gel prepared in the presence of 100 mM NaCl.

From the figure it can be seen that macro-destruction does not affect amount of water expulsed from the gel (A_{max}) (**Figure 7.10A**), but does have an effect on water flux ($k2$) from the gel (**Figure 7.10B**). A larger extent of network disruption results in a higher $k2$. These results suggest that a ruptured gel could be considered as a sum of microgels, where WH is dominated by the inherent coarseness and stiffness of the individual microgel-particles.

7.7 Impact for applications

Food products are typically multicomponent systems, where often the spatial volume is set by a protein continuous network. The ability of protein-based food products to entrap water and to prevent its exudation upon mechanical deformation is important for the texture and thus sensory perception of food products. Understanding of structural origins that determine gel water holding is therefore essential, and would allow designing foods with controlled sensory perception. Water removal from the gel (quantity, kinetics and mechanism) is related to the coarseness and deformation of the network. In the case a gel network is fine in coarseness and stiff, the applied pressure would act towards water removal rather than towards network deformation. In the case of more coarse gels (stiff and less stiff) applied pressure would act on both network deformation and water removal. An understanding of the interplay between the effect of coarseness and stiffness on WH in fine and coarse gels allows one to take a better control and tune juiciness [20] and the release of tastants from food products.

Next to taste, product texture determines sensory profile of the product. Recoverable energy correlates to sensory profiling of protein-based food products [21]. In the so-called energy balance [22], the applied work to a specimen (e.g. spatial protein network) can either be stored and recovered upon release of applied force or may dissipate via a number of physical processes. Shown RE and WH relation could be used to alter and tune product textural properties and sensory perception. A main axis in the sensorial space (PCA-plot) that positions (semi-)solid food products relative to each other is governed by the attribute "crumbing" - the effort to break a product into pieces by compressing between tongue and palate, where typically crumbly products have a low score for the attribute "spreadable" [21, 23]. It was found that there was a correlation between stored energy and crumbling effort. The more energy is stored, the more effort is needed to break the procut into smaller pieces [21]. The proportion of energy that can be used for fracture of the material, will contribute to the number of particles formed during processing between tongue and palate and has been correlated to "spreadable" [23]. If one desires to lower the energy needed to crumble the product, more energy should be dissipated towards serum flow or fracture events. To enhance spreadability during oral processing of the product, limited amount of energy should be stored, but also serum flow should be prevented. As spreadablity is related to number of particles formed during oral processing, more energy needs to be directed towards fracture instead of serum flow. By controlling the energy balance in the system, one would be able to alter product textural properties and sensory perception can be tuned.

To control texture, the correlation between RE and WH is essential and an understanding of WH and water removal (kinetics) is important. We have shown that WH is protein and network specific. The protein network is a basis for the texture of the product and thereby consumer acceptance. Water removal from the gel under applied force (during

7

consumption) is network specific, and not protein specific. However, as the type of protein used to obtain a gel defines the gel morphology, different WH for different protein systems are found. However, when coarseness and stiffness can be changed, WH of the protein systems can be varied. This means that WH can be tuned by controlling specific gel network properties. To adapt to the change in demands for alternative proteins, food industries need more flexibility in their formulation and this requires more knowledge in alternative proteins. Every protein type has inherent functional behaviour, specific solubility, denaturation and aggregation propensity and thereby also specific network-forming properties. This makes simple exchangeability of protein sources in applications difficult. In this thesis, we have shown that the type of network formed is protein specific and is defined by different parameters, as coarseness, connectivity of pores and stiffness. However, if one knows how to change network formation of the different proteins of varies sources, exchangeability of proteins would become easier. The results in this thesis could be used to identify the preferred properties of the network; e.g. what values for coarseness or stiffness would be needed to obtain a certain (rate of) water removal. This would allow one to select a specific protein source for a certain application.

7.8   Conclusion

Water holding (WH) of protein gels can be tuned by controlling the gel network properties. WH and thereby water removal from a gel is network specific, and not protein specific. In both fine and coarse gels, water removal from the gel is dominated by the coarseness of the network. For the coarseness, both the small and intermediate length scales are interesting and important in gel WH. For smaller length scales, a minimal coarseness is required before water can be removed. This lower length scale is set by gel stiffness and could be used to design gels with different coarseness without water loss. Water removal kinetics and the water removal mechanism is determined by both coarseness and stiffness of the network at intermediate length scales of the protein networ. Tuning the coarseness independent of stiffness provides an effective tool to set the water holding in food gels, and may provide opportunities to tune texture of foods and increase exchangeability of proteins.

7

References

1. Kinsella, J.E., *Relationship between structure and functional properties of food proteins*, in *Food proteins*, P.F. Fox and J.J. Condon, Editors. 1982, Applied science publishers LTD: Ireland.

2. Sikorski, E.Z., *Functional properties of proteins in food systems*, in *Chemical and functional properties of food proteins*, E.Z. Sikorski, Editor. 2001, CRC press: USA.

3. Bell, D.J., et al., *The density of protein precipitates and its effect on centrifugal sedimentation.* Biotechnology and Bioengineering, 1982. 24(1): p. 127-141.

4. Kao, F.-J., Su, N.-W., and Lee, M-H., *Effect of calcium sulfate concentration in soymilk on the microstructure of firm tofu and the protein constitutions in tofu whey.* Journal of Agricultural and Food Chemistry, 2003. 51(21): p. 6211-6216.

5. Maltais, A., et al., *Formation of soy protein isolate cold-set gels: protein and salt effects.* Journal of Food Science, 2005. 70(1): p. 67-73.

6. Puppo, M.C. and Añón, M.C., *Structural properties of heat-Induced soy protein gels as affected by ionic strength and pH.* Journal of Agricultural and Food Chemistry, 1998. 46(9): p. 3583-3589.

7. Hermansson, A-M., *Soy protein gelation.* Journal of the American Oil Chemists Society, 1986. 63(5): p. 658-666.

8. Ikeda, S. and Morris, V.J., *Fine-stranded and particulate aggregates of heat-denatured whey proteins visualized by atomic force microscopy.* Biomacromolecules, 2002. 3(2): p. 382-389.

9. Baussay, K., et al., *Influence of the ionic strength on the heat-induced aggregation of the globular protein β-lactoglobulin at pH 7.* International Journal of Biological Macromolecules, 2004. 34(1–2): p. 21-28.

10. Chantrapornchai, W. and McClements, D.J., *Influence of NaCl on optical properties, large-strain rheology and water holding capacity of heat-induced whey protein isolate gels.* Food Hydrocolloids, 2002. 16(5): p. 467-476.

11. Langton, M. and Hermansson, A.-M., *Fine-stranded and particulate gels of β-lactoglobulin and whey protein at varying pH.* Food Hydrocolloids, 1992. 5(6): p. 523-539.

12. Stading, M., Langton, M., and Hermansson, A.-M., *Microstructure and rheological behaviour of particulate β-lactoglobulin gels.* Food Hydrocolloids, 1993. 7(3): p. 195-212.

13. Munialo, C.D., et al., *Quantitative analysis of the network structure that underlines the transitioning in mechanical responses of pea protein gels.* Food Hydrocolloids, 2015. 49: p. 104-117.

14. Hermansson, A-M., *Structuring water by gelation food materials science*, J.M. Aguilera and P.J. Lillford, Editors. 2008, Springer New York. p. 255-280.

15. Urbonaite, V., et al., *Permeability of gels is set by the impulse applied on the gel.* Food Hydrocolloids, 2015(0). http://dx.doi.org/10.1016/j.foodhyd.2015.03.024

16. Urbonaite, V., et al., *Relation between gel stiffness and water holding for coarse and fine-stranded protein gels.* Submitted, 2015.

17. Pouvreau, L., et al., *Is WH the representative factor for the elastically stored energy in protein based gels?* Submitted, 2015.

18. de Jong, S., van Vliet, T., and de Jongh, H.H.J., *The contribution of time-dependent stress relaxation in protein gels to the recoverable energy that is used as tool to describe food texture.* Submitted, 2015.

19. Baumberger, T., C. Caroli, and D. Martina, *Solvent control of crack dynamics in a reversible hydrogel.* Nature Materials, 2006. 5(7): p. 552-555.

20. Northcutt, J.K., Foegeding, E.A., and Edens, F.W., *Water-holding properties of thermally preconditioned chicken breast and leg meat.* Poultry Science, 1994. 73(2): p. 308-316.

21. van den Berg, L., et al., *Energy storage controls crumbly perception in whey proteins/polysaccharide mixed gels.* Food Hydrocolloids, 2008. 22(7): p. 1404-1417.

22. van Vliet, T., Luyten, H., and Walstra, P., *Fracture and yielding of gels.*, in *Food polymers, gels and colloids*, E. Dickinson, Editor. 1991.

23. van den Berg, L., et al., *Breakdown properties and sensory perception of whey proteins/polysaccharide mixed gels as a function of microstructure.* Food Hydrocolloids, 2007. 21(5–6): p. 961-976.

7

Summary

Acknowledgments

Curriculum vitae

List of publications

Overview of completed training activities

Summary

The ability of protein-based food products to entrap water and prevent its exudation upon mechanical deformation (water holding) is important for its sensory perception and for the release of tastants from food products. This thesis provides clarity in water holding (WH) and identifies length scales most contributing to gel WH. Gel WH was defined as the sum of five different contributions representing water held within the gel microstructure at different length scales, starting at the (sub-)nm length scale for molecularly bound water to that of the mm scale, describing the contribution of fracture events to gel WH. The aim of this thesis was to understand how structural aspects at different length scales affect water holding of protein gels under applied pressure. A special focus was given to the contribution of gel morphology, where the effect of gel coarseness, gel stiffness and their interplay on water removal from the gel were evaluated and generalized. Additionally, the relation between WH and recoverable energy upon applied mechanical deformation is discussed, followed by the relevance of these findings regarding applications and possible future research.

WH of soy protein gels was investigated to identify which length scales are most contributing to WH when centrifugal force is applied. More specifically it was attempted to differentiate between the contributions of sub-micron and supra-micron length scales. In **Chapter 2**, the specificity of $MgSO_4$ and $MgCl_2$ salts on soy protein aggregation was used to create different building blocks (sub-micron contribution) and gel morphologies (supra-micron contribution). Obtained results showed that the micrometer length scale is the most important length scale to define WH of soy protein gels under applied deformation. WH of soy protein gels correlated negatively with Young's modulus and positively with recoverable energy. The occurrence of fracture events had only a limited impact on WH. The ease by which water was removed from the gel was related to the initial building block size, but not the total amount of removed water.

In **Chapter 3**, soy proteins were modified aiming to change protein clustering during network-assembly by means of modulation of calcium binding affinity to obtain gels with different morphologies at a constant ionic strength and constant protein concentration. Within this study it was aimed to differentiate between the contribution of gel microstructure and network stiffness to WH of soy protein (SP) gels. Imaged (CSLM) gel microstructures were analyzed and a coarseness parameter representing a typical length scale of the gel network was obtained. It was found that not gel stiffness, but coarseness (gel microstructure inhomogeneity) is more dominant in setting the WH ability. A higher energy dissipation of applied stress exerted onto the protein network was related to the inability of a gel network to retain water.

In **Chapter 4** it was aimed to study the interplay of gel coarseness and gel stiffness on WH and water flow kinetics from the gel once force is applied onto the material. Ovalbumin heat-set gels were used as a model system, where a range of gel morphologies and

stiffness was modulated by varying ionic strength. WH of gels was measured both as a function of time and force applied. From the experimental data (i) an effective gel permeability coefficient and (ii) an effective water flux coefficient were obtained and related to gel coarseness and stiffness. Gel coarseness determined the maximum amount of water removed from the gel at defined conditions, where lower (≤0.1 µm) and upper (≥0.4 µm) limiting length scales for water removal were identified. The lower length scale refers to the gel coarseness for which no water can be removed from the gel network at any applied pressure. The upper limiting scale refers to the limit in coarseness, for which an increased coarseness does not yield additional water removal from the gel. Gel stiffness is shown to be the major determinant for water removal kinetics from the gel. The combination of gel coarseness and gel stiffness showed a cooperative effect on gel WH.

The relationship between gel water holding and stiffness was further investigated for fine and coarse-stranded gels in **Chapter 5**. For this purpose, gels were prepared from whey protein isolate at varying ionic strength to create fine and coarse-stranded gels. These gels were characterized for their coarseness (CSLM image analysis), stiffness (Young's modulus from large deformation rheology) and water holding. Similar as in **Chapter 4**, (i) an effective gel permeability coefficient and (ii) an effective water flux coefficient were obtained and related to both gel coarseness and stiffness. Increased gel coarseness in both fine and coarse gels resulted in a larger extent of network deformation. For fine gels, the coarseness of the gel was shown to be dominant in water removal. In the case of coarse gels, coarseness and stiffness had a counteracting effect, but coarseness was still dominant. These results show that the interplay of tuning coarseness of protein networks independent of stiffness provides a balanced tool to set the water holding in food gels.

Many food products are build up from microstructural building blocks. To better understand WH on the microstructural level, the contribution of individual building blocks (aggregates) to WH was evaluated for soy proteins aggregates (**Chapter 6**). We discriminated two types of water within the aggregates: (i) entrapped water and (ii) confined water. Entrapped water is associated to (pelleted) aggregates and is not constrained in the exchangeability. Confined water in aggregates is hindered in its diffusion because of the physical aggregate structure. Larger and less dense aggregates entrap more water, but at the same time these aggregates are more deformable and result in higher water displacement from the aggregate structure when force is applied (e.g. centrifugation). Confined water in aggregates was shown to be independent on deformation and is comparable for the different aggregates prepared. Independent on the aggregate structure, the amount of confined water within the aggregates was approximately 3.5 g of water per gram of protein. In the case of soy protein aggregates, entrapped water by the aggregate could be modulated by the aggregate size and its density, while confined water, however, remained the same.

In the final chapter (**Chapter 7**) the findings of this thesis are integrated and discussed in a coherent view on the application of protein networks in food with a tailored mechanical

response. The work presented in this thesis shows that WH of protein gels can be tuned by controlling the gel network properties. WH and thereby water removal from a gel is network specific, and not protein specific. In both fine and coarse gels the coarseness dominates water removal from the gel. The water removal occurs at intermediate length scales of coarseness scales and a minimal coarseness needs to be present to induce water removal. This coarseness is presented as the lower limiting length scale and is set by gel stiffness. Gel stiffness could thus be used to design gels with different coarseness without water loss. Water removal kinetics and the water removal mechanism depend on the interplay between stiffness and coarseness of the network. Tuning coarseness of the protein networks at these intermediate length scales independent of stiffness provides an effective tool to set the water holding in food gels. The WH was shown to be related to the recoverable energy of the system, and therefore also to energy dissipation. As energy dissipation, such as fracture and serum flow, can be related to textural attributes, altering the gel network properties can be used as a tool to control the energy balance in food products for texture design.

Acknowledgements

Thank you for all who contributed to the completion of this thesis!

Curriculum Vitae

Vaida Urbonaite was born on the 4th of November 1985 in Klaipeda (Lithuania). She attended Senoji Gymnasium in Palanga, where she graduated in 2004. In the same year she started her studies in Food Technology at Kaunas University of Technology. In 2008 she acquired a Bachelor degree in Chemical Engineering and started a Master's degree program in Food Technology at Wageningen University (the Netherlands). During the MSc, she performed her thesis at the chair group of Food Quality and Design. After that, she did an internship at Danone Nutricia Research (Wageningen, the Netherlands) and participated in the Food Valley Ambassador program as an ambassador for Lithuania. After obtaining her MSc degree in 2011, she started working as a PhD researcher in the Physics and Physical Chemistry of Foods group. Her work was part of the project "Relevant time & length scales for mechanical behavior of protein-based systems" financed by TI Food and Nutrition. The results of this research are presented in this thesis. Currently she is working as a scientist in the Processing and New Technologies department at Danone Nutricia Research (Utrecht, the Netherlands).

She can be contacted by e-mail: v.urbonaite@gmail.com

List of publications

Urbonaite, V., de Jongh, H.H.J., van der Linden, E., and Pouvreau, L., *Origin of water loss from soy protein gels.* Journal of Agricultural and Food Chemistry, 2014. 62: p. 7550-7558.

Urbonaite, V., de Jongh, H.H.J., van der Linden, E., and Pouvreau, L., *Water holding of soy protein gels is set by coarseness, modulated by calcium binding, rather than gel stiffness.* Food Hydrocolloids, 2015. 46: p. 103-111.

Urbonaite, V., de Jongh, H.H.J., van der Linden, E., and Pouvreau, L., *Permeability of gels is set by the impulse applied on the gel.* Food Hydrocolloids, 2015. 50: p. 7-15.

Urbonaite, V., van der Kaaij, S., de Jongh, H.H.J., Scholten, E., van der Linden, E., Ako, K. and Pouvreau, L., *Relation between gel stiffness and water holding for coarse and fine-stranded protein gels.* Submitted, 2015.

Urbonaite, V., de Jongh, H.H.J., van der Linden, E., and Pouvreau, L., *Protein aggregates may differ in water entrapment but are comparable in water confinement.* Submitted, 2015.

Pouvreau, L., van Wijlen, E., Klok, J., Urbonaite, V., Munialo, C.D, and de Jongh, H.H.J., *Is WH the representative factor for the elastically stored energy in protein based gels?.* Submitted, 2015.

Martin, A.H., Baigts Allende, D., Munialo, C.D., Urbonaite, V., Pouvreau L. and de Jongh, H.H.J., *Modulating protein interaction on molecular and microstructural level for texture control in protein based gels.* Royal Society of Chemistry (proceedings), 2013. 404: p. 64-70.

Overview of completed training activities

Discipline specific activities

Courses

14th European School on Rheology, 2013, Leuven, BE

Image Analysis Training, 2013, Le Mans, FR

International Advanced Course Food Structure and Rheology, 2012, Wageningen, NL

Conferences and Workshops

Symposium from Molecules to Functionality, 2014, Amsterdam, NL [‡]

15th Food Colloid Conference, 2014, Karlsruhe, DE[‡]

ISOPOW XII Conference, 2013, Gothenburg, SE[†]

Symposium on Protein Folding and Stability, 2012, Liege, BE

General courses

Writing Grant Proposals, 2015, Wageningen, NL

Career Perspectives, 2015, Wageningen, NL

Mobilising Your Scientific Network, 2014, Wageningen, NL

Basic Statistics, 2012, Wageningen, NL

Scientific Writing, 2012, Wageningen, NL

PhD Introduction Week, 2011, Eindhoven, NL

Optional courses and activities

Organized and participated in the PhD trip, 2014, USA-Canada

Basic iΠ for Researchers (2012, Wageningen, NL)

Work meetings project "Food Structuring", TIFN (2011-2015, Wageningen, NL)

Science meetings in FPH group (2011-2015, Wageningen, NL)

Theme training Food Structuring (2011, Wageningen, NL)

[*][‡]Talk, [†]Poster